Magnetization and movement of glioblastoma cells loaded with magnetic nanoparticles

Dissertation with the aim of achieving a doctoral degree

at the Faculty of Mathematics, Informatics and Natural Sciences

Department of Chemistry

of Universität Hamburg

submitted by Dorothee Rose

2016 in Hamburg

First reviewer: Prof. Christian Betzel

Universität Hamburg

Institut für Biochemie und Molekularbiologie

Martin-Luther-King Platz 6

20146 Hamburg

Tel.: 040 42838 - 6069

E-Mail: Christian.Betzel@uni-hamburg.de

Second reviewer: Prof. Regine Willumeit-Römer

Helmholtz-Zentrum Geesthacht

Zentrum für Material- und Küstenforschung GmbH

Institut für Werkstoffforschung

Max-Planck-Str. 1

21502 Geesthacht

Tel: 04152 87 - 1291

E-Mail: Regine.Willumeit@hzg.de

Content

Abbreviation list

Abbreviation	Full name
AM	acetoxymethyl
ANOVA	analysis of variance
ATP	adenosine triphosphate
BBB	blood-brain barrier
BrdU	bromodeoxyuridine
CED	convection-enhanced delivery
DMSO	dimethyl sulfoxide
DNA	deoxyribonucleic acid
ECM	extracellular matrix
EGFR	epidermal growth factor receptor
FDA	food and drug administration
Fe	iron
FS	FeraSpin™ XS
Gd	gadolinium
H_2O_2	hydrogen peroxide
HGF	hepatocyte growth factor
Hz	Hertz
ICNRP	International Commission on Non-Ionizing Radiation Protection
IRP	iron regulatory protein
MA	myristic acid coated magnetic nanoparticles
MACS	magnetic-activated cell sorting
MGMT	O^6-methylguanine-DNA methyltransferase
MNP	magnetic nanoparticle
MRI	magnetic resonance imaging
mRNA	messenger ribonucleic acid
MSC	mesenchymal stem cell
NADPH	nicotinamide adenine dinucleotide phosphate
NP	nanoparticle
OH^-	hydroxyl radical

OS	overall survival
PEG	polyethylene glycol
PEI	polyethyleneimine
PLL	poly-L lysine
PTFE	polytetrafluoroethylene
ROS	reactive oxygen species
rpm	revolutions per minute
SMF	static magnetic field
T	tesla
TEM	transmission electron microscopy
VEGF	vascular endothelial growth factor
v/v	volume to volume
WHO	world health organization
w/o	without

Zusammenfassung

Glioblastome haben wegen der schnellen Rückkehr nach operativer Entfernung eine der schlechtesten Prognosen aller Gehirntumoren. Durch eine Kombination von Bestrahlung und Chemotherapie kann das Überleben der Patienten verlängert werden, allerdings sterben die meisten Patienten dennoch innerhalb des ersten Jahres nach Diagnosestellung. Deswegen ist das Interesse an alternativen Therapiekonzepten gestiegen, beispielsweise an Behandlungen basierend auf magnetischen Nanopartikeln (MNPs). MNPs sind Partikel im Nanobereich, die durch biochemische Beschichtungen vielfältige Eigenschaften besitzen und durch ein magnetisches Feld manipuliert werden können.

In der vorliegenden Studie wurden die Beladung von Zellen mit MNPs und die potentielle Zelltoxizität mit zellbiologischen und biochemischen Methoden untersucht. Dafür wurden der Eisengehalt und die Viabilität von drei humanen Glioblastomzelllinien und Astrozyten nach Zugabe von zwei unterschiedlichen MNP-Typen unter verschiedenen Bedingungen (1-3 Tage Inkubationszeit und 5-50 µg/mL Eisenkonzentration) detektiert. Im zweiten Teil der Studie wurden verschiedene Methoden für die Auswertung und Quantifizierung der Zellbewegung im Magnetfeld mit und ohne MNP-Beladung getestet, einschließlich der möglichen Zelltoxizität.

Die verschiedenen Glioblastomzelllinien besaßen sehr unterschiedliche Eigenschaften, z.B. variierte die Wachstumsrate, was auch die Beladung der Zellen beeinflusste. Außerdem zeigte sich bei den ausgewählten MNP-Arten eine konzentrationsabhängige Beladung. Durch Beobachtung der metabolischen Aktivität der Zellen konnten dosisabhängige Effekte durch die Beladung gezeigt werden, wobei die Effekte durch das Magnetfeld nur gering waren.

Die Bewertung der Magnetfeld-gerichteten Zellbewegung erforderte die Etablierung neuartiger Zellkulturverfahren, die auf ihre Praktikabilität und Qualität der Ergebnisse geprüft wurden. So konnte beobachtet werden, dass die magnetische Anziehung nicht nur durch den zellulären Eisengehalt, sondern auch durch den MNP-Typ bestimmt wurde. Wie erwartet hatte jeder MNP-Typ einen anderen Einfluss auf die Beladung und Viabilität der Zellen, dennoch sollten insbesondere die Kulturbedingungen und die Zellspender-spezifischen Eigenschaften nicht unterbewertet werden. Außerdem sollte bei der Auswahl des MNP-Typs auf die Verträglichkeit in gesunden Zellen geachtet werden, da die untersuchten Astrozyten ebenfalls auf die Beladung mit MNPs reagiert haben. Insgesamt konnten in der Studie also wertvolle Erkenntnisse für die Anwendung von MNPs im medizinischen Kontext gewonnen werden.

Abstract

Glioblastoma possesses one of the poorest prognoses of any kind of brain tumors, due to its fast recurrence after surgical removal. A combination of radiation and chemotherapeutics has prolonged the survival of the patients, however, most patients still die within the first year after diagnosis. Thus, alternative therapeutic approaches gained more interest, for example therapies based on magnetic nanoparticles (MNPs). MNPs are particles in the nano-range, that can own various properties by different biochemical coatings and that can be manipulated by a magnetic field.

In the present study, the loading of cells with MNPs and their potential cytotoxicity were examined by cytobiological and biochemical methods. For this purpose, the iron content and the viability of three human primary glioblastoma cell lines and astrocytes was detected after addition of two distinct MNP types under different conditions (1-3 d incubation time and 5-50 µg iron/mL concentration). In a second part, different setups were tested to evaluate and quantify the cell movement in a magnetic field with or without incorporation of MNPs and its potential cytotoxicity.

The different glioblastoma cell lines showed very diverse characteristics, e.g. in the growth rate, which also influenced the loading of the cells. Additionally, the MNP types selected for this study demonstrated a concentration-dependent loading. By observing the cell metabolic activity, dose-dependent effects of the MNPs were observed, while effects of the magnetic field were only low. In a non-attached state, the cells were attracted by the magnet according to their iron load and their distance to the magnet.

The evaluation of the magnetic-directed cell movement required novel cell-culture setups, which were tested in terms of practicability and quality of the results. Interestingly, the magnetic attraction was not only determined by the cellular iron content but also by the MNP type. As expected, each MNP type had a specific impact on cell viability and loading, however, particularly the culture conditions and the inherent donor-specific cell characteristics should not be underestimated. Furthermore, the choice of the MNP type should be carefully considered in terms of healthy cell tolerance, as astrocytes also responded to the MNP loading. Thus, valuable insights were achieved for the application of MNPs in the medical field.

Introduction

In this interdisciplinary study, several aspects of cell biology, toxicology and nanoscience were combined: Firstly, glioblastoma cells which display an intrinsically high migration potential were used to support the extensive research on therapies against this fatal brain tumor. Secondly, magnetic nanoparticles (MNPs) were used in order to exert a force on the cells by a magnetization of the MNPs. Thirdly, a magnetic field was introduced to induce a force on the cells, leading to a directed movement of the cells.

Glioblastoma characteristics, therapy and problems

Glioblastoma belongs to the group of primary brain cancers derived from glial cells or glial precursor cells (glioma). The specific glial cell type origin is not possible to determine, as the cells normally have reached a low differentiation level during carcinogenesis [1]. However, according to World Health Organization (WHO) classification, glioblastoma belong to the astrocytoma group [2]. The vast majority of glioblastoma are new (*de novo*) tumors, while 5 % arise from lower grade astrocytomas. Both patient cohorts differ in median age and molecular pattern, e.g. older patients mostly develop *de novo* tumors with different gene mutations [3]. The glioblastoma tumors are characterized by large necrosis areas and hemorrhages [1] and a highly heterogenic histology is partly due to the combination of neoplastic and stromal tissue [3]. The cause of the tumor formation remains mostly unclear. Mobile phone or electromagnetic fields in general were suspected to cause glioblastoma but no significant effects were measured [4]. Glioblastoma belong to grade IV (the highest grade in the WHO's tumor classification), which stands for a malignant and fast growing tumor with a very bad prognosis [2]. Indeed, even with the current standard medical therapy, the median survival of glioblastoma patients is only about 15 months [5].

Glioblastoma therapy

Many therapeutic approaches exist in the glioblastoma treatment - classical and more innovative methods, the latter being often combined with standard ones. The classical therapy concept encompasses a surgical tumor resection after glioblastoma diagnosis, followed by chemotherapeutic and radiotherapeutic treatment. Temozolomide is the standard chemotherapeutic, as other chemotherapies did not show an increased overall survival (OS) of the patient cohort [6]. Temozolomide is an alkylating agent, that is orally administered and able to cross the blood-brain barrier (BBB). After its activation, it promotes the methylation of nucleic acids and other macromolecules, causing deoxyribonucleic acid (DNA) damage and inhibition of DNA or protein synthesis leading to cell death. As systemic side effects, strong nausea, emesis and immunosuppression occurs [1], [7]. Temolozolomide is not a

specific drug against glioblastoma; however, this kind of tumor is supposed to be more sensible to alkylating agents due to the lack of the DNA repair protein O^6-methylguanine-DNA methyltransferase (MGMT) in about 40 % of glioblastoma [8].

Another agent tried for the treatment of glioblastoma is bevacizumab. This is a monoclonal antibody against the vascular endothelial growth factor (VEGF) and thus targets the increased angiogenesis occurring in glioblastoma. However, in a clinical trial, the addition of bevacizumab to the standard therapy did not show any prolongation of the OS, whereas more side effects occurred compared to the standard therapy alone [9]. In addition, the small molecule epidermal growth factor receptor (EGFR) inhibitor erlotinib treatment did not show an enhanced OS [10].

Apart from the oral administration, local delivery of the chemotherapeutics was tried to reduce the toxic side effects. Carmustine is an alkylating agent like temozolomide and was one of the first drugs administered against glioma, however, showed severe systemic side effects. Thus, Gliadel®, a polymer wafer with carmustine implanted into the brain, was introduced for glioblastoma therapy and approved by the FDA in 1996 for recurrent and 2003 for newly diagnosed glioma. The local treatment reduced the systemic side effects, whereas other complications in terms of wound healing difficulties and extensive brain edema occurred [11]. In 2014, Bregy et al. [12] reviewed nineteen studies with Gliadel® in glioblastoma treatment, concluding a marginal increase of patient survival but numerous complications. Thus, the authors did not recommend Gliadel® for glioblastoma therapy.

Problems of therapy
Special characteristics of glioblastoma tumor cells are hampering the therapy success. For example, the formation of blood vessels (angiogenesis) is strongly activated in glioblastoma, as the fast proliferating cells have a high metabolic demand. However, such vessel formation is not physiological and the pathological blood vessels are often insufficiently perfused, resulting in hypoxia [13], necrosis and edema. Hypoxia is supposed to be a major reason why glioblastoma are resistant against radiotherapy, as radiation needs oxygen to permanently damage the DNA via formation of reactive oxygen species (ROS) [14].

The invasion and a widespread distribution throughout the brain is also a typical characteristic of glioblastoma cells, causing the tumor to re-grow after surgical resection of the main tumor mass. Although glioblastoma cells can penetrate deeply in the brain tissues, in most cases the tumor recurs directly at the resection margin in the edema area [15]. As it is an important therapy hurdle, glioblastoma cell migration was the target of the present study. The migration has been intensively studied and numerous molecular pathways were

indentified that contribute to the enhanced invasion potential of these tumor cells. For example, plasma membrane associated molecules like phosphoinositides [16], intracellular NADPH-oxidase [17], hypoxia inducible factors [18] or protein kinase D2 [19] were shown to regulate the migration. These and many other molecules and their pathways offer potential targets to inhibit the invasion of glioblastoma cells in the healthy brain tissue [20]. However, up to now, most clinical trials are dealing with alkylating agents like temozolomide or anti-angiogenesis agents like bevacizumab and only a few have tested migration/invasion-relevant strategies. One phase II trial showed an enhanced progression free survival, if temozolomide was combined with marimastat, an inhibitor of matrix metalloproteinases. These enzymes are excreted by cells and are able to dissolve the extracellular matrix needed for the invasion in the surrounding tissue [21].

The disadvantage of any therapy directed against a specific molecular pathway is the high genetic flexibility of tumor cells. Even if an important tumorigenic pathway is inhibited, the cells may activate another to overcome therapy effects. In a study by Hu et al. [22], it was demonstrated that the suppression of the EGFR pathway leads to the activation of the urokinase receptor pathway and thus to an increase of the cell migration. Therefore, in the present study, the manipulation of cellular pathways was not focused. Another issue is the high patient variability, which hinders the glioblastoma therapy with chemotherapeutics. Verhaak et al. [23] described four different subtypes of glioblastoma (classical, mesenchymal, proneural and neural), distinguished by their gene expression patterns and genetic alterations, which differed also in their response to radiation or chemotherapy. For example patients of the proneural subtype seemed not to profit from a more aggressive therapy while patients of classical subtype clearly did. For this reason, an examination of different glioblastoma cell lines was considered in the present study. Because of the cancer chemotherapy difficulties, alternative therapies with new mode of actions gained more interest.

Alternative therapeutic approaches
New therapy possibilities focus on the interaction of fundamental physical principles with the tumor cell homeostasis. In 2011, the Food and Drug Administration (FDA) approved the treatment of recurrent supratentorial glioblastoma multiforme with NovoTTF-100A™ system by Novocure® after a clinical phase III trial. In this trial, transducers were fixed to the head of the patients producing an alternating electric field [24]. It was shown, that the OS of patients treated with the electric fields was not significantly higher than of the patients treated with the normal therapy of the physician's choice. However, the systemic side effects were lower and thus the quality of life was much better. In a second clinical trial, the OS was

significantly higher, however, this was in part due to a more suitable patient cohort choice for this kind of therapy [25].

Kirson et al. [26] demonstrated that the electric field is disturbing the polar microtubule molecules during the cancer cell division *in vitro*. This caused defects of the mitotic spindle, followed by apoptosis. The observations were proven to be effective against tumor growth in a mouse model, without side effects on healthy cells. This treatment is only suitable for a local therapy but as glioma cells are not able to penetrate the blood vessels, they do not form metastasis outside the brain in most cases [27] and thus, a local treatment is sufficient.

Another concept to treat cancer with physical means is the hyperthermia, where the tumor region or even parts of the body are heated to more than 40 °C. This increase of temperature is generated with the help of for example microwaves, hot water perfusion or wire implants, placed at the surface of the skin or transplanted in the tissue [28]. The cells reacted especially to temperatures higher than 43 °C with less proliferation and apoptosis. Effects on membrane fluidity and cytoskeleton changes were shown, but likely protein denaturation plays the main role in such therapy [29]. However, the targeting of the cancer cells was often insufficient with these methods, as deeper areas in the body were not reached or healthy tissue was greatly affected. So, the research headed towards magnetic nanoparticles that could be targeted to tumor cells and moved by fast alternating magnetic fields to create heat [30]. In a study by Jordan et al. [31], the prolonged survival of glioma-bearing rats was shown after MNP injection and alternating magnetic field application. Hyperthermia in combination with radiotherapy has already shown effects in a glioblastoma patient study, where the OS was increased compared to other studies. The only drawbacks shown were the necessary removal of metal implants near the application area and the MRI artifacts caused by the high iron amount that complicate the imaging of the tumor [32].

Magnetic nanoparticles (MNPs) for medical therapy

As already mentioned in the hyperthermia method, magnetic nanoparticles (MNPs) gain more interest in the medical field. MNPs are particles of nanometer range generally consisting of a metal core and a coating shell. Due to enormous combination possibilities of material, physical and chemical parameters, a huge variety of MNP types exist (Figure 1). As the MNP production does not require complicated methods or instruments, it is not restricted to companies but can be also performed in research laboratories. The metals used for clinical setups are often iron oxides (magnetite Fe_3O_4 or maghemite Fe_2O_3) or other iron composites that can be of different shapes (round, cubic or rod). Other metals, like Cobalt or Nickel, are also ferromagnetic under physiological conditions, but exhibit a lower magnetization and a higher toxicity [33]. Different types of coatings can enhance the biocompatibility of the

MNPs and enable their functionalization, for example by attaching ligands to biomolecules in drug targeting approaches. The chemistry of coatings is various, but generally consists of small organic molecules or polymers, like phospholipids, dextran, poly(ethylene glycol) (PEG) or poly(ethylenimine) (PEI) [34]. The size of the MNPs also plays an important role, especially in the distribution in the body. When MNPs are injected in the systemic circulation, they are cleared according to their size: smaller particles undergo renal clearance, while bigger ones are taken up by phagocytes and accumulate in the liver. So, the longest blood circulation is reached with MNPs in a size range 10-100 nm [35].

Figure 1: Magnetic nanoparticle composition variety. The structures of MNPs are diverse. Any free combination of magnetic compound in different shape, size and coating is possible and leads to different biophysical properties.

Clinical application and pre-clinical research

The application of MNPs in medical setups is often related with their reaction to a magnetic field. Since the 1990s, MNPs are commercially available as magnetic resonance imaging (MRI) contrast agents. Iron particles offer a good alternative to the conventional Gadolinium (Gd)-based contrast agents, as Gd is known to exert toxic effects and probably is responsible for renal fibrosis of some patients [36]. However, MNPs are mostly negative contrast agents, i.e. they darken areas, which is problematic in naturally dark areas on MRI images. Though, very small MNPs were shown to be capable positive contrast agents [37]. As MNPs are completely passively distributed upon intravenous administration, their MRI application up to now was mostly restricted to the imaging of liver lesions. A transport of these MNPs across the intact BBB could not be demonstrated in an *in vitro* model [38]. However, the

often leaky vasculature in tumors leads to an enhanced permeability for MNPs and their retention in tumor sites, so that the visualization of cancer with MNPs has gained more interest. Thus, they could be used to visualize the tumor via MRI and to define the tumor size, also in the brain, whereas a specific targeting of the cancer cells would even increase the accuracy of the tumor imaging. Indeed, Hadjipanayis et al. [39] achieved an enhanced MRI contrast by incubating glioblastoma cells with MNPs coupled with an EGFR-specific ligand in comparison to bare MNPs.

Apart for imaging, MNPs' magnetic properties are used in the concept of drug targeting. The principle of the targeted delivery is to conjugate a therapeutic component with a carrier that can deliver the drug to the intended site of action. The advantage is an enhancement of the therapeutic effect, as a higher drug concentration is reached at the target area, and in parallel there is a reduction of systemic side effects. With MNPs as carrier, drugs could be directed to a magnet fixed in or near the target area. The delivery of substances to the brain is further challenging due to the BBB, causing a restricted transport of molecules from the blood to the brain tissue. So, the ideal vector for a glioblastoma treatment should be injected systemically, remain stable in the blood stream, able to cross the BBB, target only the tumor cells and kill them. However, so far no vector system encompasses all these properties.

Some studies could show the guidance of MNPs delivered by a systemic injection with the help of a magnetic field. For example, Fu et al. [40] showed that fluorescently labeled MNPs were retained near an implanted magnetic mesh in a glioblastoma mouse model after systemic administration. Similarly, Zhang et al. [41] demonstrated in a subcutaneous glioma mouse model that PEGylated and heparin conjugated MNPs could target the tumor site more effectively by using permanent magnets. In a study by Kong et al. [42], fluorescently labeled MNPs were injected in mice, while permanent magnets were implanted in the brain or placed on the skull skin. In both setups, the MNPs were able to overcome the BBB, probably by crossing the endothelial cell membrane.

In parallel, some studies presented MNPs combined with chemotherapeutics, which were administered via convection-enhanced delivery (CED), i.e. where the fluid was injected directly in the tumor mass with a certain pressure. For example, the combination of chlorotoxin for glioblastoma cell targeting and O^6-benzylguanine (an antineoplastic agent) bound to MNPs showed to support the traditional oral telozolomide therapy in a mouse model, leading to a better OS [43]. In another study, MNPs conjugated with cetuximab, a monoclonal antibody against EGFR, were tested in three different mouse glioblastoma models. An increase of apoptosis and OS was achieved in all models in comparison to mice treated with MNPs or cetuximab alone [44].

There has been also a trial that aimed not to use MNPs as vector for drug delivery but as supportive therapy mean itself: Klein et al. [45] used MNPs in combination with radiotherapy against tumor cells. After a low dose X-Ray application, they demonstrated a drastic increase of ROS inside the tumor cells, probably because of an enhanced Fenton reaction with the MNPs, while normal tissue cells were not affected.

The variety of already existing possibilities of cancer (especially glioblastoma) treatment are represented in Figure 2. As explained already, every therapy concept has its drawbacks, leading to a lack of an efficient treatment. In the present study, a new concept is tested, dealing with the direction of cell migration after MNP incorporation by a magnetic field.
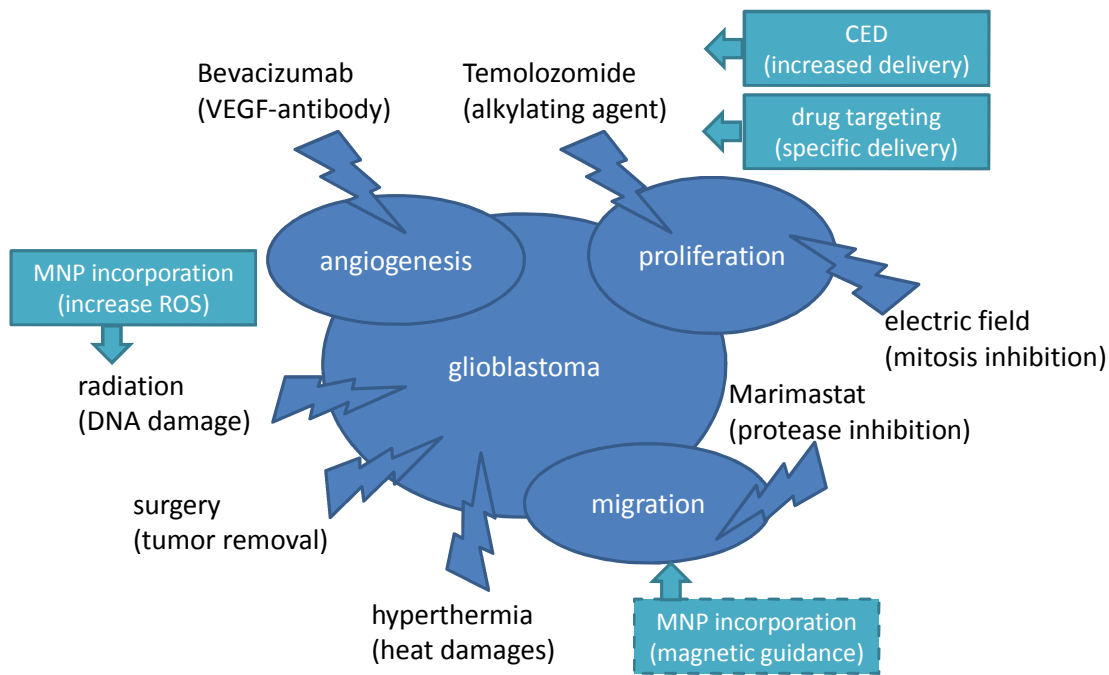

Figure 2: Therapy methods for glioblastoma treatment. The glioblastoma therapy includes classical means of cancer treatment, like radiation, surgery and chemotherapy. Temozolomide and bevacizumab belong to the most effective agents and target the proliferation and the angiogenesis, respectively of the tumors. The migration of the cancer cells can be inhibited by marimastat, which has been examined in clinical trials, but did not prolong the OS. Alternative therapy approaches include hyperthermia or electric fields. Boxes show concepts that support traditional means, while the dashed lined box demonstrates the position of the present study's aim.

Cell loading

Taken the different classical, alternative and supportive therapy concepts together, the loading of the cells with MNPs is a crucial step. The cellular loading with nanoparticles (NPs) in general can be achieved via different pathways. Very small NPs are supposed to cross the membrane by direct diffusion without a transporter, while bigger particles are likely taken up by an active mechanism, called endocytosis. Endocytosis is divided into

pinocytosis, i.e. the ingestion of fluids and solutes, and phagocytosis, i.e. the uptake of large particles (more than 250 nm). After being engulfed in endosomes, NPs are transported near the nucleus [46]. In case of an active mechanism, the uptake of NPs seems to be concentration-dependent up to saturation. However, it was shown that NPs are not excreted from the cells, so that the normal pharmacokinetic concepts are not able to explain the distribution of NPs [47].

Since the uptake of NPs is influenced by the NP properties, different NPs were tested for their loading efficiency. As already implied by the internalization pathways, the size of the NPs has an influence on the uptake efficiency [48]. The optimal NP size for an efficient receptor-mediated uptake was calculated to be 20-60 nm, whereas it was stated that for other endocytosis pathways different sizes would be optimal [49]. Indeed, for silica NPs, an optimal uptake was achieved with 50 nm size, while smaller (30 nm) and bigger particles (up to 280 nm) showed less uptake [50]. Similarly, Huang et al. [51] found that 37 nm MNPs were taken up best in macrophages in a group of similar, 8-64 nm MNPs. Another important and often discussed factor is the coating of the MNPs. In some studies, it was shown, that the coating has more influence than the size [52] or the iron concentration applied [53]. Murase et al. [54] tested the loading of similar-sized dextran MNPs modified with a carboxy-methylation or an alkali treatment, showing differences in uptake and MRI imaging. Even small changes in coating chemistry change the cell response [55].

Another factor influencing the cell loading arises from the *in vitro* setup, especially the cell culture medium, in which the MNPs are suspended. The serum proteins added to the cell culture medium often leads to the formation of a protein corona around the MNPs, causing them to aggregate and change their properties like size or surface charge [56]. Among the serum proteins, especially immunoglobulins, complement factors and apolipoproteins were detected in the MNP corona. Concerning the adsorption of immunoglobulins or complement proteins, the uptake of MNPs could facilitated by specialized cells of the immune system [57]. Normally, the MNP uptake is enhanced without serum proteins in the medium [58], maybe due to an enhanced adherence of the particles on the surface of the cells. Also, the coating could influence the uptake pathway. In a study by Lesniak et al. [57], electron microscopy images indicated that bare NPs were also found freely in the cytosol and not enclosed in vesicles of the endosomal or lysosomal pathway like particles with a protein corona.

In any case, the cells also influence the uptake. In a study by Jordan et al. [59] four different cell types (a neuronal cell line, a glioblastoma cell line, a colonic adenocarcinoma and a fibroblast line) were incubated with similar MNPs showing completely divers iron uptake.

As each cell has a different gene expression, the uptake mechanism may be responsible for this phenomenon [60]. Furthermore, it was suggested that cancer cells can generally take up more particles, as they have less specific membranes [59]. Kim et al. [61] showed that even the cell cycle has an effect of the iron load per cell. Firstly, cells express different membrane proteins in each phase of the cell cycle and thus may take up NPs better or worse. Secondly, the iron agglomeration of a cell that just divided after NP exposure is less, due to the separation of the NPs to the daughter cells and thus the iron amount per cell is diluted.

All these fine variations in the setups together with the differences in incubation time and concentration render the comparison of loading studies or the prediction of the cellular iron load treated with MNPs nearly impossible - even *in vitro*. Thus, the first part of this study dealt with the systematic testing of the cell loading efficiency under varying conditions.
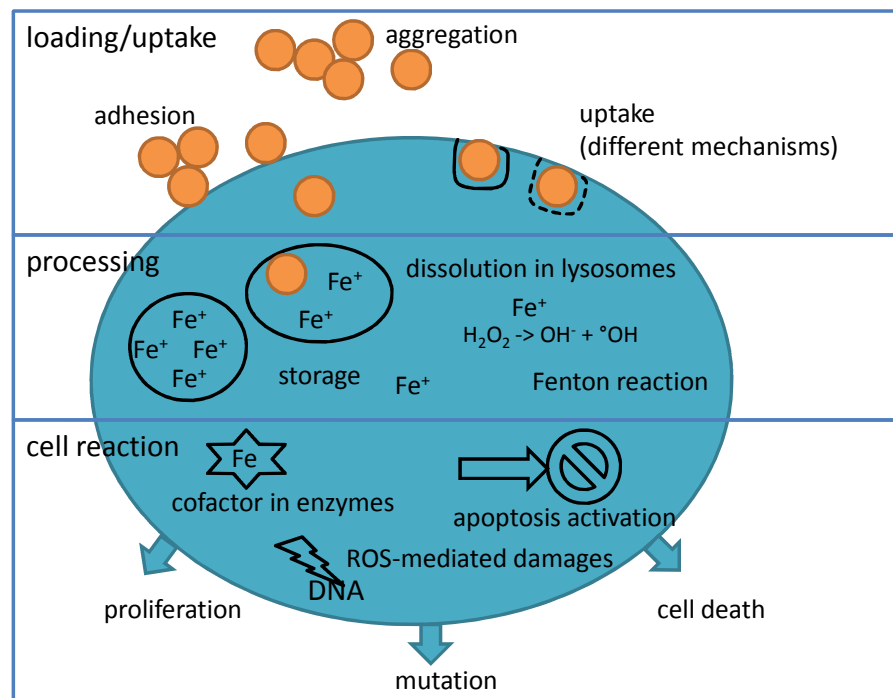

Figure 3: The interaction between MNPs and cells *in vitro*. The MNP cellular loading can be roughly divided in three steps: the loading or uptake of the MNPs, their processing inside the cell and the cell reaction towards the MNPs. Each step includes several proceeding possibilities. The loading is influenced by the aggregation of the MNPs outside the cells and their adhesion on the cell surface. The uptake itself can be achieved by different mechanisms, according to size and coating. The processing most likely takes place in the lysosomes, where the MNPs are dissolved in iron ions (Fe^+), which are exported into the cytosol and can be stored. Free iron ions can cause reactive oxygen species (ROS) generation by the Fenton reaction. The cell reaction towards the iron probably depends on the iron dose. In normal levels, iron is incorporated in enzymes, that can induce proliferation. In higher levels, ROS can cause DNA damages leading to mutations or even to cell death, for example by apoptosis.

MNP toxicity

Similar to the NP/MNP uptake, numerous studies have examined the toxicity of MNPs. However, it is still difficult to predict the cytotoxicity of MNPs, as small variation of the MNP properties or cell characteristics can cause pronounced differences in cytotoxicity reaction. As mentioned above for the uptake, the physical MNP properties (size, charge or coating) influence the cell reaction. It is expected that the MNP dose (concentration in the medium) and the incubation time, both supposedly connected with the MNP amount per cell, can affect the toxicity. Additionally, the protein corona may also mask potential toxicity of the bare NPs [62] and avoid binding of intracellular proteins [57]. Additionally, each cell type seems to react more or less sensitive on MNP loading [63].

Several studies show that the intracellular ROS concentration is increased after iron-based MNP treatment. This increase can be related to the enhanced iron amount in the cells, as MNPs are metabolized and eliminated via the normal iron pathway [14]. As most MNPs are taken up by endocytosis, they reach the acidic milieu of the lysosomes, where they are supposed to be dissolved into iron ions. Indeed, it was demonstrated in TEM images that MNPs coated with PLL were lysed in the cellular lysosomes latest by day 5 after incubation start, whereas not the whole amount of iron was processed at once [64]. Probably, iron is already released earlier, as the up-regulation of the iron storage protein ferritin, which is only triggered by free iron in the cytosol, occurred in astrocytes already one day after MNP incubation [65]. The dissolution of MNPs and processing of liberated iron may also explain why MNPs are barely excreted by the cells [66].

Iron is an important co-factor of many cellular enzymes, such like ribonucleotide reductase which is responsible for DNA synthesis, or of electron transfer proteins [14]. As iron is an essential element of the body, an additional amount of iron derived from MNP degradation is supposedly tolerated by the body. Iron-regulatory proteins (IRP1 and 2) can regulate the iron levels in cells by blocking the translation of iron storage protein ferritin and by stabilizing the messenger ribonucleic acid (mRNA) of iron transporters [67]. However, iron catalyses the conversion from hydrogen peroxide (H_2O_2) to the hydroxyl radical (OH^-) which is considered as highly reactive and as a damaging molecule [68]. By this Fenton reaction, cancer initiation (due to DNA mutation) or cancer cell death could be promoted [14]. Furthermore, the IRP system is also regulated by ROS and thus demonstrates a cellular defense mechanism against iron mediated toxicity [67].

The toxicity of iron in the brain tissue is largely unknown, though higher iron concentrations were found in brain tissue of patients with neurodegenerative diseases. However, this iron accumulation in the brain is more a consequence than a cause of the pathological events of

these diseases [69]. Hemochromatosis, a genetic disease with massive storage of iron, is often correlated with fatal damages of the liver and pancreas [1] and even liver tumors, demonstrating a possible connection between iron and cancer [70]. Indeed, in several mouse models, the correlation between iron exposure and carcinogenesis was demonstrated. The exact mechanism is not defined, however, the ROS-mediated damages were supposedly the main reason for DNA mutations [70]. Curcumin, which is known to decrease the iron levels *in vivo* [71], was found to decrease the proliferation of glioblastoma cells [72]. Elstner et al. [73] demonstrated that the lack of iron promote glioblastoma cell invasion, probably by enhancing the degradation of the extracellular matrix, while an increase of iron reduced the invasive behavior. Interestingly, the proliferation was not affected by the iron depletion. In a study about lymphoma, an increase of iron induced of cell death, probably by a massive generation of ROS [74]. Surely, the dose of iron is important in toxic effect consideration (see Figure 3). While a low dose is mandatory for normal cell function, higher amounts of iron could increase the cell proliferation, until the generated ROS is too high and the cell dies [70]. In order to evaluate probable effects of the MNP loading on glioblastoma cells in the present study, the proliferation, the metabolic activity and the membrane integrity were checked after each MNP treatment.

Magnetic field impact in biological matter

Another influencing factor in this study is the magnetic field. A magnetic field can be created by permanent magnets, materials that were magnetized or moving electric charges (electromagnetic fields) [75]. There are different types of magnetic fields, shown in Figure 4. Generally, static magnetic fields (SMF) do not change in time, while the strength or orientation of dynamic fields varies with time. The MNP reaction differs along the magnetic field types. In SMFs, MNPs align according to the field lines, or move along a gradient, if the field is inhomogeneous. The effects of rotating or oscillating fields, that changes the orientation or strength over time, are more complex. Oscillating fields can dissipate heat due to the fast changing magnetization of the material, which is used in the hyperthermia approach [76]. Oscillating fields can be classified into ionizing (very high frequency) and non-ionizing fields. The latter is also classified according to its frequencies (in Hz): extremely low frequency fields, intermediate frequency and radiofrequency fields [75].
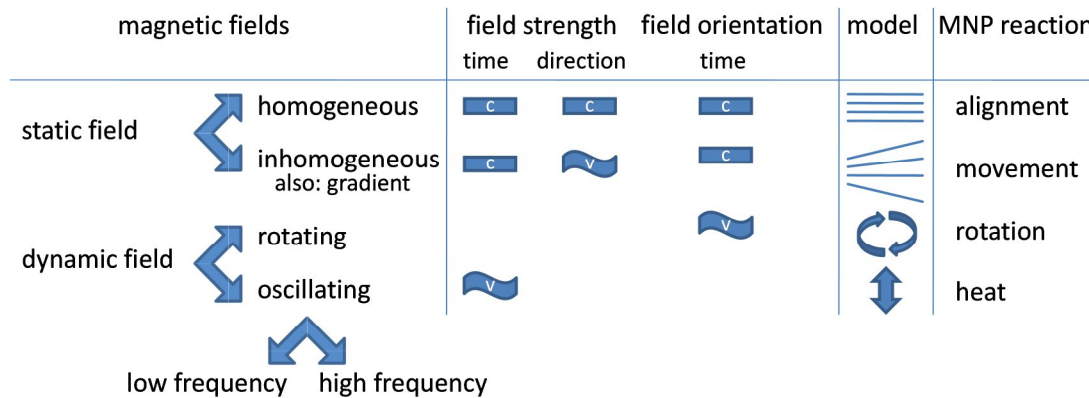
Figure 4: Overview of magnetic field types. Magnetic fields can be divided into static and dynamic fields. Homogeneous static fields have constant field strength and orientation (box with "c" for constant), while inhomogeneous field strength changes in direction (wave with "v" for variable). Dynamic fields can be rotating, where the field orientation changes over time, or oscillating, where the strength changes over time. Dynamic fields can be homogeneous or inhomogenous. The frequency of oscillating fields is very important for their biological consequences. The reaction of MNPs to the different magnetic field types varies: MNPs can be aligned, moved, rotated or used to create heat [76]. The model shows the arrangement of magnetic field lines in the homogeneous or inhomogeneous fields, and the symbolic change of the field for dynamic fields.

All organisms are exposed to the 0.05 mT earth SMF and some of them are even able to take advantage of this field. Magnetotactic bacteria have magnetite nano-crystals surrounded by a phospholipid membrane, so called magnetosomes, which form chains to align with the earth magnetic field. With these magnetosomes, the bacteria can move along the field to find special sediments [77]. But also higher organisms, like migrating birds, lobsters or bats are known to orient with the magnetic field of the earth. However, there are only hypotheses available about how the perception of magnetic fields takes place, most commonly about magnetite-based or chemical reactions due to magnetic input [78].

In a more abstract concept, magnetic fields are an interesting tool for biomedical research, by enabling the possibility to move MNPs without a direct contact. The most advanced application is the cell separation or isolation according to their magnetic properties. The magnetic-activated cell sorting (MACS) technique from Miltenyi Biotech is probably the best-known example: magnetic beads coupled with antibodies selectively bind cellular surface antigens and are then separated with a strong magnet to purify specific cells from mixtures. For the separation of magnetic or magnetized materials, not static but gradient fields are needed, which can be also created by a permanent magnet as used in immunomagnetic cell separation [79]. Other *in vitro* strategies include the magnetic separation of tumor cells from the blood stream [80], the magnetic enhanced seeding of corneal cells on contact lenses [81], or the 3D glioblastoma cell culture with magnetic

levitation [82]. A classic example for a clinical application is the hyperthermia treatment with MNPs, where heat is generated with the help of radiofrequency fields of 100 kHz up to several hundred MHz [83]. For the MRI technique three different types of magnetic fields, homogeneous and gradient static magnetic fields and radiofrequency magnetic fields are combined [75].

Magnetic field positive and negative effects

As stated in the review by Markov [84], the effect of the magnetic field depends on various parameters, like field type, localization or exposure time, and the type of tissue. Thus, it is consistent that the effects of magnetic fields on human beings are controversial, ranging from negative to non-influential to beneficial effects.

The positive effects were observed in bone and wound healing and in pain relief. For example, in a double blind study, a significant reduction of pelvic pain perception was reached by the application of magnets on pain pressure points for several weeks [85]. In another study, the influence of a SMF on the vascular tone was shown *in vivo*, whereas the response was both dilatation and constriction [86]. The effect of different magnetic field strengths and types on wound healing was demonstrated in an *in vivo* study, where the proliferation of cells and the generation of fibrous tissue was enhanced [87]. The cellular mechanisms how magnetic fields are influencing are not yet clarified, but a lot of hypotheses were drawn [84]. A theoretical model presented the influence of static and dynamic magnetic fields on the movement of water molecules at binding sites thus modifying the binding ability of molecules to enzymes [88]. Buchachenko [89] reviewed that irreproducible effects of magnetic fields on biological matter may occur due to magnet-mediated catalysis of biochemical reactions. Lin et al. [90] suggested that specific DNA sequences are susceptible to magnetic fields and thus, the expression of genes could be regulated by weak fields. An example for such gene regulation is the activation of the heat shock factor, which induces a temporary resistance against cell stress [91].

However, despite the positive results of magnetic fields on biological matter, reports dealing with risks of magnetic fields are more common. The negative effects on the whole body detected in some studies are for example vertigo [92], nausea and a metallic taste. However, these sensory effects were transient and mostly observed when the person moved inside the field [93]. The guidelines of the International Commission on Non-Ionizing Radiation Protection (ICNRP), also accepted by the WHO, advise an occupational exposure limit of 2 T, whereas up to 8 T are acceptable in controlled conditions. For public exposure, a limit of 400 mT was set due to indirect adverse effects for medical implants and flying metal objects [93].

Nevertheless, the toxicity of magnetic fields depends vastly on their characteristics and in some *in vitro* and *in vivo* studies, effects of magnetic fields were observed. Especially the toxicity of static magnetic fields has been discussed controversially. Some researchers state effects of magnetic fields on biological tissues, especially on ion fluxes [94], while other reviewers declared that none of the biological hazardous effects have been yet verified [95]. Tenuzzo et al. [96] reported that 6 mT SMFs caused reproducible cell effects, particularly on mitosis and apoptosis in several different cell types. Mice exposed to a SMF showed a significant weight loss after 12 d, indicating a pathological response, due to reactive oxygen species according to the authors' opinion [97]. Ghodbane et al. [98] reviewed that often the SMF alone is not toxic but in combination with other toxins (drugs or radiation) showed an increased effect. They mentioned that an enhanced permeability of the cell membranes may be responsible for these observations.

Static magnetic fields (SMF) in combination with MNPs could be regarded as more hazardous due to a potential synergistic effect of the magnetic potential and the addition of metals on biological tissues. Indeed, Bae et al. [99] showed a decreased viability of cultured mouse liver cells, that were treated with MNPs following exposure to a SMF with a mean flux of 0.4 T. They found that among others the formation of ROS lead to apoptosis. Additionally, keratinocytes incubated with MNPs and a SMF of 0.5 or 30 mT exhibited an increased cell proliferation, mainly addressed to the SMF [100]. In a study by Shawn et al. [101], healthy and cancer cells were incubated with MNPs and placed in a 70 mT SMF for 12 h. The DNA integrity of the cancer cells was remarkably disturbed by a SMF alone and especially after MNP incorporation, while healthy cells were not affected.

The toxicity of dynamic magnetic fields is supposedly bigger, as already demonstrated in the heat generation of oscillating fields for hyperthermia. Interestingly, cytotoxic effects were also shown with lower frequency magnetic fields, not producing heat, for example presented in astrocyte cultures by Schaub et al. [102]. As dynamic fields are not needed to move MNPs, only static fields were applied in the present study, which reduces also the expected toxicity by the magnets.

Cell migration

The final goal of the study was to influence the cell migration by the forces exerted from MNPs in a magnetic field. Cell migration is the active movement of cells on a surface. The main actors of this cell movement are three protein polymers, actin filaments, microtubules and intermediate filaments, which form the cytoskeleton. The cytoskeleton not only organizes the inner cell space but also manages the forces to cause cellular shape changes and movement. Thus, during cell migration, a protrusion at the leading edge of the cell body is

formed by actin polymerization. Then, connections to the extracellular matrix are formed, while adhesion molecules at the rear side are cut and the cell body contracts to move forward [103].

The cytoskeleton is able to change in reaction to inner and outer cell signals. So, external contacts to other cells and to extracellular matrix (ECM) molecules can influence the cell migration [104]. Indeed, the surface of the material is important for the cell movement, e.g. glioblastoma cells prefer to migrate along white matter tracks or blood vessels in the brain [105]. Thus, the imitation of natural ECM structures became an important part of migration studies, e.g. the production of nanofibres that could enhance the cell migration in comparison to flat substrates [106]. However, Giese et al. [107] showed cell-specific preferences for coating proteins, even within cell lines of the same origin. Laminin was demonstrated as the best coating for the majority of astrocytoma cell lines, while collagen and fibronectin showed best adhesion for single cell lines. Additionally, different patterns of migration out of a dense cell spot were observed: some cell lines had a compact front and others a more spread one. This is in accordance with the finding, that glioblastoma cells migrate either alone or in groups [108]. Interestingly, substrates showing stronger cell adhesion were also supportive for cell migration [107].

In a study by Lamszus et al. [109], the hepatocyte growth factor (HGF), also called scatter factor, caused enhanced cell motility. Different glioma cell lines were examined in a Boyden chamber assay, where the cells pass a membrane, and a fence migration assay, where cells were seeded in a spot and the outgrowth was evaluated. Verkhovsky et al. [110] examined the dynamics of cell fragments and presented, that a pipetting stream could induce a directional movement of these fragments. Thus, it could be suggested, that mechanic stimuli can influence the migration of cells as well.

Adherent magnetic cell migration

Only few studies are reporting the manipulation of the natural cell migration by using forces generated by MNPs in a magnetic field. With this strategy, it should be possible to reassemble the glioblastoma cells that are scattered in the brain tissue after main tumor resection. As it is feasible to design MNPs preferably targeting tumor cells and as glioblastoma cells are known to migrate naturally to a high degree, the cells could potentially react to magnets fixed on the skull or even implanted in the tumor resection cavity. The following three studies are explained more in detail to present the conditions and setups, which were used so far for the observation of directed cell migration by magnetic fields.

Bradshaw et al. [111] examined typical skin cell lines (keratinocytes and fibroblasts) to support the outgrowth of cells from the edges of a skin wound with the help of MNPs and a 0.6 T magnetic field. They seeded keratinocytes (HaCaT) on a cover slip and loaded them with MNPs, before the cover slip was transferred to a cell culture well near a permanent magnet. After 4 d, they observed that the cells migrated from the cover slip, however, mostly at the side heading towards the magnet, while the migration without MNP or without magnet showed no preferred direction. In a second experiment, MNP-loaded fibroblasts were seeded in a transwell insert with a magnet fixed below the plate. The cells treated with MNPs and incubated in the magnetic field showed an enhanced migration after 24 h in comparison to the cells without magnetic field treatment. The decrease of the supposed magnet-driven migration at later time points was assigned to a dilution of MNPs due to cell division.

In another study, White et al. [112] tested the migration of MNP-loaded microglia with a magnetic field to guide the cells to deep brain tumors and to activate the immune response. By putting magnets of different shapes below the cell culture plates, they demonstrated an accumulation of MNP-treated cells at the edges of the magnets, while control cells without MNPs or without magnetic field did not follow any patterns. Also, live-cell imaging was performed in a 3D-printed chamber to show that the cells are moving to the magnet side.

Riggio et al. [113] aimed to support the neuronal regeneration after injury by creating a mechanical force on axons to increase its elongation by MNP and magnetic field application. The researchers seeded MNP-loaded neuroblastoma cells and control cells without MNPs, placed a magnet near the culture wells and counted the cells at different distances to the magnet after 3 d incubation. The cells treated with MNPs accumulated in areas near the magnet, while control cells stayed evenly distributed. They found a weaker migration of primary Schwann cells which they accounted to a stronger adhesion of these cells to the laminin-coated surface.

The same group [114] also performed experiments with carbon nanotubes to direct the migration of cultured cells by a magnetic field. Few neuroblastoma cells were fluorescently labeled and their displacement was detected after 1, 2 and 3 d by a grid placed below the culture well and microscopy. They developed a mathematical model, which was in good agreement with the measurement data, proposing the cells to move 1-2 mm per day. The mechanism suggested is the application of a magnetic field-derived force on the reversible bonds of the cell to its surface, causing a creeping of the cell to the magnet. In other words, for a migration guidance of the cells, the adhesion points at the rear side would have to be removed, so that the cell is pulled towards the magnet [115].

These studies demonstrate, that in principle, the movement of magnetically labeled cells, e.g. by MNP-loading, is possible with different cell types. However, the directed movement of MNP-loaded glioblastoma cells by a magnetic field was not tested so far. Thus, the setups used in the migration studies above were evaluated and developed for the detection of the glioblastoma cell movement.

Aim of the study

Glioblastoma cells are known to migrate into the healthy brain tissue in a very early state of the cancer development, causing recurrence of the tumor after surgical removal. Thus, as strategy could be the direction of scattered glioblastoma cells towards a concrete superficial brain location, where they could be treated with traditional therapies. This strategy would rely on the possibility to direct the natural glioblastoma cell migration by a magnetic field after the loading of the cells with magnetic nanoparticles (MNPs).

Thus, the objective of the study was to induce and observe the movement of MNP-loaded cells in a magnetic field.

For this, intermediate steps were carried out:

- material characterization

Several parameters, different MNP types, various cell lines, magnets and their combination were selected. As all these materials have different properties, preliminary experiments were performed to characteristics them and identify factors which may influence further steps.

- MNP cell loading efficiency

The success of the MNP-loading supposedly differs between the glioblastoma cell and MNP types. In loading efficiency experiments, the influence of different parameters (time and concentration) was examined to obtain a high intracellular iron concentration for optimizing the magnetically directed movement.

- MNP cell loading toxicity

Together with the optimal loading, the toxicity of the MNP incorporation needed to be considered to define an optimal loading protocol. For this, the proliferation ability, the cell integrity and metabolic activity were examined.

- effects of the magnetic field on cells with or without MNPs

Magnetic field side effects were evaluated to demonstrate the safety of the use of magnets for the directed cell movement.

- Movement of MNP-loaded cells in a magnetic field

Finally, different setups for the observation and quantification of cell movements in a magnetic field were tested and evaluated, including MNP-loaded cells in a non-attached and attached state.

Materials

Chemicals

chemical name	abbreviation	purchaser
(+)-sodium L-ascorbate, crystalline	sodium ascorbate	Sigma-Aldrich, St. Louis, USA
Alexa Fluor® 488 Phalloidin	Phalloidin-488	Fisher Scientific GmbH, Schwerte, Germany
ammonium acetate for analysis EMSURE® ACS	ammonium acetate	Merck KGaA, Darmstadt, Germany
Calcein, AM	Calcein	Fisher Scientific GmbH, Schwerte, Germany
CASY®ton	CASYton	Roche Diagnostics GmbH, Mannheim, Germany
4',6-Diamidino-2-phenylindole dihydrochloride, BioReagent, suitable for fluorescence	DAPI	Sigma-Aldrich, St. Louis, USA
dimethyl sulfoxide ReagentPlus®	DMSO	Sigma-Aldrich, St. Louis, USA
DMEM, high glucose, GlutaMAX™ supplement, pyruvate	DMEM GlutaMAX	Fisher Scientific GmbH, Schwerte, Germany
Dulbecco's Modified Eagle's Medium	DMEM	Fisher Scientific GmbH, Schwerte, Germany
Faramount mounting medium	DAKO mounting medium	Dako Deutschland GmbH, Hamburg, Germany
fetal bovine serum	FBS	GE Healthcare, Frankfurt, Germany
formaldehyde solution	formaldehyde	Sigma-Aldrich, St. Louis, USA
hydrochloric acid fuming 37 %	HCl	Merck KGaA, Darmstadt, Germany
iron (III) oxide nanopowder<50 nm particle size (BET)	iron oxide nanopowder	Sigma-Aldrich, St. Louis, USA
iron(III)chloride, reagent grade	$FeCl_3$	Sigma-Aldrich, St. Louis, USA
Leibovitz's L-15 medium (1x)	Leibovitz medium	Fisher Scientific GmbH, Schwerte, Germany
phosphate buffered saline	PBS	see preparation below
Penicillin/Streptomycin (10,000 U/mL)	Penicillin/Streptomycin	Fisher Scientific GmbH, Schwerte, Germany
potassium hexacyanoferrate (II) trihydrate, ACS reagent	Prussian blue	Sigma-Aldrich, St. Louis, USA
potassium permanganate ACS reagent	$KMnO_4$	Sigma-Aldrich, St. Louis, USA
sodium hydroxide solution, 1 mol/l	NaOH	Merck KGaA, Darmstadt, Germany
thiazolyl blue tetrazolium bromide	MTT	Sigma-Aldrich, St. Louis, USA
Triton™ X-100 for molecular biology	Triton X-100	Sigma-Aldrich, St. Louis, USA
laminin from human placenta, liquid	laminin	Sigma-Aldrich, St. Louis, USA

recombinant human HGF (hepatocyte growth factor)	HGF	PeproTech Germany, Hamburg, Germany
Rhodamine123, mitochondrial specific fluorescent dye	rhodamine	Sigma-Aldrich, St. Louis, USA
sodium chloride for analysis EMSURE® ACS	NaCl	Merck KGaA, Darmstadt, Germany
potassium chloride for analysis EMSURE®	KCl	Merck KGaA, Darmstadt, Germany
di-Sodium hydrogen phosphate dihydrate	Na_2HPO_4	Merck KGaA, Darmstadt, Germany
potassium dihydrogen phosphate anhydrous	KH_2PO_4	Merck KGaA, Darmstadt, Germany
fibronectin from human plasma, liquid, 0.1 % (solution)	fibronectin	Sigma-Aldrich, St. Louis, USA
poly-L-lysine (0.01 % solution)	PLL	Sigma-Aldrich, St. Louis, USA
Trypsin-EDTA (0.05%), phenol red	Trypsin	Fisher Scientific GmbH, Schwerte, Germany
5,6-Diphenyl-3-(2-pyridyl)-1,2,4-triazine-4′,4″-disulfonicacidsodium salt for spectrophotometric det. of Fe	ferrozine	Sigma-Aldrich, St. Louis, USA

Equipment and Software

name	device	purchaser
Lab-Tek®II chambered #1.5 German coverglass system, 8 chamber	8-well chambered coverglass	Fisher Scientific GmbH, Schwerte, Germany
Adobe® Photoshop® CS6, Version 13.0	Photoshop software	Adobe Systems Inc.
CASY® - Cell counter and Analyser System, Model TT	CASY	Roche Innovatis AG, Reutlingen, Germany
CASY®ConverterXL	software	Olaf Rose, Hamburg, Germany
CASY®excell Version 2.3	software	Roche Innovatis AG, Reutlingen, Germany
ClinScan®	MRI device	BrukerBiospin, Ettlingen, Germany
femm Version 4.2	femm software	David meeker http://www.femm.info/wiki/Download
Gaussmeter Model 421	Gaussmeter	Lake Shore Cryotronics, Inc., Westerville, Ohio, USA
Thermomixer comfort	heating block	Eppendorf Vertrieb Deutschland GmbH, Hamburg, Germany
Heraues™ Pico™ Microcentrifuge	microcentrifuge	Fisher Scientific GmbH, Schwerte, Germany
ImageJ 1.46r	ImageJ software	Wayne Rasband, http://imagej.nih.gov/ij
Leica TCS SP8	confocal microscope	Leica Mikrosysteme Vertrieb GmbH,

		Wetzlar, Germany
neodymium magnets	permanent magnets	Webcraft GmbH, Gottmadingen, Germany
Nikon Eclipse Ti microscope	fluorescence microscope	Nikon GmbH, Düsseldorf, Germany
NIS-Elements Advanced Research (Version 3.00)	NisElements software	Nikon GmbH, Düsseldorf, Germany
Rotina 420	benchtop centrifuge	Hettich lab technology, Tuttlingen, Germany
SpectroSize™300	DLS	Xtal Concepts GmbH, Hamburg, Germany
Tecan Sunrise™	Tecan plate reader	Tecan Group Ltd., Männedorf, Switzerland

Disposables

name	abbreviation	purchaser
8-well chambered coverglasses Nunc™ Lab-Tek™ II, no°155409	8-well chamber slide	Fisher Scientific GmbH, Schwerte, Germany
cell culture flask, PS, red filter screw cap, clear, cellstar® TC	cell culture flasks	Greiner Bio-One GmbH, Frickenhausen, Germany
cell culture multiwell plate, PS, clear, cellstar®, TC	multi-well plates, or more detailed: 6-well plates, 12-well plates or 96-well plates	Greiner Bio-One GmbH, Frickenhausen, Germany
Bellco glass cloning cylinders	cylinder	Fisher Scientific GmbH, Schwerte, Germany
Marienfeld glass coverslips	coverslip	VWR International GmbH, Darmstadt, Germany
culture-inserts 2 well for self-insertion	ibidi® insert	ibidi GmbH, Martinsried, Germany
Marienfeld objective slides	obejctive slide	VWR International GmbH, Darmstadt, Germany
Parafilm® M	Parafilm	Sigma-Aldrich, St. Louis, USA
SafeSeal tube	micro tube	Sarstedt AG & Co, Nümbrecht, Germany
tube, PP, conical bottom, cellstar®, blue screw cap	tube	Greiner Bio-One GmbH, Frickenhausen, Germany
Nunc® surface cell culture dish, 35 mm	dish	Sigma-Aldrich, St. Louis, USA

PBS preparation

For the preparation of phosphate buffered saline (PBS), following salts were dissolved in 800 mL ultrapure water: 8.00 g NaCl, 0.20 g KCl, 1.78 g Na_2HPO_4, 0.24 g KH_2PO_4. Then, the pH was adjusted to 7.4, the solution was filled up to 1 L with ultrapure water (final concentration of 137 mmol/L NaCl, 2.7 mmol/L KCl, 10.0 mmol/L Na_2HPO_4 and 1.76 mmol/L KH_2PO_4) and the solution was sterilized by autoclaving.

Magnetic nanoparticles (MNP)

Myristic acid MNPs (MA)

MA were synthesized in the Laboratory of Magnetic Fluids (Romanian Academy-Timisoara Branch, Romania) as described in Bica et al. [116]. They consist of a magnetite (Fe_3O_4) core with a double layer of myristic acid (MA) and are suspended in water. By transmission electron microscopy (TEM) detection, the iron core diameter was 2-7 nm with a mean size of 4.3 nm. A structural testing of these nanoparticles was performed in the study by Avdeev et al. [117], where MA were shown to have near superparamagnetic behavior and a high stability even in cell culture medium. Myristic acid is naturally fixed to proteins, where it enables the irreversible interaction with other proteins and membranes and regulates protein targeting and function [118]. Pham et al. [119] tested how well fatty acids of different lengths bound to a peptide were taken up by HeLa cells and found that myristic acid showed the highest incorporation compared to lauric or palmic acids. In a further study [120], they discovered that myristoylated polyarginin is suitable to cross the BBB effectively and fast. In another study [121], myristic acid was shown to bind to PEI-DNA complexes, enhancing the transfection of glioblastoma cells *in vitro* compared to PEI-DNA complexes alone. Myristic acid was also used to form inhalable MNPs to treat lung cancer by hyperthermia [122]. These findings demonstrate that the application of myristic acid as coating for MNPs could be suitable to support the treatment of brain cancer.

FeraSpin™XS (FS)

FeraSpin™XS (FS) is manufactured by nanoPET Pharma GmbH (Berlin, Germany) and is a registered trademark of Miltenyi Biotec GmbH (Bergisch Gladbach, Germany). They belong to a series of MRI contrast agents of different sizes for pre-clinical imaging. FS are superparamagnetic iron oxide nanoparticles with a iron core size of 5-8 nm (TEM) and a coating of carboxydextran. Dextran is a widely used branched polysaccharide, which can be well adsorbed to the iron oxide nanoparticle surface and show good biocompatibility. Thus, many of the commercially available MNPs possess a dextran coating [34].

Sigma MNPs (Sig)

The abbreviation "Sig" stands for MNPs purchased from Sigma-Aldrich in the form of iron(III) oxide nanopowder with less than 50 nm particle size and coated with 0.1 % poly-L lysine (PLL). Briefly, the nanopowder was weighted and suspended with PLL to 50 mg/mL concentration, following mixing by vortex and short sonication on ice. Then, the suspension was further diluted 1:10 in PLL to a final concentration of 5 mg/mL and stored at 4 °C. Sig were used as control group for migration tests, as they were already used in a study about the imaging of MNP-loaded glioblastoma cells. In this study [123], they were found to form

large (up to 10 µm) clusters in the cells and were thus recommended by Professor Ben Fabry (biophysics group of the Friedrich-Alexander University of Erlangen-Nürnberg).

Magnets

Three types of Nickel-coated Neodymium magnets, from similar type and company but of different sizes (see Table 1), were used for the application of a magnetic field.

Table 1: Permanent magnets data

Name	Dimensions	Pole area	Magnetization	Remanence
W-05-N	5x5x5 mm	5x5 mm	N42	1.29-1.32 T
Q-10-10-05-N	10x10x5 mm	10x10 mm	N42	1.29-1.32 T
Q-20-20-05-N	20x20x5 mm	20x20 mm	N42	1.29-1.32 T

The Nickel coating was chosen to avoid the magnet's corrosion under cell culture conditions (37 °C and 95 % relative humidity). The resistance against the warmth in the incubator was guaranteed, as the magnets resist temperatures until 80 °C. The use of permanent magnets was preferred over electric ones due to the easier handling, in terms of smaller size and no need of cooling. The biocompatibility of the magnet material was not important, as the magnets were fixed outside the cell culture vessels, so that no direct contact to the cells or the medium occurred.

Cell types

The human glioblastoma cell lines G62, G44 and G112 were derived from patients of different age (4-64 years) and sex [124] and were kindly provided by Professor Katrin Lamszus from University Medical Center Hamburg-Eppendorf (Hamburg, Germany). Normal human astrocytes were purchased from Invitrogen (Fisher Scientific GmbH, Schwerte, Germany) and also delivered by Prof. Dr. Katrin Lamszus.

For live-cell imaging, immortalized mouse embryonal fibroblasts NEDD9-2 (wild type) were used, which were isolated as described before by Zhong et al. [125]. These cells showed a higher motility *in vitro* compared with the glioblastoma cell lines G62 and G44, as investigated in live-cell imaging trials. Thus, they were preferred in live-cell imaging trials about the directed cell migration, which were performed in the laboratories of the biophysics group of Prof. Ben Fabry at the Friedrich-Alexander University of Erlangen-Nürnberg.

Methods

Magnetic nanoparticle (MNP) characterization

Dynamic light scattering

Principle

The dynamic light scattering method uses the scattering of laser beams to measure the size of particles in a suspension. Particles in solution perform Brownian motion, which is related to the particle size, viscosity of the solution and temperature, as described in the Stokes-Einstein equation. The velocity of the moving particles in the solution is detected by the changes of light scattering in a certain angle. As all particles in a solution are moving together with a shell of water molecules, the hydrodynamic size is detected. This is normally bigger than the core size [126].

Procedure

After dilution of MA and FS with water or complete cell culture medium to 25 µg/mL iron concentration, samples were measured 3 times with the SpectroSize™300. For measurements, the viscosity of water (1.007 g/mL) was chosen as it is similar to cell culture medium [127]. A scattering angle of 90 °, a temperature of 20 °C and a wavelength of 660 nm were selected. Each run comprised 10 measurements of 15 s each and every sample was run in duplicate. A histogram plot was used to show the frequency of occurrence of each radius in nm. Cell culture medium dilutions were stored at 4 °C without agitation and measured again after 3 d after only soft shaking.

Cell characterization

General cell culture

Principle

In order to examine biological processes, isolated cells are cultured in an artificial environment with controlled conditions. As these cells continue to divide, the substrate and space availability in the closed system becomes scarce, so that a subculturing is necessary. In this procedure, the cells are transferred in a new vessel, offering more place and nutrients for growth.

Procedure

All glioblastoma cell types were cultured in Dulbecco's Modified Eagle's Medium (DMEM) completed with 10 % fetal bovine serum (FBS), hereinafter called "cell culture medium", and passaged every 3 to 4 d. Astrocytes were kept in DMEM GlutaMAX™-I supplemented with

20 % FBS and 10 % Penicillin/Streptomycin. For MNP experiments, the medium for astrocytes was exchanged to 10 % FBS without antibiotics in order to gain better comparability between astrocyte and glioblastoma loading (see also appendix, Figure 38). NEDD9-2 cells were cultured in cell culture medium supplemented with 10 % Penicillin/Streptomycin.

For normal subcultivation routine and seeding in multi-well plates, the cells were washed shortly with PBS and detached by using 0.05% Trypsin-EDTA in the incubator (37°C, 5 % CO_2, humidified atmosphere) for 2 and 5 min for glioblastoma cells and astrocytes, respectively. After stopping the Trypsin reaction by addition of at least the double amount of medium, cell suspension was centrifuged at 1500 rpm for 5 min with the benchtop centrifuge. Cells were resuspended with fresh complete culture medium, counted automatically and seeded at desired density in cell culture flasks or multi-well plates.

MNP loading

MA iron concentration was calculated by the volume fraction of magnetite and the density (44 g/L). The iron content of FS was 10 mmol/L (585.5 µg/mL), according to the supplier. For dilution factors see Table 2.

Table 2: Dilution factors for MNPs

	5 µg/mL	25 µg/mL	50 µg/mL
MA	8800	1760	880
FS	112	22	11

For Sig-MNPs experiments, 10 µL/mL cell culture medium were used (= 50 µg/mL MNP and 35 µg/mL iron concentration).

For all magnetic experiments, cells were first incubated with MNPs followed by an exchange to cell culture medium without MNPs and by magnetic field application.

Cell analysis by automatic counting (CASY®)

Principle
The CASY®-technology is based on a resistance measurement principle. The cells suspended in an electrolyte solution (CASY®ton) are passing a capillary in a constant flow speed. A low voltage field is applied in a pore with two platinum electrodes during the measurement. The electrolyte resistance is increased if a healthy cell passes the pore since the membrane acts as an electrical barrier. The displacement of resistance is a dimension of the

cell volume. If the cell membrane is not intact, as in dead cells, only the dimension of the cell nucleus is detected. The viability is calculated as a rate of viable to dead cells.

Procedure

For the measurement, 50 µL of the cell suspension was mixed with 10 mL CASY®ton and 3 cycles with each 400 µL were measured. The viable cells/mL were used to calculate the total cell number. The peak diameter (µm) and the viability (%) were recorded. CASY®excell and CASY®ConverterXL software were used for data management.

Proliferation assay

Principle

To characterize the different cell types, the cells were seeded at different seeding densities and trypsinized at regular time periods to evaluate their growth and viability. In parallel, their morphology was observed with microscopic pictures.

Procedure

The cell proliferation behavior without MNP exposure was examined by seeding glioblastoma cells and astrocytes in 6-well plates at 2.5×10^4 or 5×10^4 cells/cm² density. For glioblastoma cell lines, also 1×10^5 cells/cm² seeding density was considered.

For the proliferation assay without MNPs, the cells were examined after 1 to 4 d, n=12 for glioblastoma cells, n=8 for astrocytes (2 trials with triplicates or duplicates, 2 technical replicates). Additionally, microscopy was performed.

The proliferation behavior after MNP incubation was checked during the cell preparation for the ferrozine assay (see corresponding section).

MNP loading of cells

Ferrozine assay

Principle

Ferrozine is a chelator of ferrous iron (Fe^{2+}) that is used since decades for the detection of Fe, also in biological samples [128]. After binding of Fe^{2+}, the ferrozine complex strongly absorbs light at 570 nm, so that it is possible to detect the iron amount of a single cell culture well. Fe^{3+} is reduced to Fe^{2+} by ascorbate. Disturbances from other divalent metal ions were not detected, except of copper ions (Cu^{2+}), however, copper levels in brain tissue are not sufficient to interfere with the assay [129]. For cell-based studies, firstly the cells has to be lysed and the iron is released from proteins by an acid potassium permanganate ($KMnO_4$) solution. For our setup, the dissolution of MNPs with hydrochloric acid (HCl) was included.

Procedure

All cells were seeded in 12-well plates at $5x10^4$ cells/cm² densities for G62 and G112 and at $2.5x10^4$ cells/cm² densities for G44 and astrocytes. The different seeding densities were chosen because of cell morphology and proliferation properties, as explained in the results part. After one day, the medium was exchanged to complete medium without (control) and with MNPs at 5, 25 and 50 µg/mL iron concentration. Then, the cells were incubated for 1 to 3 d. Afterwards, the cells were washed twice with PBS to remove MNPs from the cell surface. The cells were detached with 500 µL Trypsin for 2 min in the incubator and reaction was stopped with 500 µL culture medium. Cells were resuspended by pipetting and transferred to an Eppendorf tube. An aliquot of 50 µL was taken for CASY® measurement.

The remaining cells were centrifuged at 2000 rpm for 5 min with the microcentrifuge, supernatant was discarded and the cell pellet was resuspended in PBS. This washing step was repeated followed by removal of the supernatant and freezing of the pellet at -20 °C until further processing to break the cell membrane and store the samples.

The ferrozine assay was adapted from Riemer et al. [129]. Before the biochemical assay, the cell pellets were thawed and vortexed rigorously. The cells were lysed completely by incubation with 300 µL sodium hydroxide (NaOH) for 2 h on the shaker at room temperature. Afterwards, the MNPs were lysed by addition of 20 µL HCl conc. (37 %) and incubation at 70 °C for 15 min on the shaker. Then, 300 µL 10 mM HCl and 300 µL freshly prepared mixture of equal volumes of 1.4 M HCl and of 4.5 % (w/v in ultrapure water) $KMnO_4$ were added to the samples. The samples were incubated at 60 °C for 2 h on a shaker at 750 rpm.

Afterwards, the samples were cooled for 10 min to room temperature and 90 µL of the iron-detection reagent, containing 6.5 mM ferrozine, 2.5 M ammonium acetate and 100 mM sodium ascorbate in water, was added and vortexed thoroughly. After an incubation of 15 min at room temperature, samples were centrifuged at 13000 rpm with the microcentrifuge for 5 min to remove cell debris. Then, 280 µL of the supernatant were transferred to a 96-well plate in triplicate and the absorbance was measured at 570 nm with a Tecan plate reader.

For the standard curve, a serial dilution of iron(III)chloride ($FeCl_3$)in 10 mM HCl from 30.00 to 0.23 nmol Fe was performed. To check the results of the assay, 1.5 nmol pure MNPs were examined as positive control.

Prussian blue staining

Principle

Prussian blue is a very old histochemical stain, also known as Perls reaction. In acid environment, ferrocyanide combined with ferric iron (Fe^{3+}) is forming a blue insoluble complex [130].

$$K^+ + [Fe(CN)_6]^{4-} + Fe^{3+} -> K[Fe_2(CN)_6] \text{ [130]}$$
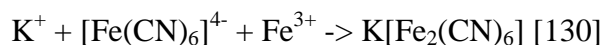
Procedure

The cells were seeded in 24-well plates at 6250 cells/cm² density for G44, G62 and astrocytes and at 12500 cells/cm² for G112. After 1 d, the medium was exchanged to normal cell culture medium without MNPs (control) or with 50 µg/mL MA or FS. Then, the cells were incubated for further 3 d.

The cells were washed shortly with PBS and fixed with 3.7 % formaldehyde in PBS for 15 min at room temperature. Afterwards, the cells were washed twice with ultrapure water. Prewarmed 1 M HCl and 20 mg/mL potassium ferrocyanidetrihydrate were mixed shortly before use at a ratio of 3:7 (v/v), added to the cells and incubated for 10 min at 37 °C. Afterwards, the cells were washed 3 times with water. Pictures were acquired with Nikon Eclipse Ti microscope in color camera mode with NisElements software.

Loading effects

MTT assay

Principle

The biochemical assay is based on the intracellular conversion of the soluble yellow tetrazolium salt (MTT) into the insoluble purple formazan product by cellular enzymes within several hours of incubation. Afterwards, the crystals have to be dissolved by addition of chemicals like dimethyl sulfoxide (DMSO) or sodium dodecyl sulfate (SDS) before reading the absorbance at a wavelength of 570 nm.

Although this assay has been used in numerous studies since decades, the exact mechanism remains unclear [131]. For the conversion, mostly NADH but also succinate or NADPH as reducing agents are needed. It has been suggested that mitochondrial enzymes are responsible for the MTT reduction; however, also enzyme systems from other compartments may play a role [132],[133]. Berridge et al. [134] found that the endoplasmic reticulum was the major localization of MTT conversion supporting his theory of less respiratory chain but more glycolysis influence.

The outcome of the assay has been referred to as "viability" [135], as damaged cells produce less formazan, or "proliferation" [134], because the inhibition of cell division reduces the amount of formazan. Since the reason of the absorbance changes are unknown, the term "metabolic activity" was chosen in this study.

Procedure

Glioblastoma cells and astrocytes were seeded in 96-well plates ($2x10^4$ cells/cm²) and incubated 24 h for proper attachment to the surface. Then, the medium was removed and pure medium (as control) or medium containing MNPs in 5, 25 or 50 µg/mL was added. After 1, 2 or 3 d, 10 µL of MTT was added and the cells were further incubated for 4 h. Then, the supernatant was removed completely and 100 µL dimethyl sulfoxide (DMSO) was used to dissolve the crystals by shaking. The absorbance (optical density, OD) was measured at 570 nm and 655 nm (reference) by Tecan plate reader, n=8. The metabolic activity was calculated using following formula:

cell viability [%]=(OD570 sample-OD655 sample)/(mean(OD570 control-OD655 control))*100

Magnetic field characterization

Magnetic field simulation

For the visualization of the magnetic fields, the software femm by David Meeker was used. A cut through a permanent magnet was created by a rectangle with the dimensions of the magnets. The material properties were set to NdFeB permanent magnet with 40 MGOe, that equals N42 quality. A boundary with a radius of 20 mm was set around the magnet rectangle and the area inside the circle mimicked the air compartment. Afterwards, the magnetic field lines were calculated and the flux density was plotted in a heat map, where blue color was correlated with 0 T and dark purple color with 1 T.

Magnet strength measurement

Principle

The calculation of magnetic field strength is complex. Thus, the magnetic density flux was detected by a Gaussmeter, where the probe was placed at various distances from the magnet in air. Furthermore, pictures of the behavior of MNPs in the magnetic field were taken. The gaussmeter measurement principle is based on the Hall effect. In the probe of the device, a small plate is installed, through which a current flows in one direction, and the voltage difference in the other axis is measured. If a magnetic field is applied, the current flow is disturbed and the voltage changes proportionally to the magnetic flux density [136].

Procedure

To investigate the influence of the magnet size on the magnetic field strength, the different permanent magnets were examined with a Gaussmeter Model 421 with a hand held transverse probe (MMT-6J04-VG, 300 G – 30 kG). The magnets were fixed on the surface and magnetic flux density was measured from 0-40 mm distance towards the pole area in 5 mm steps.

Static magnetic field effects

Permanent magnetic field effects

For the investigation of the magnetic field influence, 6000 cells/well in a 96-well plate (5×10^3 cells/well for G62) were seeded for 1 d MNP incubation or 3×10^3 cells/well for 3 d MNP incubation. After 1 d, the medium was exchanged to cell culture medium without MNPs (control) or with 25 or 50 µg/mL MA and FS. The incubation with MNPs was interrupted after 1 or 3 d by an exchange to medium without MNPs, followed by 1 d incubation in a magnetic field. The cells for each condition were seeded in groups of 4, so that 20 mm permanent magnets could be attached below the plate covering the 4 wells (see Figure 5). A second plate was treated similar, except of the magnetic field incubation. Each trial was repeated.
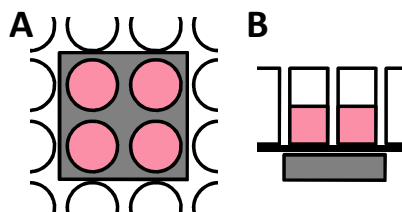
Figure 5: Seeding scheme of the magnetic field effects. The top view (A) and side view (B) of the setup is depicted. The cells were seeded in the wells of 96-well plates (circles in A and rectangles in B) as illustrated by the brighter filling. The 20 mm permanent magnet (grey rectangle) was placed below the plate, covering 4 wells.

High static magnetic field effects

Principle

The high static magnetic field was produced by a magnetic resonance imaging (MRI) device, which had a magnetic field strength of 7 T with field lines in horizontal direction. During the image scanning, a combination of magnetic field types are used (static, gradient and alternating fields). However for this trial, only the static component was applied to the cells,

in order to test the amplification of potential effects observed in the permanent magnet experiment.

Procedure

For MRI experiments, G62 cells were seeded in 8-well chamber slides ($1x10^4$ cells/well) in a final volume of 300 µL/well. Medium was exchanged after 1 d to 200 µL complete medium without MNPs or with 25 µg/mL FS. The chambered cover glasses were sealed and transported to the Molecular Imaging North Competence Center (MOIN CC) in Kiel. Directly before experiment (after 1 or 3 d of MNP incubation), medium was exchanged to 300 µL Leibovitz medium supplemented with 10 % FBS. The Leibovitz medium was designed for cell culture experiments without CO_2 related pH-stabilization [137]. The effect of the Leibovitz medium on glioblastoma cells was tested in a preliminary trial (see appendix, Figure 40). One chamber was put in a 7 T MRI device and one in a plastic box in the adjacent room to the MRI, both heated with hot water tubing to approximately 33 °C, and incubated overnight.

Afterwards, the medium was exchanged to 300 µL complete culture medium and in 6 wells (3 control, 3 FS) 30 µL MTT was added. After 4 h incubation in the normal cell culture incubator, the supernatant was removed and 300 µL DMSO per well were added. The solution was thoroughly mixed by pipetting and transferred to Eppendorf tubes for transport. Solutions were measured and evaluated as described in MTT section.

Non-adherent cell movement

Cell seeding with magnet

Principle

A fast, but only qualitative examination of the magnetic field influence on MNP-loaded cells was gained by seeding the cells in a well with a magnet fixed below. During sedimentation of the cells, they could be more or less attracted by the magnet and assemble above it. The cell distribution can then be visualized by microscopy.

Procedure

G62 cells were incubated with MNPs for 3 d and seeded in 6-well plates, followed by an immediate fixing of 10 mm magnets below the plate. After 6 h adherence time, large images were acquired with the Nikon microscope.

Swimming discs setup

Principle

To see how far the magnetic field has an influence on the MNP-loaded cells, the movement of non-attached cells was quantified. If the cells in suspension were attracted by the magnet on top, they had been pulled against a disc on the surface of the culture medium, where they adhered and later could be detected (Figure 6).
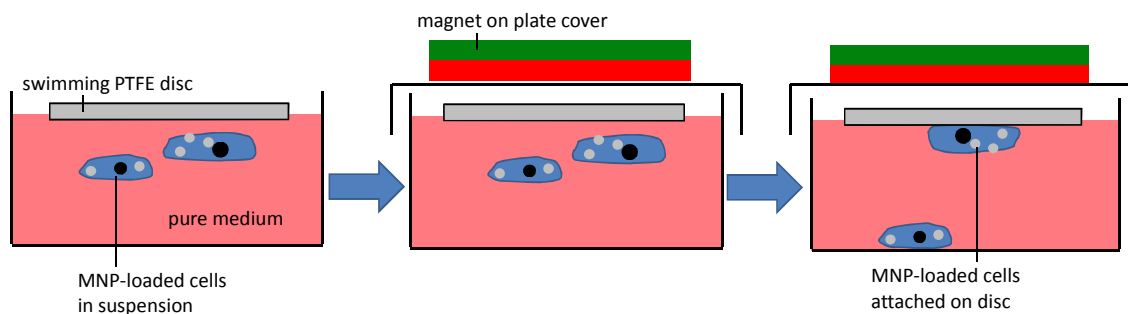

Figure 6: Swimming discs assay. The cells were loaded with MNPs and detached before transferred to wells with fresh culture medium and addition of a coated PTFE disc on the medium surface. Afterwards, the plate cover was mounted and a magnet was fixed on top of the cover. In the course of time, the MNP-loaded cells either sank to the bottom of the well or were attracted by the magnet and could attach on the disc.

Procedure

The PTFE discs were sterilized and coated in a drop of 10 µg/mL fibronectin solution in PBS for 1 h at room temperature. After washing with PBS, they were stored in PBS until use. Glioblastoma cells were incubated with 25 µg/mL MA or FS for 1 and 3 d, trypsinized and counted. Two wells in opposite corners of the 12-well plates were filled with 4 mL medium and a drop of 50 µL cell suspension ($3\text{x}10^4$ cells) was added to each well. A PTFE disc with the coated side down was placed carefully on the surface, so that it swam. Immediately, the plate was covered with the lid and a 20 mm permanent magnet was fixed on top. As controls, cells without MNP treatment were used, as well as the setup without magnetic field.

After 1 d, the swimming discs were removed and washed with PBS. The cells on the discs were fixed with methanol and stained with DAPI in one step by a solution of 5 µg/mL DAPI in methanol for 15 min in the incubator. Then, the cells were washed with PBS and mounted on objective slides with mounting medium.

By fluorescence microscopy, 5 images were taken and particles were counted (see section "image evaluation"), n=20 (4 discs from 2 independent trials), using an excitation filter of 340-380 nm and an emission filter of 435-485 nm.

Magnet channel setup

Principle

For the quantification of the magnetic field influence on MNP loaded cells, a setup for the microscopic evaluation was developed. For this, a self-built chamber forming a channel was used (see Figure 7). Cells were stained with Calcein-AM to only observe living cells and to allow the particle counting by ImageJ. Calcein AM is a non-fluorescent dye, which is used to label living cells. After entering the cells, it is converted to the fluorescent form by enzymatic cleaving of the AM groups in the cytosol. This assay was useful to gain insight in how many cells from the population are affected by the magnetic field and how far away from the magnet the cells can be moved, if they are not attached on the surface.

Procedure

Glioblastoma cell lines were seeded in 12-well plates at 2.5×10^4 cell/cm² density (G44) or 5×10^4 cells/cm² (G62 and G112), like for iron loading studies. After 1 d, the medium was exchanged to cell culture medium without MNPs (control) or medium containing MA or FS at 25 µg/mL concentration for 1 or 3 d. Then, cells were stained with Calcein AM in complete cell culture medium (1.6 µL/mL) for 30 min in the incubator, before the cells were trypsinized and counted. The cell pellet was resuspended in medium to a concentration of 3×10^5 cells/mL.
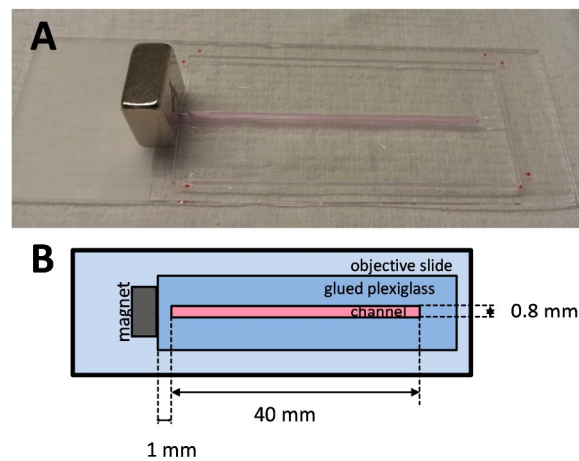
Figure 7: Magnet channel assay. The photograph (A) shows the setup of the magnet channel assay, which is also illustrated in the scheme (B) by a top view, including dimensions (scheme not in scale).

After cleaning the chamber with ultrapure water, 40 µL of the cell suspension was transferred to the channel. The objective slide was mounted on the microscope table and cells were allowed to settle down for 5 min. Then, a large image was acquired. A 10 mm permanent magnet was fixed with modeling clay in 1 mm distance to the channel for 5 min.

Subsequently, microscopy was repeated. All trials were performed twice, total n=5. For data evaluation, see section "Microscopy image evaluation".

Adherent cell movement

Cylinder setup

Principle

The cells were seeded in a clear spot with the help of a glass cylinder put inside the cell culture well. After removal of the cylinder, the outgrowth from the spot was evaluated by bright field microscopy. In this experiment, the effect of a laminin coating was examined. Laminin is a protein that has been shown to increase the glioma cell motility *in vitro* [138].

Procedure

The 24-well plates were coated with 10 µg/mL laminin in PBS for 1 h at 37 °C and washed with PBS before storage at 4 °C until use. Then, the glass cylinders were put in the well-plates and 6000 G62 cells without MNPs per cylinder in 30 µL normal cell culture medium were added. The gap between the glass cylinder and the outer well was filled with 200 µL to prevent the laminin from drying out, and the cells were incubated for 6 h to adhere to the surface. Afterwards, the cylinders were removed and non-adherent cells were taken out by medium wash. Large images were taken at the start and after 3 d of culture.

Ibidi® insert setup

Principle

The trials with the ibidi® culture-inserts 2 well, hereafter called ibidi® inserts, underlie the similar principle as the cylinder trials. However, due to the even edges, the outgrowth evaluation was easier and the silicone material attached better to the surface. The side facing to the magnet was compared with the opposite side of the cell spot and a control without MNPs was used to show effects of the MNP incubation.

The ibidi inserts were used for migration experiments with magnets in combination with recombinant hepatocyte growth factor (HGF) or rhodamine as these chemicals are supposed to support the cell migration.

Procedure

G62 cells were incubated with 25 µg/mL MA or FS for 1 d, trypsinized and counted by CASY. Ibidi® inserts were placed in a 24-well plate and one chamber was filled with 70 µL medium containing $5x10^4$ cells treated with MA or without (control, see Figure 8). After 6 h adherence time, the cells were washed with medium and 1 mL normal cell culture medium

supplemented with 50 ng/mL HGF was added. Bright field images were acquired with the microscope.

In another experiment, G62 cells were seeded in the inserts with medium containing 50 µg/mL rhodamine or the similar volume of DMSO. After 6 h adherence, the cells were washed with normal cell culture medium and 1 mL medium without dye was added. Then, large fluorescence and small bright field images were acquired with the microscope. The positions of the pictures were saved to acquire the same areas after the magnetic field incubation of 1 d.
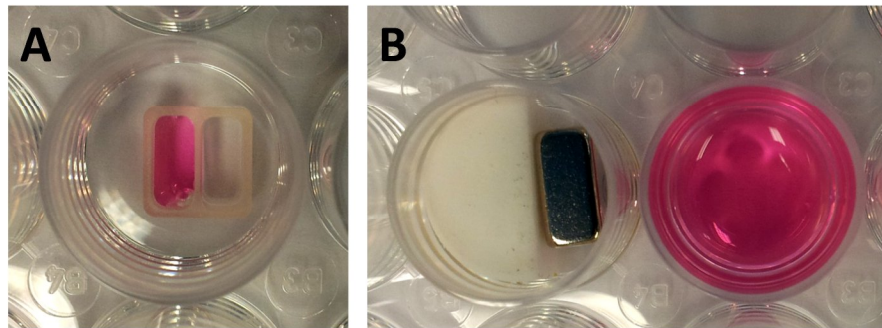
Figure 8: Ibidi® insert setup. The ibidi® insert was placed in a well of a 24-well plate, one chamber filled with cell suspension (A). Then, the insert was removed and the well was filled with fresh medium. A 10 mm permanent magnet was placed in the adjacent well with a white spacer (B).

A 10 mm permanent magnet was fixed in the adjacent well with the help of a self-made Teflon spacer and modeling clay (see Figure 8). After 1 d incubation in the incubator, microscopy was repeated.

Transwell assay

Principle

The cells were seeded on a membrane with 8 µm pores, which were hung in a well filled with medium so that the cells were able to migrate through the pores to the other side of the membrane. The permanent magnets were fixed below the plates to examine whether the natural migration behavior was enhanced by the magnetic field (Figure 9).

Procedure

G62 cells were incubated with 25 µg/mL MA for 3 d, trypsinized and counted. A volume of 500 µL normal cell culture medium was added per well of a 24-well plate and the transwell insert was added. Then, 7.5×10^4 cells in 100 µL were seeded in the upper compartment. After 1 h adherence, a 10 mm permanent magnet was fixed below the well and the cells were incubated 1 d in the magnetic field.
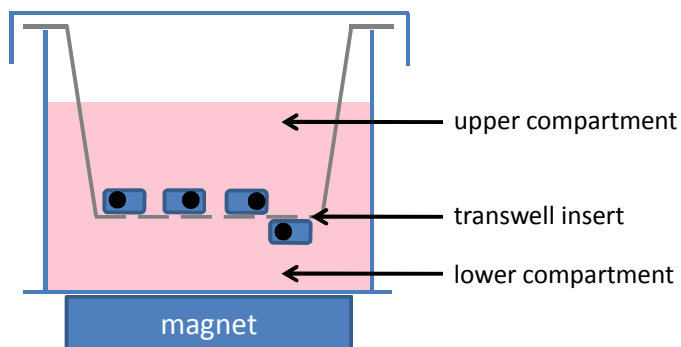
Figure 9: Transwell insert. The transwell insert was placed in a well of a 24-well plate, and cells were seeded in the upper compartment. After the migration through the pores of the membrane, the cells could be detached in the lower compartment. The magnet was fixed below the plate.

For the evaluation, the medium from both compartments was removed and 500 µL staining medium (1.6 µL/mL Calcein-AM) was put in the lower compartment. After 30 min incubation in the incubator, the medium was removed and the cells were washed with PBS. Trypsin was put in the lower compartment and incubated 5 min, before the insert was removed from the well and 500 µL medium was added. The cell suspension was transferred to Eppendorf tubes and centrifuged for 5 min at 2000 rpm in the microcentrifuge. The supernatant was removed and the pellet was resuspended in 450 µL medium. Afterwards, 100 µL cell suspension was pipetted in triplicate in a 96-well plate and cells were incubated for 15 min in the incubator to settle down. Then, fluorescence pictures of the whole wells were acquired and particles were counted (see section "Microscopy image evaluation").

12-well assay

Principle
For the quantification of the reaction of adherent cells on the magnetic field, similar principles as for the magnet channel trial were used. The cells were incubated for few hours to attach to the surface, following Calcein-AM staining and magnet attachment directly at the outer side of the well. As the biological answer towards the field was expected to be slower, the cells were incubated with the magnet for 1 or 3 d.

Procedure
Glioblastoma cells were seeded in 12-well plates (5×10^4 cells/well), followed by a medium exchange after 1 d to complete cell culture medium without MNPs (control) or with 50 µg/mL MA or 25 µg/mL FS. As high-load control, Sigma-PLL sample was used (35 µg/mL). Cells were incubated for 3 d, trypsinized and counted. Then, 6250 cells/cm² (2.5×10^4 cell/well) were seeded in a new 12-well plate in two opposing wells each.

After 4-6 h adherence time in the incubator, 100 µL Calcein-AM staining solution (16 µL/mL medium) was added (final concentration = 1.6 µL/mL) and cells were incubated for 20-30 min in the incubator. The medium was exchanged to fresh complete medium and stitched microscopic images were taken. The 10 mm permanent magnets were fixed directly at the cell culture well with a small piece of modeling clay. In order to avoid misinterpretation due to seeding differences, the magnets were fixed either on left or on right side of the well (see Figure 10). After 1 or 3 d of incubation the magnets were removed and the staining with Calcein-AM was repeated without medium exchange followed by microscopy. Each trial was repeated 3 times, total n=6. For evaluation see section "Microscopy image evaluation".
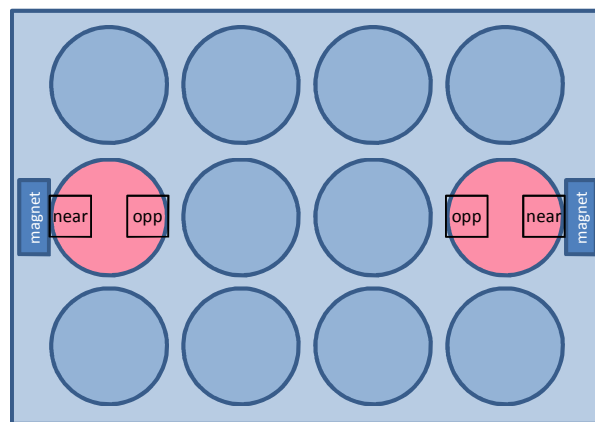
Figure 10: Scheme of 12-well assay setup. The cells were seeded in the outer wells of a 12-well plate and magnets (dark rectangles) were fixed directly at the wall at the outer sides. The marked areas "near" (= near magnet) and "opp" (=opposite of the well) were evaluated.

Microscopy

Fluorescence microscopy

Principle

Fluorescence microscopy is based on the excitation of fluorophores with a special wavelength. During this excitation, some electrons from the fluorophores get in a higher energy state and fall back to their original state, while emitting photons of a longer wavelength. In the microscope, bright light is filtered to the excitation wavelength and is diffracted by a dichroic mirror to reach the object. The emitted light of the object passes the mirror due to its higher wavelength and is then collected by a camera for the acquisition of an image [24].

Procedure

Fluorescence images were acquired with a Nikon Eclipse Ti-S inverted microscope with NisElements software (Version 6), using an excitation filter of 465-495 nm and an emission filter of 515-555 nm for Calcein-AM or rhodamine detection.

Microscopy image evaluation

Principle

Microscopy is usually applied for qualitative analysis, as quantification of picture data, for example particle counting, is considered as time-consuming and user-dependent process if done manually. For (semi-)automation of particle counting, pictures should

a) be not too large that they can be processed in a reasonable time;

b) consist of a strong, clear signal so that digital processing can be performed without causing artifacts;

c) contain mostly single particles without overlapping.

For this reason, we used relatively low cell numbers, stained the cells with a fluorescent dye and examined only a part of the cell culture well.

Procedure

For particle counting, the first part of the channel or the middle part of the cell culture well was recorded by large image acquisition, i.e. stitching of single pictures to a large one. Several images were taken with a 4x objective in x- and y-direction (see Table 3) with 5 % overlap in the FITC setup and saved the starting position for better reproducibility. With Photoshop, a grid was projected on the images to divide it into areas of different distance to the magnet. Then, we loaded the pictures in ImageJ, cut the single areas and defined a threshold between background and fluorescence signal (automatic calculation "Li"). By watershed algorithm, cell duplets were separated before particles were counted (size=20-infinity, circularity=0-1).

Table 3: Image quantification parameters

	magnetic channel	adherent movement
image dimensions (pictures)	x=12 , y=1	x=8, y=3
grid areas	1 mm sections (channel breadth ca. 0.8 mm)	1x4 mm
counted areas	5	4 near and 4 opposite magnet

Confocal microscopy

Principle

The laser scanning confocal microscopy underlies the same principle as the normal fluorescence microscopy. However, the fluorophores are excited by a laser beam only at one point of the specimen, so that the diffraction is limited. By scanning the whole specimen, an image can be composed by the computer [6]. With this technique, it is possible to acquire a higher resolution than in traditional fluorescence microscopy. Additionally, 3D images can be produced.

Fluorescence dyes are normally designed to stain special sites or organelles of the cells. For the experiments, following dyes were used:

- DAPI, that intercalates in the DNA of fixed cells.

- Phalloidin, that binds to actin of fixed cells and shows an important part of cytoskeleton structure.

Procedure

For confocal microscopy, round glass cover slips were sterilized by autoclaving and coated with 10 µg/mL fibronectin in PBS for 1 h at room temperature. Then, the coated cover slips were transferred in a 12-well plate and washed with PBS. G62 cells and astrocytes were seeded on cover slips ($1x10^4$ and $4x10^4$ cells/well) and medium was exchanged after 1 d to complete medium without (control) and with MA and FS at 25 µg/mL concentration.

After 3 d incubation, medium was exchanged to medium without MNPs and a 10 mm permanent magnet was fixed at the side of the well with modeling clay. By a forceps, it was assured that the cover slips are placed near to the magnet. The cells were fixed with 3.7 % formaldehyde for 10 min at room temperature after 1 d incubation in the magnetic field.

The cells were permeabilized with 500 µL 0.1 % Triton X-100 solution in PBS per well and incubated for 10 min at room temperature. After washing with PBS, the staining solution was prepared containing 25 µL Phalloidin-488 and 12 µL 7.5 % BSA per 1 mL PBS. The cells on the cover slips were stained in 90 µL drops of staining solution on Parafilm for 1 h at room temperature in the dark. Afterwards, the cells were washed twice with PBS in a fresh 12-well plate.

The cell nucleus staining was performed by DAPI. For the stock solution, 5 mg DAPI was dissolved in 10 mL ultrapure water. Afterwards, the stock solution was diluted 1:100 in PBS for working solution. The cells were washed shortly with PBS and 500 µL DAPI working

solution was added per well. After 15 min incubation in cell culture incubator, the cells were washed thoroughly with PBS.

The cover slips were mounted on objective slides with DAKO mounting medium and pictures were acquired with the Leica TCS SP8 in the center of each cover slip to achieve similar distances to the magnet.

Live-cell imaging

Principle

In order to follow the movements of a cell, the camera of a microscope can take pictures of cells at defined time points, which afterwards can be converted into a video. The hurdles of this method lie in the maintenance of cell culture conditions on the microscope stage and the evaluation of the video data, especially the movement quantification. Live-cell imaging was performed in the biophysics laboratories under the direction of Professor Ben Fabry (Friedrich-Alexander University of Erlangen-Nürnberg).

Procedure

For live cell imaging experiments, $2x10^4$ NEDD9-2 cells were seeded per dishes. After few hours, 35 µg/mL Sig MNPs were added and the cells were incubated for 1 d. Then, the dish was placed in a self-build incubator system on the microscope stage and a 10 mm magnet was fixed at the wall of the dish. Every 2 min, a brightfield picture was captured automatically and recorded.

Statistics

The statistical analysis was performed by SigmaPlot (Version 11, Systat Software GmbH, Erkrath, Germany). For all experiments, an analysis of variance (ANOVA) was used for significance testing towards control and between the samples. If only one condition (e.g. the MNP concentration) was affecting the measurement variable (e.g. the cell number or the metabolic activity), a 1-way ANOVA was used. If several nominal factors influenced the measured variable (e.g. in the iron load/cell detection), a 2-way ANOVA was chosen. By using this test, the means of the measured variable were tested, whether they are similar within each factor, and whether there is an interaction of the factors [139]. If a difference of variance was observed, the Holm-Sidak test was performed for multiple pairwise comparison. The significance level was set to 5 %. The ANOVA was only performed within the cell lines, as the cells consisted itself of inherent properties affecting the measurement. Additionally, a third factor could lead to less reliable significance test results.

To test the relation between growth and Fe/cell rate, the Pearson correlation was applied. With this test, the significance of the correlation was tested, but also the strength of association was determined by the factor R^2 and the equation described the kind of relationship. The pairs of growth rate and iron/cell rate of the two examined time periods were chosen for each cell line and condition.

Results

In advance of the combination of the MNPs with the cells, both MNP types and cell lines were characterized to understand the extent of differences within the starting material. Afterwards, MNPs and cell lines were combined and the loading efficiency and the cellular effects were detected, before the magnetic field was introduced. Afterwards, different setups for the movement of non-adherent and adherent cells were tried to gain information about the reaction of MNP-loaded cells to magnets.

MNP characterization

Some properties of the MNPs are already declared by the suppliers, like the materials for core and coating or the size of the iron cores observed in transmission electron microscopy (TEM) images. As the size of the MNPs in suspension is crucial for the cell uptake, the hydrodynamic radius or diameter detected by dynamic light scattering (DLS) is one of the most important parameters.

Dynamic light scattering (DLS)

The DLS measurement is often conducted in water, however, the MNP size is probably changing in cell culture medium containing electrolytes and proteins, which interfere with the MNPs. This interaction leads to the increase of the size and to agglomerations of the MNPs. To test the impact of the medium with the MNPs used for this study, both MA and FS were mixed with cell culture medium and the effects were observed directly after the combination and again after 3 d incubation, the longest incubation time chosen for the cell experiments afterwards. As negative control, pure cell culture medium was also tested.

The cell culture medium, supplemented with 10 % FBS but without MNPs, showed a peak of particles with 5-7 nm radius size and few particles with 10-40 nm radius (Figure 11). A large particle radius distribution from 10-50 nm with a maximum at 30 nm was detected for MA diluted in water, while the FS size distribution in water was very narrow with 8-10 nm radius. When MNPs were diluted in cell culture medium, the size distribution of the particles changed as expected. MA showed two main size distributions at 10-20 nm and at 30-60 nm, so that the range of particles sizes increased only slightly, but a sharp decrease of middle-sized particles (between 20 and 30 nm) occurred. After 3 d incubation, the MA particles sizes between 10 and 20 nm decreased, leading to a small distribution about 30-50 nm radius size. The changes in FS particle distribution were more remarkable than observed in MA samples. When diluted in medium, FS showed fewer particles in original 8-10 nm radius in water dilution, and particles with 5-6 nm and 10-20 nm size appeared. When incubated for 3 d, FS

showed a higher number of large particles in a larger distribution from 10-30 nm but also still some particles of original size.
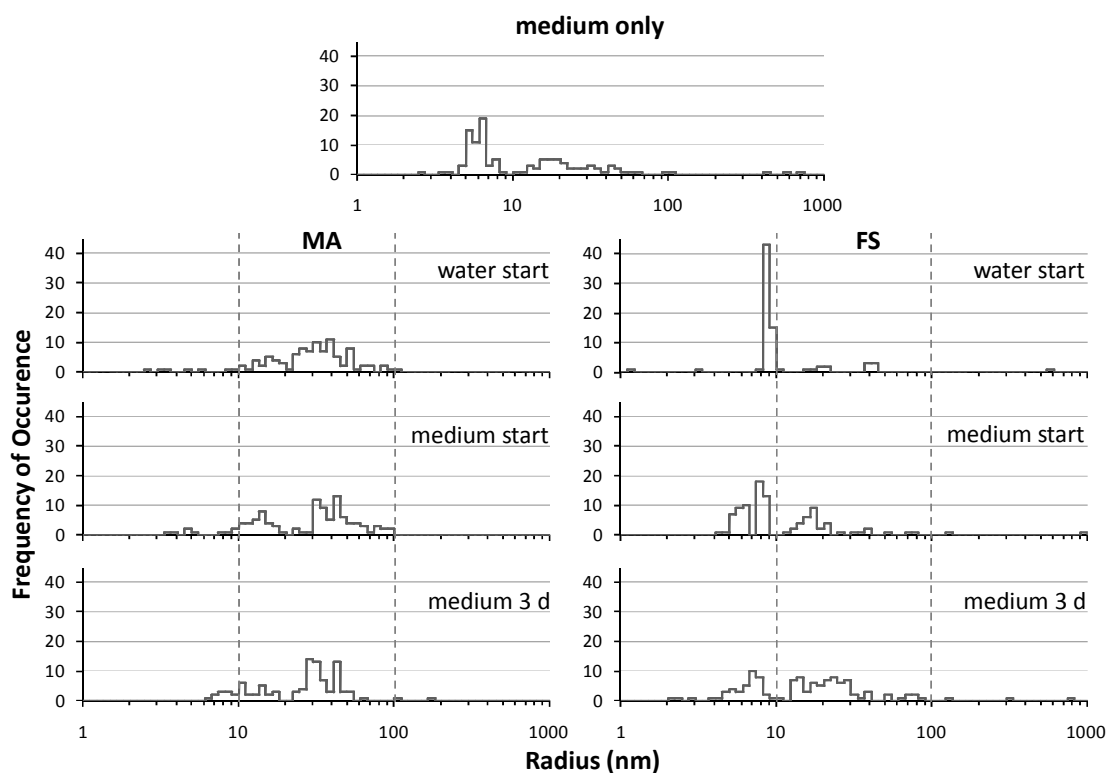

Figure 11: MNP radii in water and cell culture medium. The hydrodynamic radii distributions of medium alone (top), MNPs (MA and FS) diluted in water and in medium are shown in a range from 1-1000 nm, dashed vertical lines show 10 and 100 nm radius. The frequency of occurrence shows the number of particles with each radius (nm).

To summarize, the introduction of complete cell culture medium did change the MNP size of both MA and FS. However, the changes were more drastic in FS compared to MA samples. While the MA size distribution narrowed, the FS particle sizes were more variable. The longer incubation showed only a slight enhancement of the effects.

Cell characterization

The different glioblastoma cell lines were chosen to mimic the patient variability in the uptake of MNPs. It was likely, that the cell properties influence the loading with MNPs, thus, trials without MNPs were conducted to enlighten basic cell culture parameters, like the proliferation rate, the viability and morphology in the course of time.

Proliferation assay

The proliferation ability and characteristic of cells depends largely on the cell culture conditions, especially on the initial cell number seeded, defining the cell density. Thus, the

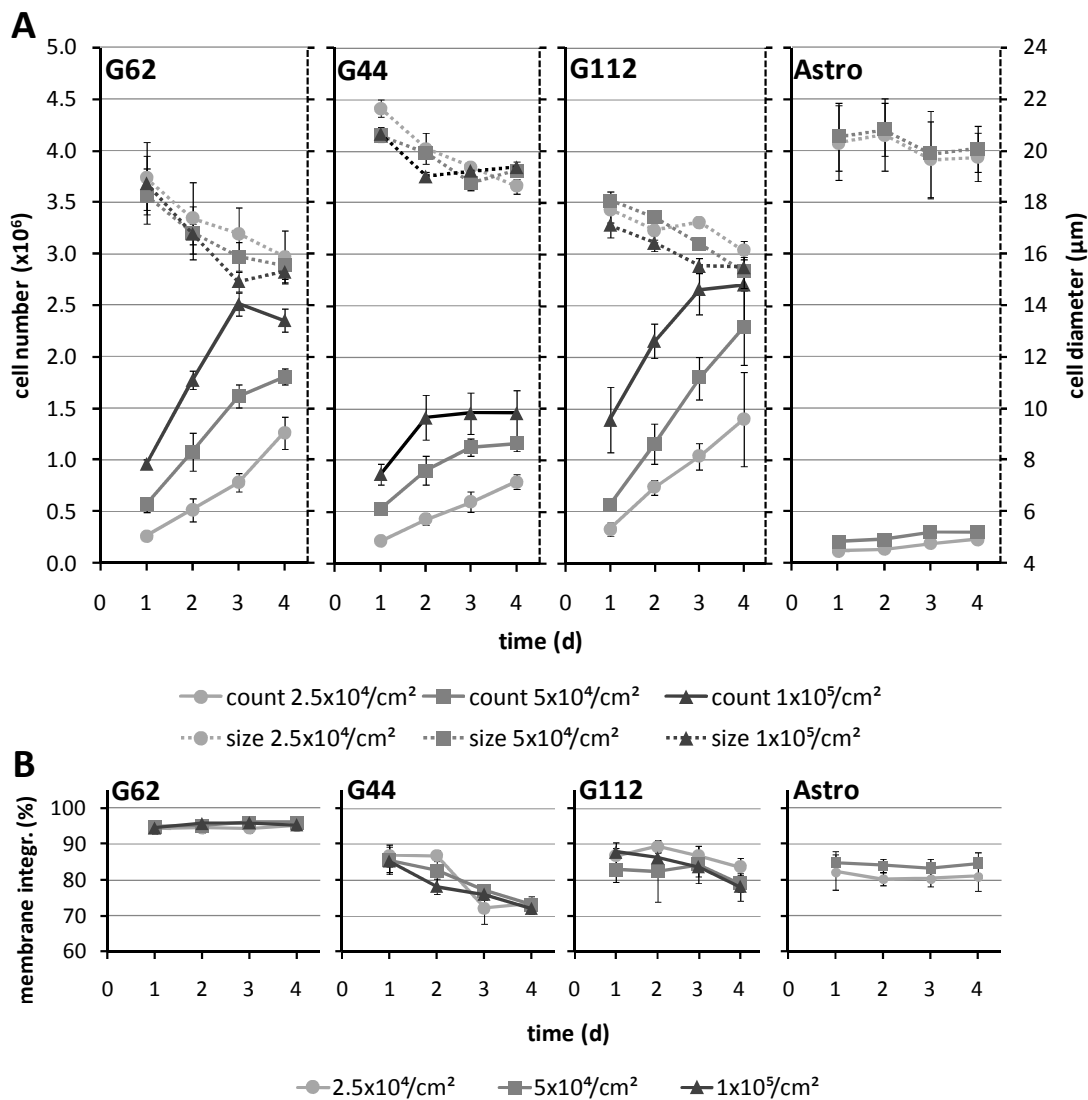cell lines were seeded in different densities and some general culture characteristics were measured by CASY®.

Figure 12: Glioblastoma and astrocyte cell growth, diameter (A) and membrane integrity (B) evolution without MNP exposure. The mean values and their standard deviation of cell number (A, solid lines), diameter (A, dashed lines) and membrane integrity (B) are depicted for glioblastoma (G62, G44, G112) and astrocytes (Astro) at different seeding densities ($2.5x10^4$ to $1x10^5$ cells/cm²) after 1-4 d culture.

It was shown, that the glioblastoma cell lines differed in size and growth velocity (Figure 12A). G44 were the biggest cells (18.7-21.7 µm), while G62 (14.9-18.9 µm) and G112 (15.3-18.1 µm) had a smaller but similar diameter. Over time, the mean cell diameter of all cell types decreased. With the highest seeding density, it remained constant from day 3-4. The

higher the seeding density, the smaller the cells were; however, the differences were only small.

The cell proliferation was reduced at later time points, mainly with the highest seeding density ($1x10^5$ cells/cm²), so that the growth rate differed not only between the cell lines but also between the time periods. When less cells ($5x10^4$ cells/cm²) were seeded, only small reductions of the growth rate were observed for G62, while G44 proliferation was more affected. With the lowest seeding density ($2.5x10^4$ cells/cm²), the increase of cell number stayed mostly linear in all cell lines. So, with higher seeding densities, the cell number increased until reaching a plateau. Similarly, the cell diameter decreased and formed a plateau, assuming a connection between cell growth and size. Astrocytes grew more slowly than glioblastoma cells but also showed the growth rate reduction at later time points, particularly with higher seeding densities.

Also, the cell membrane integrity differed remarkably between the glioblastoma cell lines (Figure 12B). While G62 showed stable high viability (95 %), G112 and particularly G44 membrane integrity decreased in the course of time from 85-90 % to 80 % and 70 %, respectively. The differences between the seeding densities were low.

The proliferation was remarkably influenced by the seeding density. The highest density ($1x10^5$ cells/cm²) led to a drastic inhibition of cell division at the late time points, therefore, it was not considered for further experiments. At middle seeding density ($5x10^4$ cells/cm²), G62 and G112 showed a division ability until 4 d after seeding, while G44 and astrocytes showed also a large decrease in growth rate. Thus, for G44 and astrocytes, the lowest seeding density ($2.5x10^4$ cells/cm²) was used for further trials.

Growth pattern
The morphology of the cells could also indicate their integrity and thus their reaction to cell culture conditions. Microscopy pictures visualizing the cell shape was used to confirm the usability of the cell seeding densities chosen.

The glioblastoma cells showed a different shape and spreading when seeded on cell culture multi-well plates (Figure 13A). G44 cells were more spread than G62 or G112 and showed a prominent nucleus with nucleoli. G62 were more spindle-like and G112 shape varies from small round to long triangular. While G62 and G44 single cells were distributed quite evenly on the surface, G112 cells grow together in small islets. Astrocytes were far the most spread cells with an irregular shape.

The inherent morphology differences are changing with growth (Figure 13B). G62 cells grow closer together and became more fiber-like. G44 cells became spindle-like that led to the

impression of lower cell confluence at later time points. G112 cells islets got bigger and finally fused. Astrocytes decreased their spreading during proliferation in culture and formed a confluent layer.
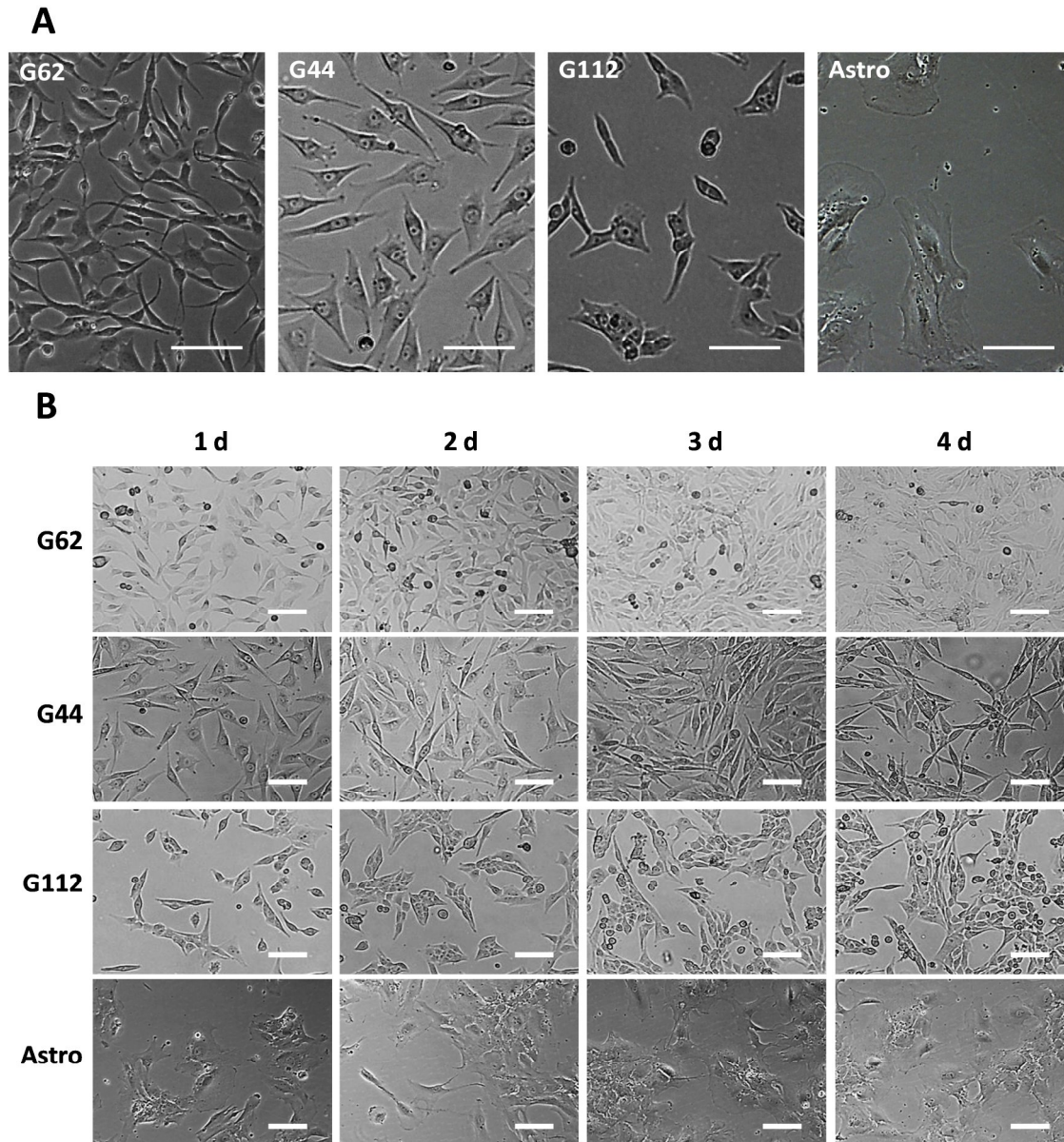

Figure 13: Cell morphology changes during growth. A: Microscopy images of the glioblastoma cell lines and astrocytes. B: The glioblastoma cell and astrocyte morphology was monitored by microscopy at the seeding densities chosen for MNP loading experiments (G62 and G112 $5x10^4$ cells/cm², G44 and astrocytes $2.5x10^4$ cells/cm²), scale=100 µm.

Due to the very large spreading of astrocytes and the pronounced morphological changes of G44, their very low seeding density was justified. In the case of G44, a lower cell number could be even better, however, the automatic cell counting procedure would have been more

inaccurate in the earlier time points. G112 and especially G62 cells seemed only slightly affected by increasing cell number.

Loading of cells with MNPs

After information about different reactions of the MNP types and cell lines due to the cell culture conditions were gathered, every cell line was loaded with both MNP types concerning different parameters. The most important information were firstly, how many MNPs were loaded onto or into the cells, and secondly, where the MNPs were situated. As both MNP types consisted of an iron core, assays based on the detection of iron were chosen, to guarantee a direct comparison. The ferrozine assay for quantitative iron detection and the Prussian blue staining for iron visualization were proven convenient for MNPs in former studies, thus they were chosen for this study.

Quantitative loading

The influence of two parameters on MNP cell loading was examined by ferrozine assay, the incubation time and the MNP concentration. The incubation time was maximal 3 d to keep the fast dividing cancer cells alive in culture. The concentration of MNPs in the cell culture medium was set by the iron concentration in the MNP suspension (5, 25 or 50 µg/mL) to evaluate the effects of the MNP properties (size, coating) and not the effectiveness of a certain amount of particles. The main reason of this trial was to achieve optimal conditions for the highest iron loading, as a high iron level was likely correlated with a better magnetic attraction. Another aim of this experiment was the detection of relationships between the parameters and the loading success to transfer these on other MNP types. Finally, the cell line-derived influences on cell loading were in focus, including the loading of astrocytes as healthy control cells.

Differences in MNP loading between the cell types occurred (Figure 14). With both MNP types, the far lowest iron loads were detected in G112 cells, ranging from 0.0011 to 0.0031 pmol iron/cell for MA and 0.0019 to 0.014 pmol iron/cell for FS. G62 and G44 showed higher iron loads; however, differences between the MNP types appeared. G62, compared to G44, reached slightly higher iron levels with MA (0.017 versus 0.014 pmol iron/cell), while with FS, G62 loads were only half as high as the ones of G44 (0.045 versus 0.104 pmol iron/cell). The highest loads were detected in astrocytes with a maximum of 0.024 pmol iron/cell after MA and 0.221 pmol iron/cell after FS treatment.

The iron loads were higher using FS for all conditions, except with 5 µg/mL MNPs in the medium, where it was higher with MA or at least in a comparable range. With higher iron concentration in the medium, also the iron concentration in the cells increased. However, the

effect was far stronger after FS than after MA treatment. For example, in G62 cells after 3 d, the iron amount/cell increased from 0.014 to 0.017 pmol with an increase of MA dose, while a 5-fold increase occurred with FS (from 0.009 to 0.045 pmol).
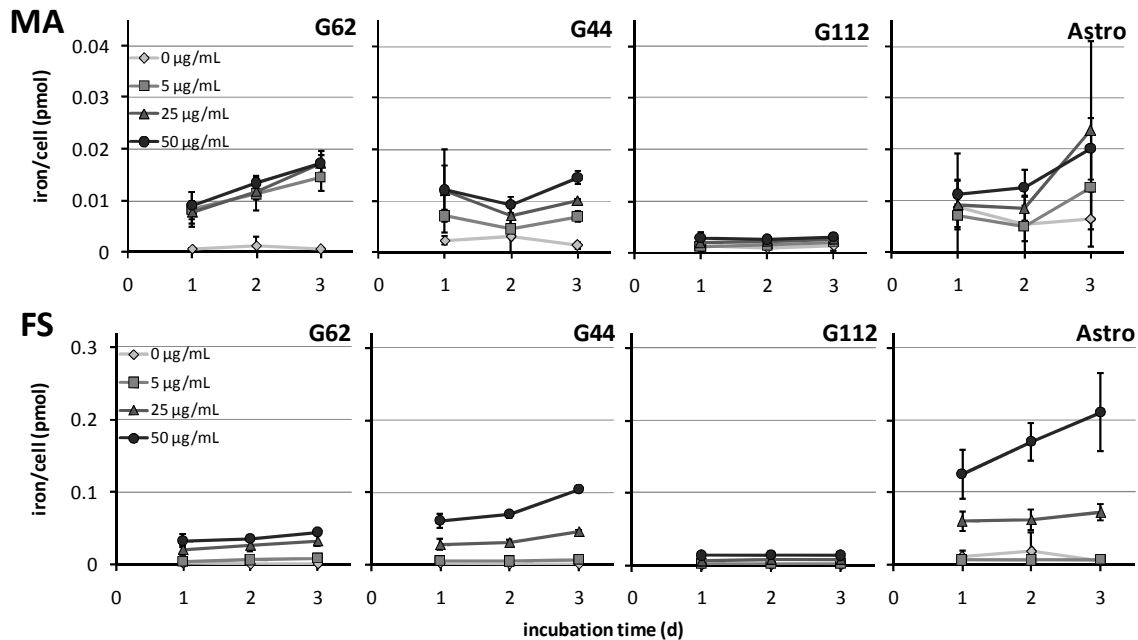

Figure 14: MNP cell loading with MA and FS. The mean ± the standard deviation of the amount of iron per cell are presented after 1-3 d incubation with MA or FS and 0-50 µg/mL MNPs in the medium (statistics see appendix, Figure 41).

While the increase of iron with time was mostly linear with FS treatment, more irregular increases and also decreases occurred with MA. Especially with G44 cells and MA, the iron load/cell decreased from 0.012 pmol at day 1 to 0.009 at day 2 and increased again to 0.014 pmol after 3 d of incubation. When the rate of growth and Fe/cell for 24 h intervals was calculated (Figure 15), a negative correlation for both MNP types was shown considering all glioblastoma cell lines together (Pearson MA p=0.0003; FS p=0.0098). The slope of the regression line was higher with MA loading (-0.779) compared with FS (-0.403) and also the coefficient of determination (R^2), referring to the relationship of both rates, was higher with MA (MA = 0.57; FS = 0.35). For astrocytes, the dependency between growth rate and MNP loading rate was similar for FS, but much higher for MA treatments.
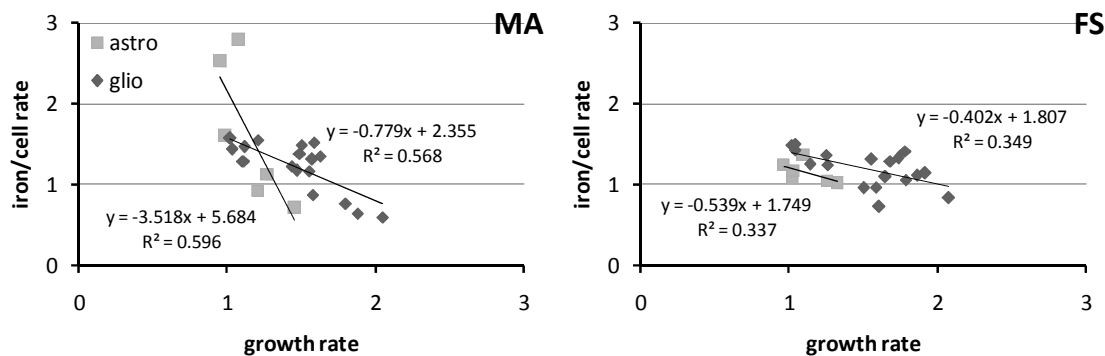
Figure 15: Growth-dependent MNP loading. The rates of the iron amount/cell and growth for all glioblastoma cell lines (Glio) and astrocytes (Astro) were calculated for 24 h intervals and correlated. The lines show the regression.

To summarize, FS yielded a higher iron amount per cell than MA using 25 or 50 µg/mL concentration. Furthermore, the FS loading was less affected by the cell growth and thus showed a good time-dependence. However, the loading of astrocytes was much higher than of glioblastoma cells, unlike to MA, where the astrocyte loading was nearly similar. While the maximal iron amount per cell was gained in G62 with MA and in G44 with FS, G112 had far the lowest iron levels with both MNP types. This indicated, that MNP-loaded G112 cells might show the least attraction in a magnetic field.

Qualitative loading

By the visualization of iron deposits in the cells, the success of the MNP loading can be confirmed. As the highest MNP concentration and the longest incubation time showed the highest amount of iron per cell in all cell lines, it was chosen as condition for the Prussian blue staining.

Regarding a sub-confluent cell layer, no traces of iron could be detected in MA treated cells in glioblastoma cells (Figure 16). In images with a comparable cell density, iron deposits near the nuclei were found after FS treatment. The iron signals after FS incubation were not even distributed among all cells; especially in G112 samples, where the cells in the center of the islets were deeper stained. In images with a very high cell density, iron could also be visualized in G62 after MA treatment, demonstrating cell density effecting the loading of MNPs. Astrocytes showed iron signals after MA loading that were detected in the perinuclear region. However, with FS, the staining of iron was more located at the edges of the cells or perhaps even outside the cytosol. The shape of the glioblastoma cells seemed not to be affected by the MNP loading, while astrocytes showed an islet formation after FS treatment.
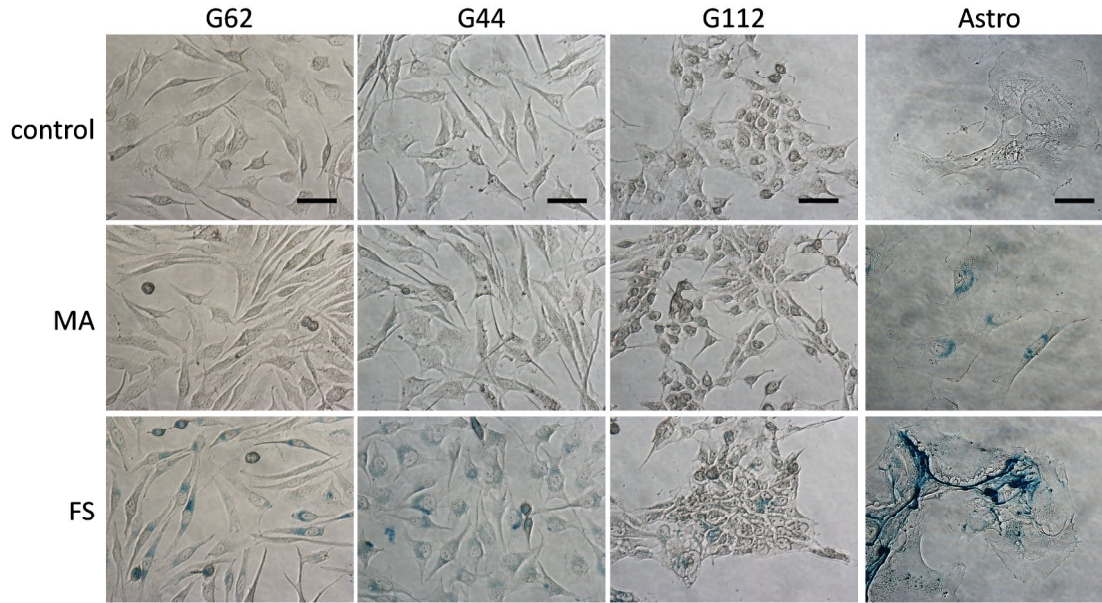
Figure 16: Prussian blue staining after MNP loading. Microscopic pictures of the iron staining of glioblastoma cell lines (G62, G44, G112) and astrocytes (Astro) after 3 d loading with 50 µg/mL MA or FS, or without MNP incubation (control), scale = 50 µm.

The perinuclear iron deposits could indicate that the MNPs are taken up by the cells and not only attached at the cell surface, as this would stain the whole cell body. The difficulties of iron staining in MA-treated glioblastoma cells could be connected with a too low iron amount per cell. The staining success with a very high cell density show the functioning of the assay for this MNP type. The unusual FS staining observed in astrocytes could be an evidence for a cytotoxic reaction, which were examined in further experiments.

Loading effects

The successful loading is as important as a sufficient cell health for observing the cell movement in a magnetic field. Thus, several aspects of cellular effects after the MNP treatment were tested and compared with cells without MNP incubation. The cell number, the cell membrane integrity and the metabolic activity were chosen for a comprehensive overview.

Cell number

If cells are treated with MNPs, they may reduce their proliferation due to the interference of the particles with cellular processes. Additionally, a lower cell number could explain cell losses because of cell death. To examine the potential effects of MNP loading on cell health, the cell number after MNP loading was compared with control cells.
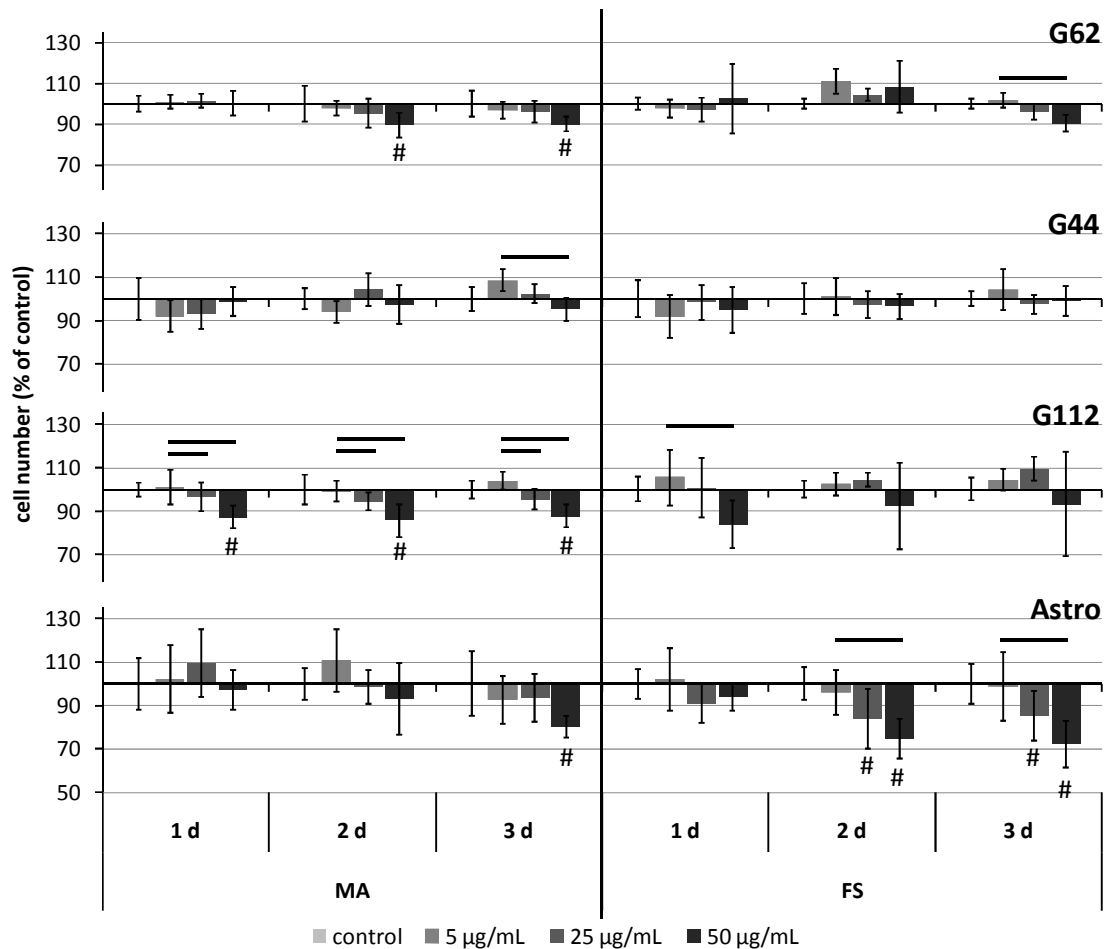
Figure 17: Cell number after MNP loading. The glioblastoma cell lines (G62, G44 and G112) and astrocytes were loaded with MA or FS for 1, 2 and 3 d. Control cells without MNPs were set as 100 %. Bars show mean values ± standard deviation, # significant towards control, horizontal lines significant between the conditions, p<0.05 (2-way ANOVA), n=6.

The glioblastoma cell number after MNP loading was significantly but not drastically decreased in several conditions: about 20 % less cells as compared to control were found (Figure 17). Differences between the cell lines occurred, as G112 showed the most, G62 less and G44 fewest changes of cell numbers compared to control. All significant decreases were detected with 50 µg/mL MA in G62 (90 %) and G112 (86-87 %), while only small reductions of cells occurred in G44 cells (95 %). With lower concentrations and/or earlier time points, also non-significant increases of cell number were observed.

In contrast to glioblastoma cells, in astrocyte cultures higher cell number reductions were detected after FS treatment (72 %) compared to MA-treated cells (80 %). Also, significant effects were observed already with 25 µg/mL FS concentration (75 %).

The reduction of cell number with the highest MNP concentration could indicate mild toxic effects, which are more pronounced in healthy control cells. In order to distinguish growth reduction from cell death, the membrane integrity of the cells was further evaluated.

Membrane integrity

The membrane integrity was also detected by CASY® measurement, showing defects of the cellular membrane. The results of this experiment can only show a percentage of damaged cells compared to the total cell number at the moment of detection. As a damaged cell membrane leads to cell death, cells with a disturbed membrane integrity might have been lost in the time before the detection. Additionally, dying cells often detach from the surface and could be washed away in the procedure of the experiment. Thus, the results from this measurement are likely demonstrating less MNP toxicity than in reality.
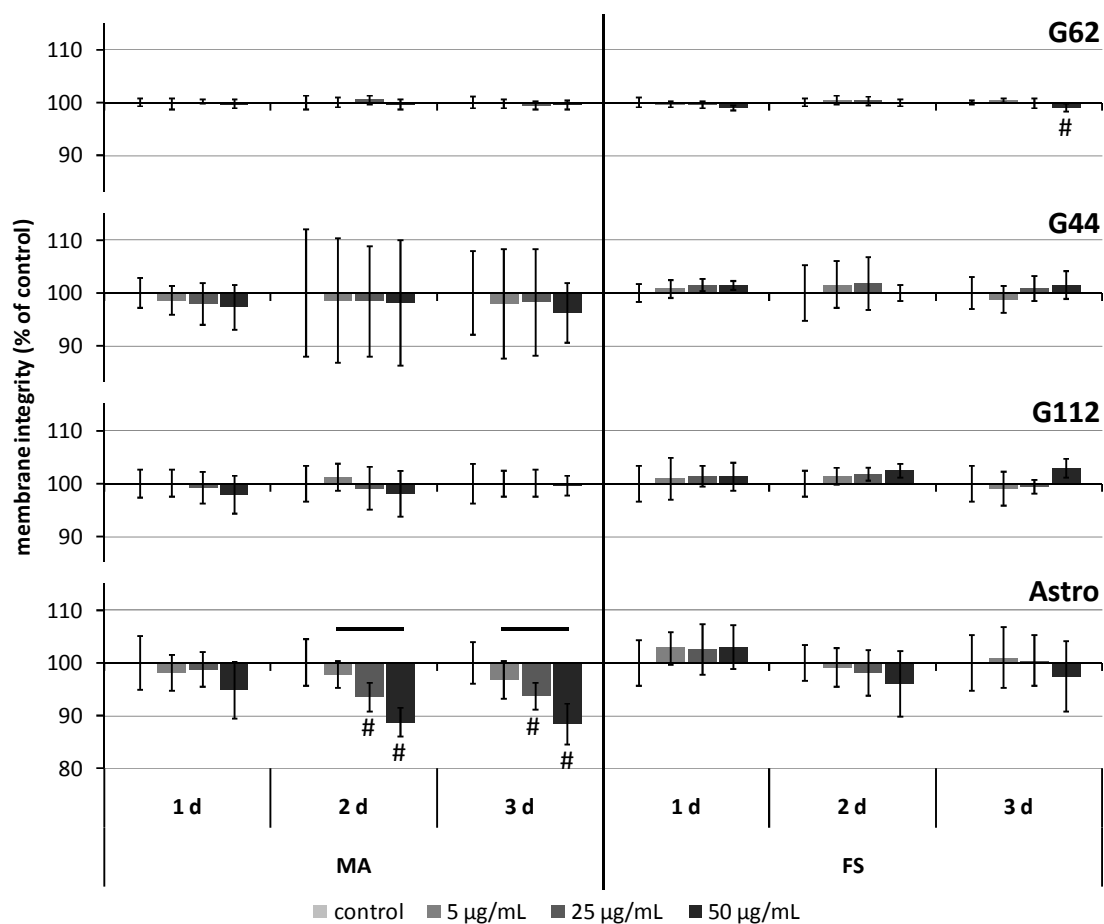

Figure 18: Membrane integrity after MNP loading. The glioblastoma cell lines (G62, G44 and G112) and astrocytes were loaded with MA or FS for 1, 2 or 3 d. Control cells without MNPs were set as 100 %. Bars show mean ± standard deviation, # significant towards control, horizontal lines significant between the conditions, p<0.05 (2-way ANOVA), n=6.

The membrane integrity of all glioblastoma cell lines was not significantly impaired by MNP loading, except for G62 with 50 µg/mL concentration after 3 d (Figure 18). The mean changes varied between 96 and 103 %. However, astrocytes showed a significant loss of viability with MA in correlation with the MNP concentration to 88 % with 50 µg/mL compared to control. In contrast, no significant changes of astrocyte membrane integrity were measured after FS treatment.

The cell membrane disintegration was only detected in healthy control cells, not in glioblastoma cells. For a deeper analysis, the metabolic activity of the cells after MNP incubation was tested.

Metabolic activity
The MTT assay is a common method for the detection of cytotoxicity, as it shows the ability of a cell population to convert MTT to a formazan product. If the cells are damaged, the conversion ability is reduced, resulting in lesser end product detected. Similarly, a reduction could occur, if the cell number of the population is decreased due to a proliferation inhibition.

The loading with MNPs significantly affected the metabolic activity of all glioblastoma cell lines, although higher effects were observed with FS than with MA (Figure 19). A pronounced concentration dependent rise of activity was detected with MA.

In G44 and G112 cells treated with 5 µg/mL MA, a significant increase of activity to 110 % and 115 %, respectively, occurred already after the first day of incubation. The activity was even higher using 50 µg/mL concentration in G112 cells (143 %) and G44 (124 %), whereas with G62 the increases were very low (105 %). After 2 d of incubation, the activity decreased, especially for 50 µg/mL treated samples to 114 % for G112, 122 % for G44 and 93 % for G62. The activity went back to control level or declined further after 3 d to 87 % in G112, 99 % in G44 or 78 % in G62. With increasing concentrations, more drastic the changes were observed.

Using FS, the differences between the cell lines were smaller. However, similar to MA, G112 showed more changes than G44 and least variability was observed with G62. In contrast to MA, most increases of activity occurred at day 2 with maximal 110 % in G112, 111 % in G44 and 106 % activity in G62, followed by decreases to control level in G62 and G44 or more negative in G112 (91 %). The concentration dependence was less compared to MA.

Astrocytes showed high concentration-dependent increases with MA that had their maximum at 2 d of incubation (142 %), but low time-dependent effects. In contrast, with FS there were only small changes until significant decreases of viability at day 3 to 80 %.
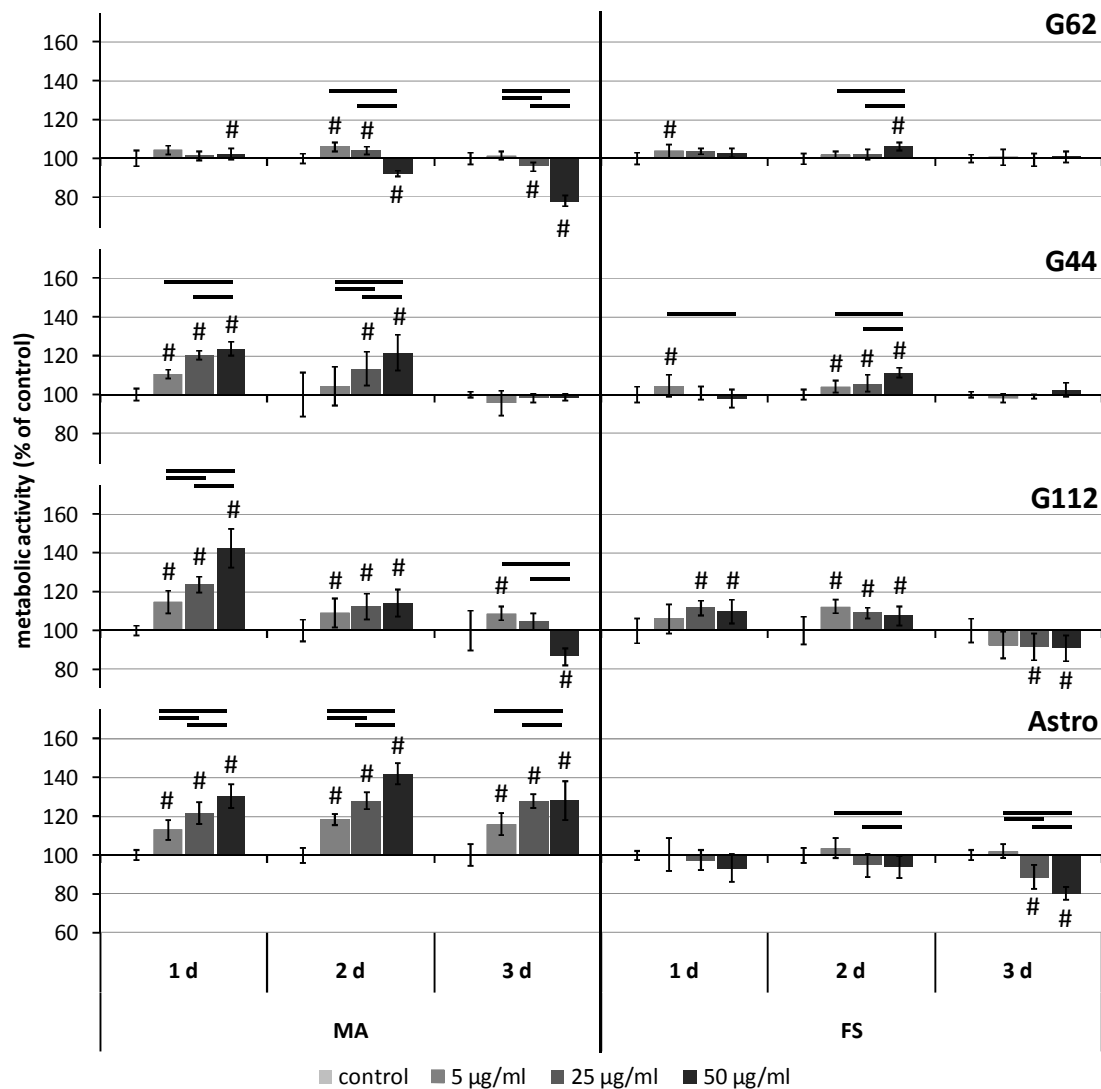
Figure 19: Metabolic activity after MNP loading. The glioblastoma cell lines (G62, G44 and G112) and astrocytes were loaded with MA or FS for 1, 2 or 3 d. Control cells without MNPs were set as 100 %. Bars show means ± standard deviation, # significant towards control, horizontal lines significant between the conditions, p<0.05 (2-way ANOVA), n=8.

The metabolic activity of all glioblastoma cell lines and astrocytes was more effected by MA than by FS treatment. Unexpectedly, more increases than decreases of the metabolic activity occurred after MNP treatment during the first days of incubation, indicating other than toxic effects.

Concluding from the characterizing and MNP loading experiments (Table 4), MA showed higher stability in the cell culture medium, but FS treatment lead to higher iron amounts/cell in the glioblastoma cells. G112 cells had the lowest MNP loading and thus are probably worst attracted by the magnetic field. The effects on viability were low on all glioblastoma

cell lines and did not remarkably differ between the MNP types. The highest concentration (50 µg/mL) and the longest incubation time (3 d) lead to highest iron loads/cell, but also to pronounced metabolic declines. Thus, 5 µg/mL MNP concentration and 2 d incubation time were not regarded in further examinations.

Table 4: Parameter choice for magnetic experiments after characterization and loading results

parameter	choice	reason
MNP type stability	MA	similar size after medium incubation
MNP loading	FS	higher iron amount/cell
MNP concentration	25 and 50 µg/mL	5 µg/mL too few loading
MNP incubation time	1 and 3 d	3 d highest loading, but highest toxicity
glioblastoma cell type	G62 and G44	G112 too low iron/cell

Magnetic field characterization

For the movement of the MNP-loaded cells, a magnetic field needed to be introduced. Similar to the different cell lines and MNP types, the magnetic field created by permanent magnets of variable sizes was examined, in terms of strength, field line appearance and ability to attract pure MNPs.

Magnetic field simulation

In order to visualize the magnetic field of the three different magnet sizes, a magnetic flux density plot was created by the femm software. As the magnetic flux density is connected with the magnetic field strength, the images present an overview about the performance of the magnets.

According to the manufacturer, the remanence, defined by the magnetic flux density inside the magnet, was similar for all magnet sizes, namely 1.3 T. In the simulation of the magnetic field lines and flux density by the femm software, differences of the magnetic field due to the sizes of the magnets were illustrated (Figure 20). The homogeneity of the magnetic field was the highest at the pole surface of the 20 mm magnet, demonstrated by the highest linearity of the field lines. However, the highest field strength was achieved at the surface of the smallest magnets, as shown by the bright yellow color and the accumulation of field lines. The gradient of the magnetic field, which induce the attraction of MNPs, seemed to be also the highest in the air compartment around the smallest magnet. Similarly, the field intensity of

the smallest magnets strongly declined within a short distance, whereas the decrease of field strength was much lower with the bigger magnets.
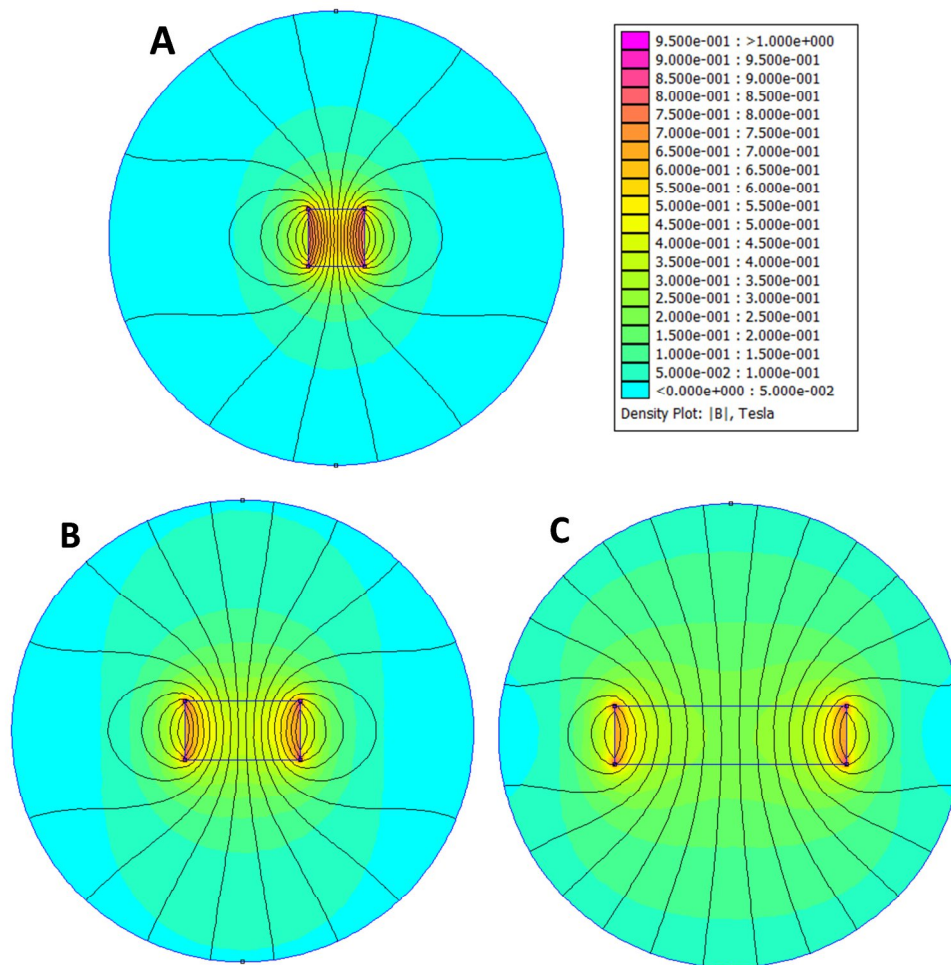

Figure 20: Visualization of the magnetic field by software simulation. A cut through the 5 mm (A), 10 mm (B) and 20 mm (C) permanent magnets are shown by the blue rectangles, where the bottom is the south and the top the north pole of the magnets. The circles indicate the air compartment with a radius of 20 mm from the center of the rectangle. The black lines illustrate the field lines and the different colors mark areas with similar magnetic flux densities as referred to the legend.

Due to this magnetic field simulation, the highest field strength and gradient was shown by the smallest magnet; however, the higher penetration of the magnetic field was demonstrated by the biggest magnet. In order to proof these relations between magnet size and magnetic field properties, the magnetic field strength of the magnets was measured.

Magnet strength measurement

The magnetic flux density of the different permanent magnets was detected by a Gaussmeter in different distances to the magnet surface. This investigation was important for the decision about the right magnet for further MNP-loaded cell movement setups.
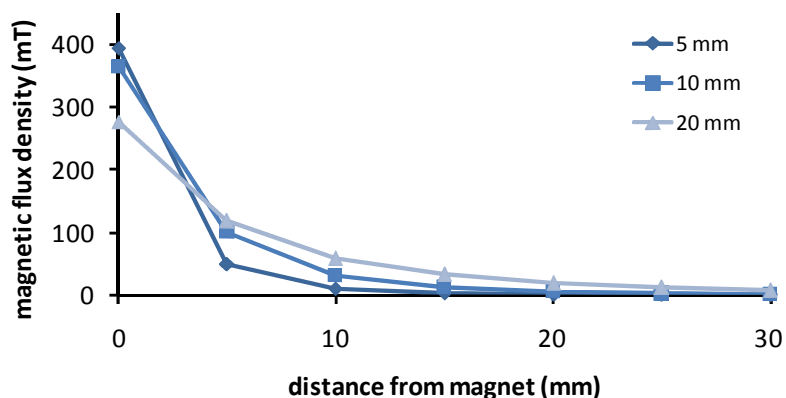

Figure 21: Magnetic flux density of permanent magnets. The flux density of the permanent magnets (5, 10 and 20 mm size) was detected in increasing distance to the magnet surface.

The magnetic flux density measured directly at the magnet surface (Figure 21) was the highest with the smallest magnet (400 mT), followed by the 10 mm magnet (360 mT) and the biggest magnet (280 mT). The reduced strength measured is explained by the sharp loss of the remanence during the passage from the magnet to the air phase, also observed in the simulation. The decline of the flux density was the biggest with the smallest magnet, so that in 10 mm distance to the magnet surface, the highest field strength was achieved with the 20 mm magnet (60 mT), followed by the 10 mm (30 mT) and the 5 mm magnet (10 mT). In 20 mm distance to the magnet, which is roughly the size of a well from a 12-well plate, the flux density differed between 2 and 19 mT from the smallest to the biggest magnet.

The measurement of the magnetic flux density supported the simulation of the magnetic properties. Due to the very sharp decrease of the magnetic field strength, the 5 mm magnet was excluded from further trials. As the higher flux density and the pronounced gradient should lead to a better magnetic attraction of the MNPs, the 10 mm magnet was preferred for the experiments. However, the bigger dimension of the 20 mm magnets was required for some of the setups.

Magnetic attraction of MNPs

As the brown color of the magnetic fluids offered a good possibility to estimate the MNP attraction by a magnet, 10 mm magnets were fixed at the wall of the cell culture well with water-diluted MA or FS.
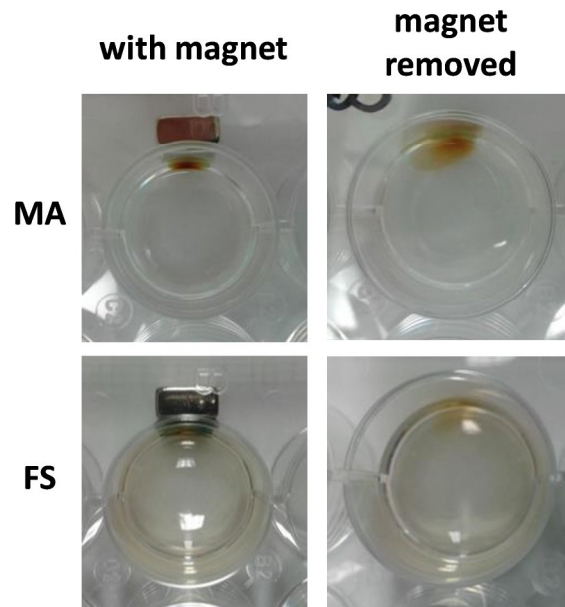
Figure 22: Magnetic attraction of MA and FS. A 10 mm permanent magnet was fixed at the cell culture well filled with 25 µg/mL MA or FS suspension in water for 3 d (left images) and removed afterwards (right images).

After 3 d incubation of 25 µg/mL MNPs in a magnetic field, differences between the attraction of the MNP types became visible (Figure 22). In the well with the water-diluted MA, the brown color by the iron oxide particles disappeared and the water in the well was completely clear, while a dense brown spot was observed at the magnet side of the well. In contrast, FS seemed to remain distributed in the well, as the water was still brownish after 3 d magnet incubation. After removal of the magnets, the MA attached to the wall started to distribute in the water again, due to Brownian motion. Also in the well with FS, a small accumulation near the magnet was observed after the magnet removal. This experiment indicated the lower attraction of pure FS in comparison to MA, which needs to be considered in the MNP-loaded cell reaction to the magnetic field.

Static magnetic field toxicity

Like the MNPs, also the magnetic field could lead to cellular effects, especially if the cells were loaded with MNPs before. As the MTT assay was most sensible to the MNP effects, it was also chosen for the detection of cellular reactions towards a magnetic field. Additionally, microscopy was performed to visualize cytoskeleton changes, that were observed in former cell culture studies with a magnetic field incubation.

Permanent magnets influence

The biggest permanent magnets were placed in close vicinity to the cells to test the effect of a 200-250 mT magnetic field on the cellular metabolic activity. The lowest MNP concentration

(5 µg/mL) from the loading tests was excluded due to the low iron content gained in all cell types.

The effects from the magnetic field on the metabolic activity were not very significant, but cell type-dependent (Figure 23).
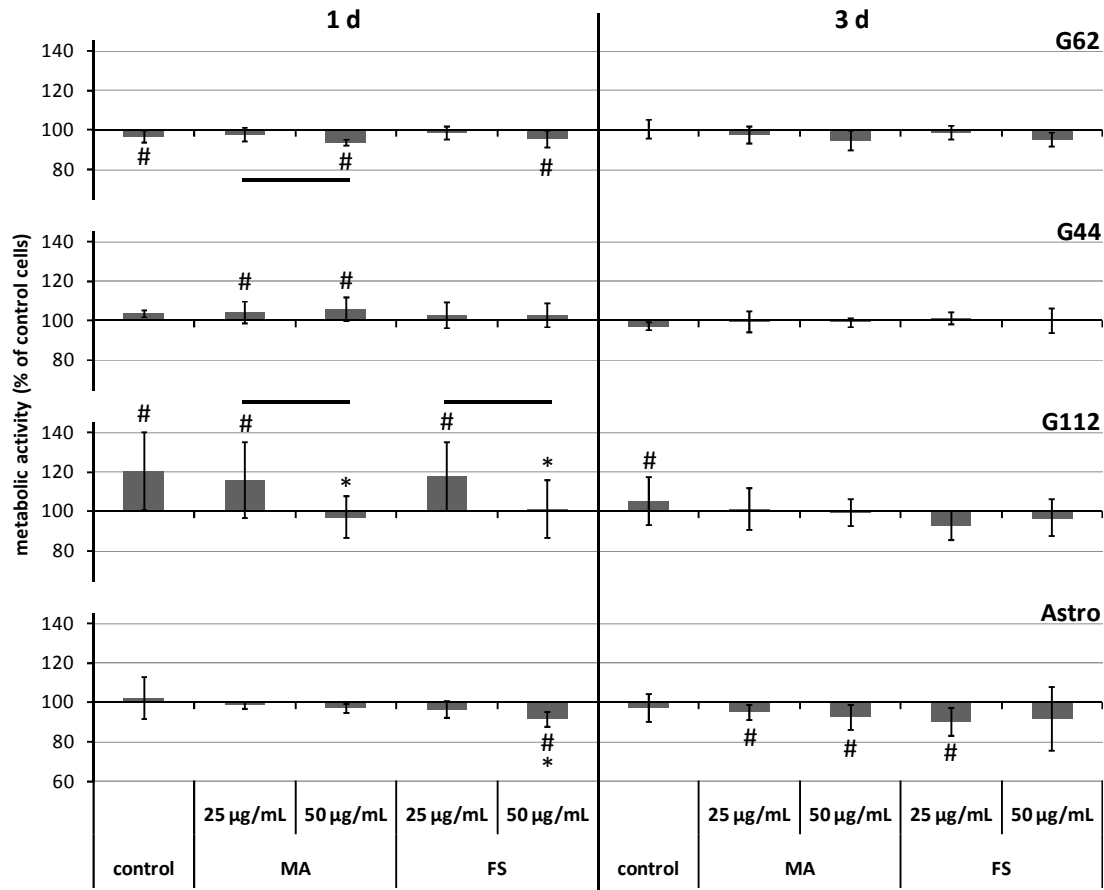

Figure 23: Metabolic activity after MNP loading and magnetic field application. The metabolic activity is depicted in percent of the according samples without magnetic field incubation after 1 or 3 d incubation without (control) or with MNP treatment and subsequent 1 d incubation in a magnetic field, mean ± standard deviation, n = 8, p < 0.05, # towards control without magnet, * towards control without MNPs, line between samples, 2-way ANOVA (Holm-Sidak post-hoc analysis).

After 1 d of MNP incubation, G62 cells showed low negative effects (94 % metabolic activity), when a magnetic field was applied. These decreases were similar to cells incubated for 3 d with MNPs. Low positive effects were detected in G44 cells (increases to maximal 106 %) which were reduced to normal level after 3 d of MNP incubation. In both glioblastoma cell types, MA treated cells were slightly more influenced compared to FS. After 1 d of MNP incubation, G112 cells showed relatively high increases of activity in control and 25 µg/mL MNP samples, when a magnetic field was applied (to 120 %), whereas

with higher MNP concentration, the activity declined to 97 % with MA and 101 % with FS, respectively. With longer MNP incubation time, the metabolic activity was not significantly influenced. Astrocytes showed decreases of the metabolic activity to 91 % with 50 µg/mL FS incubation after 1d. However, after 3 d of MNP incubation, also MA treated astrocytes had a reduced activity.

To summarize, the effects were small in all cell lines, except of G112, and the metabolic activity showed both, increases and decreases after the magnetic field incubation. There was a tendency, that higher MNP concentrations lead to decreases of metabolic activity. However, this effect was cell-line-dependent.

For confocal microscopy imaging, G62 cells were chosen as example for the glioblastoma cell lines due to their robust cell culture features. It was expected that they were the least influenced by the seeding on glass cover slips to gain meaningful data. Astrocytes were chosen as healthy control group.

Considering the actin staining in G62 and astrocytes, no remarkable distortions of the cytoskeleton were shown (Figure 24). The actin fibers were longer and more dense in astrocytes compared to G62, whereas mostly in areas with a lower cell density. The cell density differences resulted from an uneven cell distribution on the cover slips. Regions of similar cell density were not chosen due to the comparability of the distance to the magnet. The cells did not show a remarkable alignment or any drastic morphology changes that could refer to a MNP or magnet toxic effect, except of the islet formation in astrocytes incubated with FS.

According to the experiments above, the toxicity of the magnetic field on MNP-loaded cells in comparison to pure cells is negligible.

High strength magnetic field influence
In order to test the toxicity of a higher magnetic field strength, the static magnetic field of a magnetic resonance imaging (MRI) device was introduced. The 7 T field strength was applied to test the possibility of movement trials with MNP-loaded cells in such a device, as a higher magnetic field could not only increase the force on the MNP-loaded cells, but also the toxic effects.
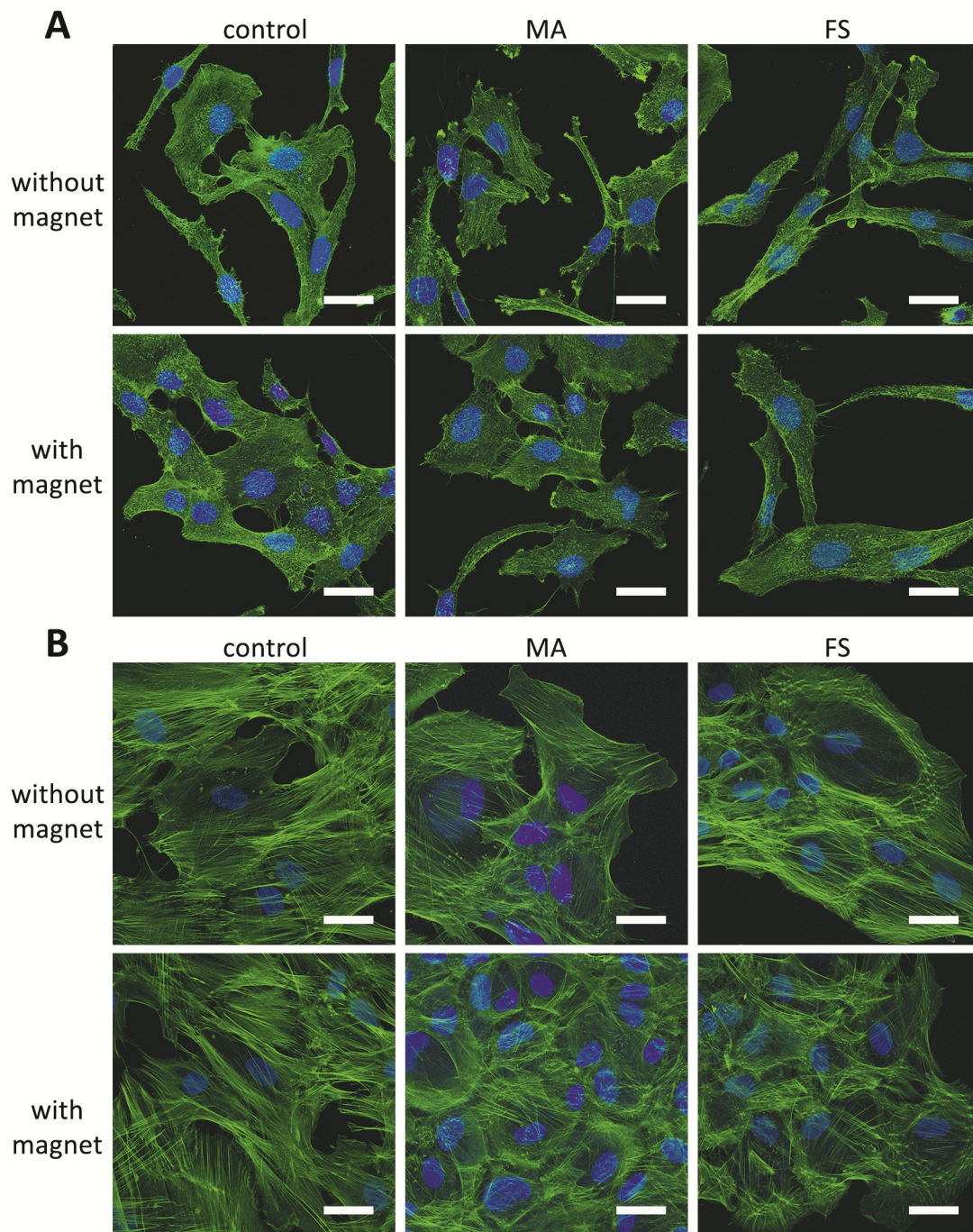
Figure 24: Actin staining with exposure to MNPs and magnetic field. G62 cells (A) and astrocytes (B) were incubated with 25 µg/mL MA or FS for 3 d and exposed to a magnetic field. Confocal microscopy pictures show actin fibres (green) and nuclei (blue).

The homogenous magnetic field of the MRI did not cause any differences of metabolic activity between samples without MNPs or with 25 µg/mL FS after 1 d of MNP incubation

(Figure 25). After 3 d MNP incubation, a significant but very small decrease of metabolic activity was detected in G62 cells exposed to the homogenous MRI magnetic field. Differences between the incubation conditions occurred in both MNP incubation times, while after 1 d a small increase and after 3 d a decrease occurred.

Thus, the high strength of the MRI static magnetic field is not harmful for MNP-loaded cells and could be used for further movement trials.
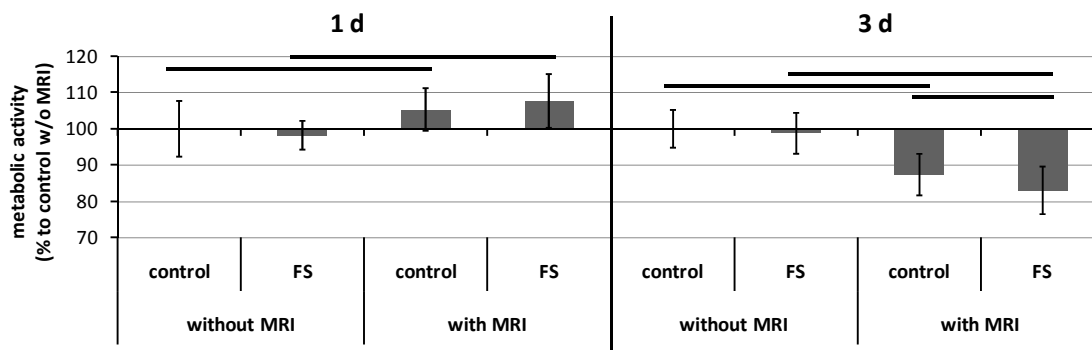

Figure 25: Metabolic activity of FS loaded G62 in MRI. G62 loaded with 25 µg/mL FS for 1 or 3 d were incubated overnight in a warmed chamber without magnetic field (without MRI) or in a warmed chamber in a 7 T MRI device (with MRI) before detection of the metabolic activity, mean ± standard deviation, n = 4 in sample 1d with MRI, remaining n = 4-6.

Non-adherent magnetic cell movement

Before testing the movement of MNP-loaded glioblastoma cells attached on a surface by a magnetic field, a setup for the evaluation of the force on the cells using permanent magnets was necessary. For this, cells were loaded with MNPs and detached before the magnet was added. Three setups were performed to evaluate their suitability for the task and to gather information about the most promising combination of cell line and MNP type, in order to see an attraction in the assays with adherent cells.

Magnetic cell seeding

The first setup tested was the fastest and easiest method to visualize the attraction of MNP-loaded cells by a magnet. The cells were seeded in a well with a magnet fixed below. MNP-loaded cells were expected to be pulled to the center of the well, where the magnet was placed, while control cells without MNPs should attach distributed in the whole well.

Indeed, control cells without MNP treatment remained largely spread over the whole well-surface and MNP-loaded cells were more distributed in the center of the well, above the magnet (Figure 26). The centralization seemed to be more effective with MA but the differences to the FS were low. The highest agglomeration in the center was achieved by incubation with Sig, where the cells were arranged in linear patterns. These patterns could

indicate the magnetic field lines, suggesting a high influence of the magnetic field forces on the Sig-loaded cells.

The microscopy pictures showed the forces of the 300 mT magnetic field on the MNP-loaded cells, that differed between the MNP types. However, a quantification of the attracted cells was impossible, supporting the development of other setups.
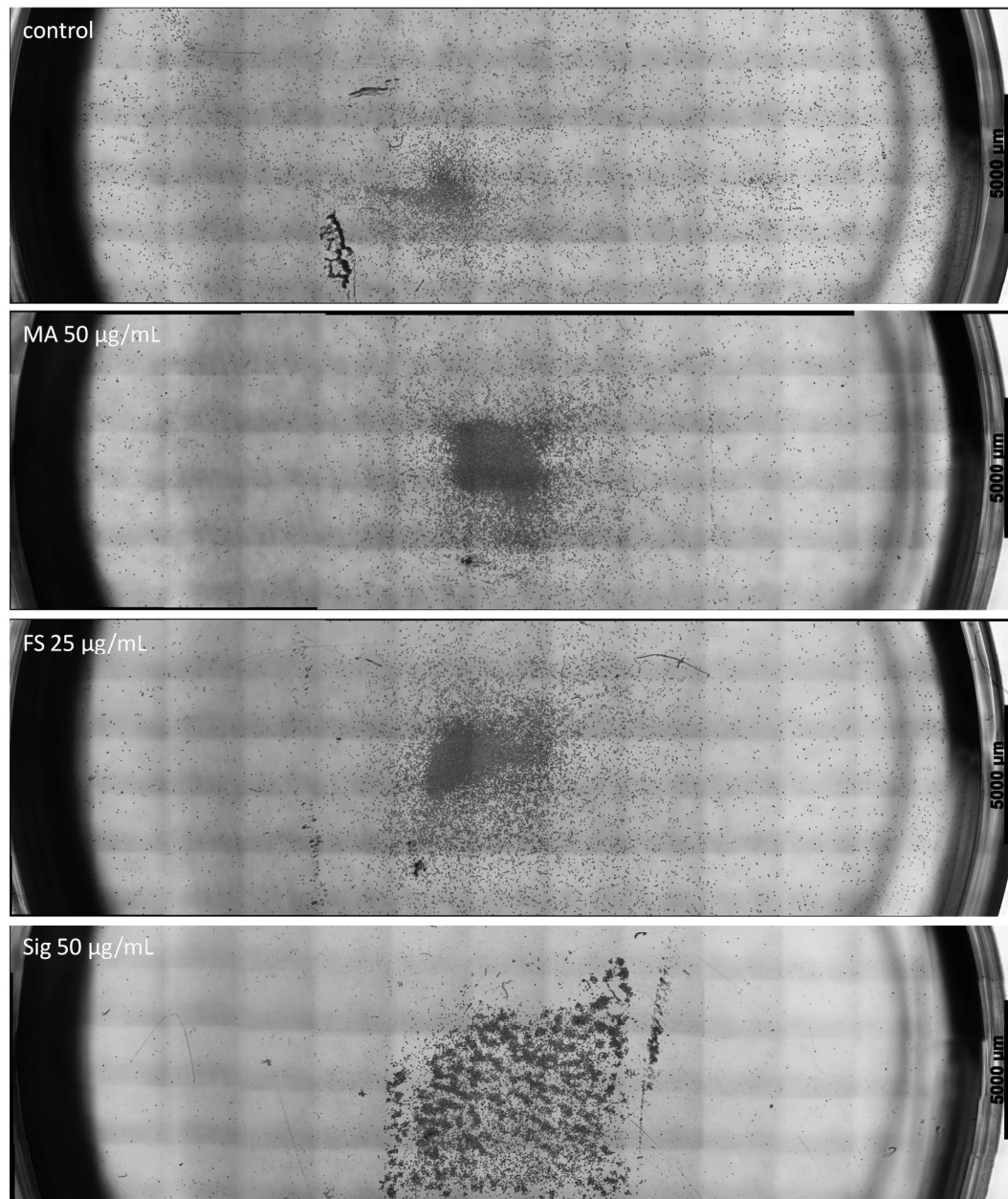

Figure 26: MNP-loaded glioblastoma cells seeded with a magnetic field. Overview microscopy images of G62 without MNPs (control) or incubated with 50 µg/mL MA or Sig or 25 µg/mL FS for 3 d, which were seeded in a well with a permanent magnet fixed below the plate, in the middle of the well.

Swimming discs assay

In the swimming discs assay, a quantification of the results was possible, as the cells pulled to a disc swimming below the magnet could be stained and counted. The cells, that were not attracted, were sinking to the bottom of the well and were thus separated from the attracted ones.
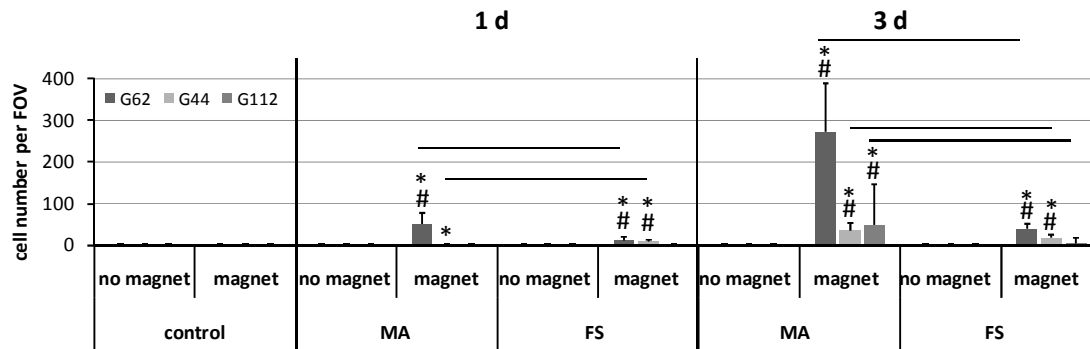

Figure 27: Swimming discs assay. Mean values per field of view ± the standard deviation of glioblastoma cells (G62, G44 and G112) attached on the swimming discs are shown after incubation without (control) or with MA or FS for 1 or 3 d, and with or without a magnet on top. Bars represent the mean, p≤0.001, # against control without MNPs, * against control without magnetic field, 2-way ANOVA (Holm-Sidak post-hoc analysis).

All types of glioblastoma cells without MNP incubation as well as MNP treated cells without magnetic field application showed any cell adherence on the swimming discs (Figure 27). After 1 d MNP incubation, most cells were counted on discs swimming with MA-loaded G62 cells and a magnet installed (52 cells). However, G44 and G112 cells treated with MA showed only few attached cells. With FS incubation, only 8-10 G62 or G44 cells were attracted, but still no G112 cells appeared.

After 3 d MNP incubation, more cells adhered on the discs incubated in the magnetic field, while there were still barely cells detected without magnet. Again, the highest numbers were detected in MA-treated G62 cells (272 cells), followed by G112 (49 cells) and G44 (34 cells) incubated with MA. The cells incubated with FS grew less on the discs, counting 39 G62, 18 G44 and 4 G112 cells.

The differences between the cell lines were expected due to variable iron levels after MNP loading, as well as the increased cell attraction after a longer MNP incubation time. However, a huge variability was also detected between the experiments, relying probably on the cell counting of five field of views and not of the whole disc. A great disadvantage of the assay was the difficulty to reproduce the dropping of the cell suspension and especially the handling of the discs. Thus, a further assay was developed.

Magnet channel assay

In this assay, the cells were pulled in a horizontal direction towards the magnet, allowing also judgements about the maximal distance for the cell attraction, as the cells were counted in 1-mm-areas. A similar MNP concentration was used for both MNP types to achieve a better comparability of the MNP type effectiveness.
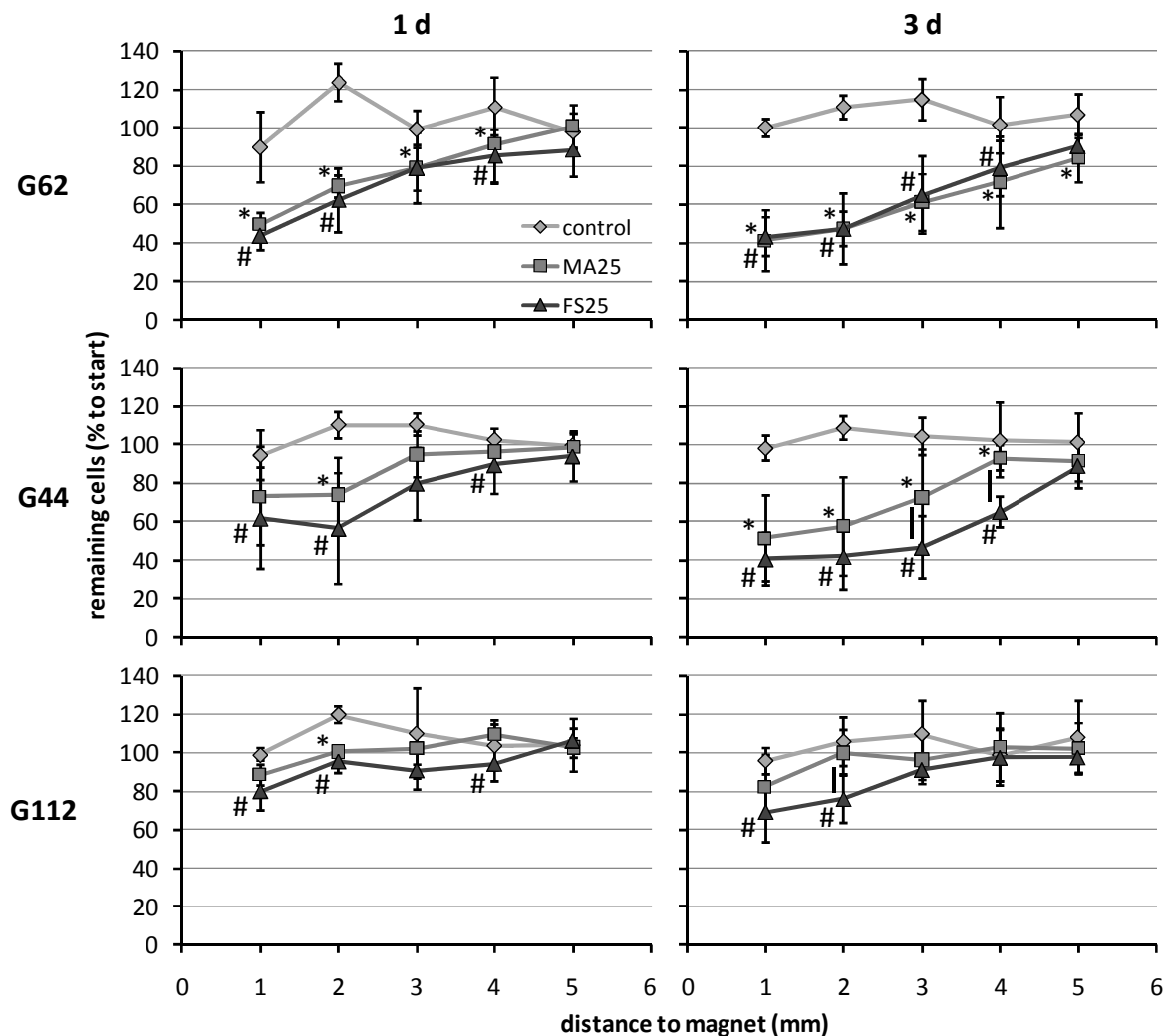

Figure 28: Magnet channel assay. Glioblastoma cells were loaded with 25 µg/mL MNPs for 1 or 3 d and the magnetic attraction was tested in a magnet channel trial. Data points represents the means ± standard deviations of remaining cells in different distances to the magnet, n=5 (2 independent trials), p<0.05, * MA towards control, # FS towards control, vertical lines between MA and FS, 2-way ANOVA (Holm-Sidak post-hoc analysis).

After 1 d MNP incubation G112 cells showed the lowest attraction to the magnet with more than 80 % remaining cells even in the nearest field at the magnet (Figure 28). G44 showed minimal 56 % remaining cells followed by G62 with 44 %. With a longer incubation time,

the attraction towards the magnet got stronger, especially for G44 and G112 cells (41 % and 69 %, respectively), while only minor more G62 cells were attracted compared to a shorter incubation (41 %).

Considering the distance, significant differences towards control cells were detected until 2-3 mm for G112, 3-4 mm for G44 and 4-5 mm for G62 cells. In most cases, higher distances towards the magnet were overcome after 3 d MNP incubation. If the cells were attracted in a higher distance, the amount of remaining cells near the magnet was also lower.

FS loaded cells were better attracted than MA loaded ones, however, only few significant differences between the MNP types occurred, and all of them after 3 d of MNP incubation. The slight increase of control cells after magnet application shows that likely not all cells were sedimented after 5 min and settled down during the incubation in the magnetic field.

As expected after the MNP loading experiments, the attraction of the cells differed between the cell lines. Thus, G112 cells were neglected for further trials, due to their weak attraction in comparison to G44 and G62, which gained more similar results. However, the differences between the MNP types was low, so that neither MA nor FS could be excluded from the further trials.

Adherent magnetic cell movement

Similar to the non-adherent cell movement, also several methods were tested to find the most suitable assay for the movement of cell attached to the surface. During the directed movement testing, also means to increase the cell migration *in vitro* were examined.

Cylinder assay

Firstly, the outgrowth of cells, which were seeded in a spot with the help of a glass cylinder, was evaluated without MNP incubation. The handling of the cylinders was tested during an experiment about the possible migration enhancement of glioblastoma cells after a surface coating with the protein laminin, which was shown to increase the glioblastoma cell migration *in vitro*.

By the comparison of the microscopy images after 3 d of growth, the cells did not remarkably enhance the migration out of the original circle than control cells without any coating (Figure 29). Thus, laminin coating was not used for further experiments.
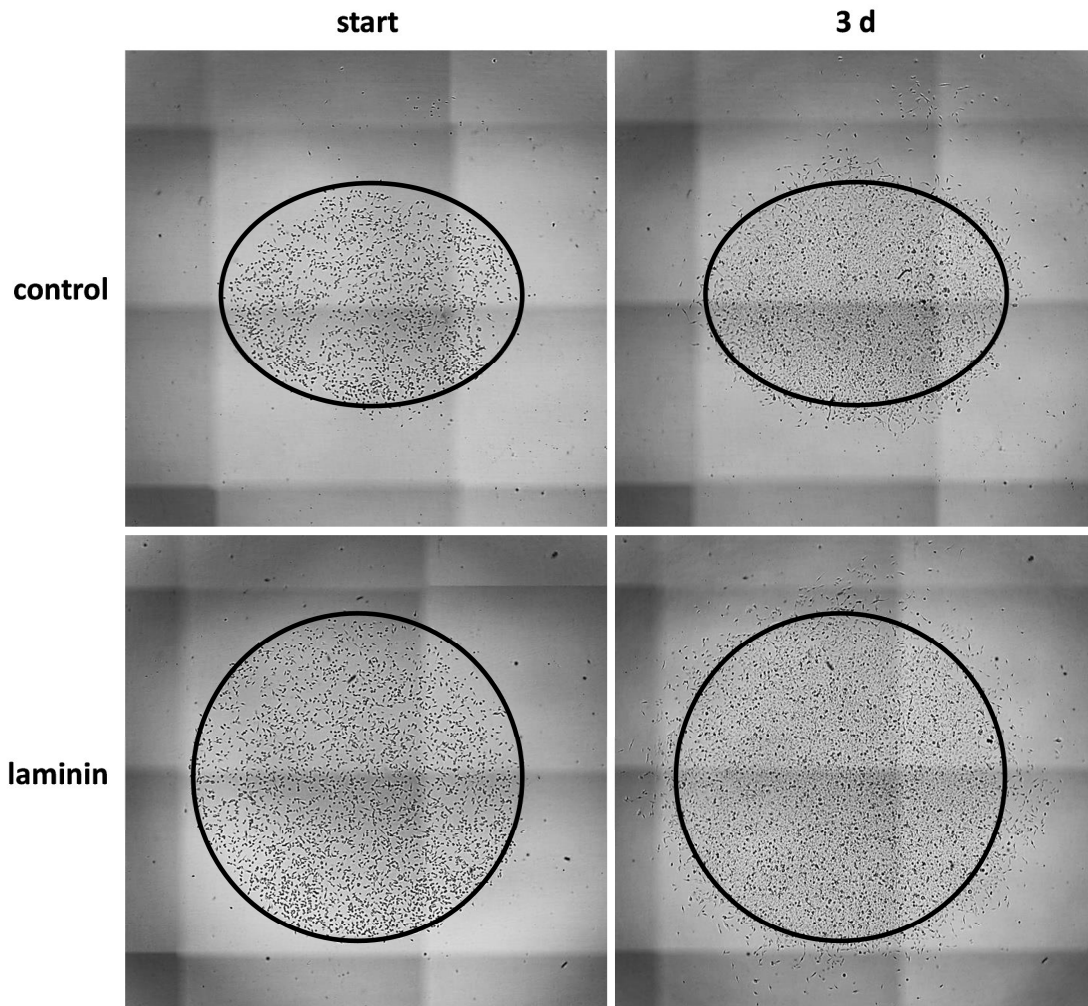
start 3 d

control

laminin

Figure 29: Laminin coating test with cylinder assay. G62 cells without MNP exposition were seeded in a spot (marked by the black circles) and the growth out of the spot was examined with laminin coating and without (control) for 3 d, scale=1 mm.

Considering the setup, it was not always possible to prevent the cylinders with the cell suspension to stay at the initial position during the cell adherence phase. Reasons for this slipping were probably the low adherence of the cylinders at the surface, also because of the coating solution, and movements during the transport of the plates to the cell culture incubator. This led to non-circular or even completely scattered patterns on the surface, which were difficult to compare with other samples. Furthermore, the round shape was not suitable to observe a clear cell front, thus, a quantification of the observations was difficult.

Ibidi® insert assay
The assay with the inserts from ibidi® GmbH was based on the similar outgrowth principle like the cylinder assay. However, the ibidi inserts had even edges, that enabled an easier comparison between different samples and time points. The outgrowth at the side pointing to

the magnet can be compared with the opposing side. Due to the silicone material, they stuck perfectly on the surface of a multi-well plate, if no coating was applied before. With this setup, rhodamine and the hepatocyte growth factor (HGF) in the medium were tested to increase the natural glioblastoma cell migration *in vitro*. This could be useful to fasten the experiments of the magnetic guidance and to show the effect more clearly.

Indeed, in a first experiment, MA-loaded G62 cells showed a clear shift to the magnet with rhodamine treatment, while in control cells, a quite similar outgrowth to both sides was observed (Figure 30). However, this result was not reproducible in the second trial. By fluorescence microscopy of rhodamine-treated cells, the seeding densities within the cell spot were visualized. In Figure 31, the areas evaluated for the migration trial were marked with white frames, showing that in the first trial, the cell density on the right edge (to magnet) was much higher than on the left side (away from magnet). In the second trial, the densities on both sides were more similar. Besides the lack of reproducibility, G44 cells showed less adherence when incubated with rhodamine and cells additionally treated with FS even reduced the cell number (Figure 32).

In trials with the HGF, no clear difference in cell outgrowth was observed between samples with or without HGF treatment (Figure 33). Considering the magnetic guidance, the outgrowth seemed always stronger on the right side, independent from the magnet position.

Both, the cell migration from a cell spot and the addition of migration-enhancing chemicals was not convincing. Thus, assays based on a normal cell seeding were focused.

Rhodamine trial 1

Rhodamine trial 2

start

1 d

start

1 d
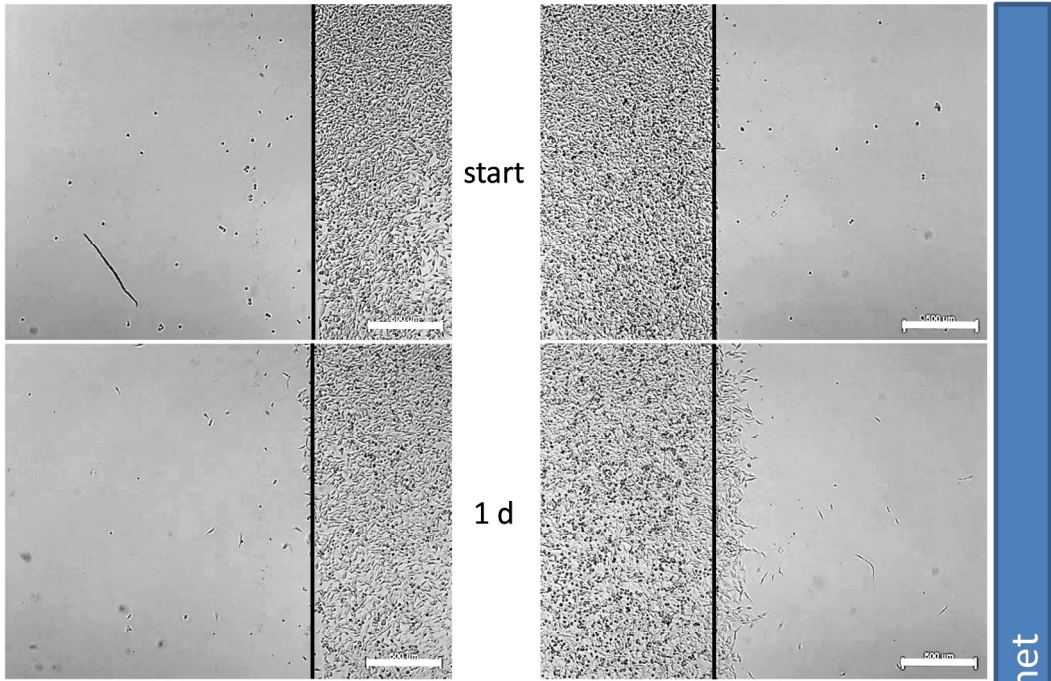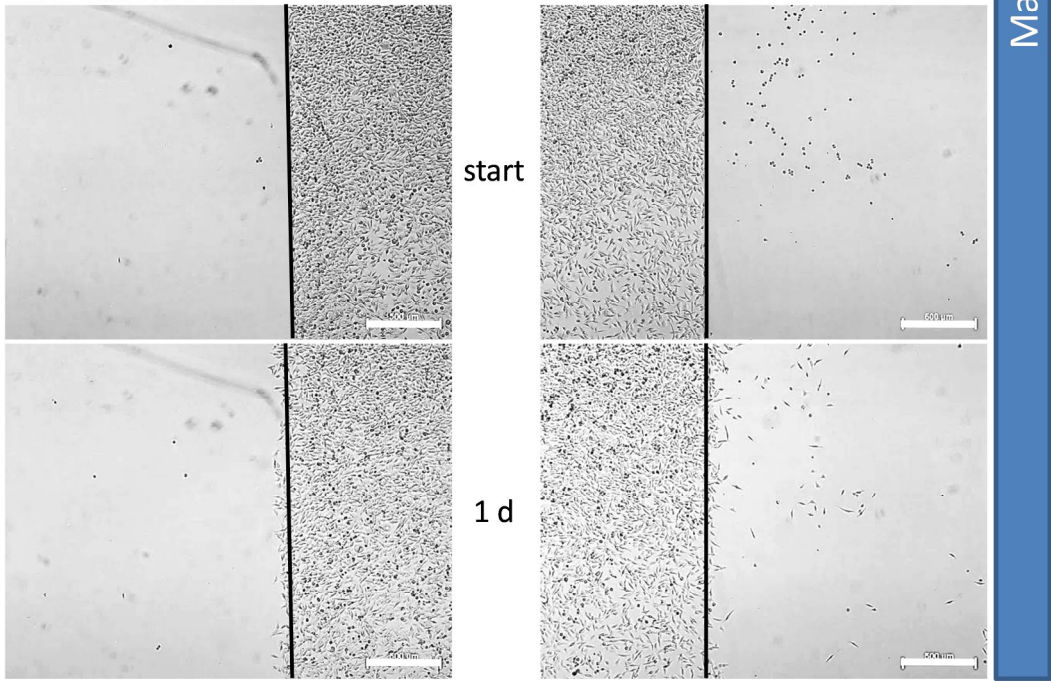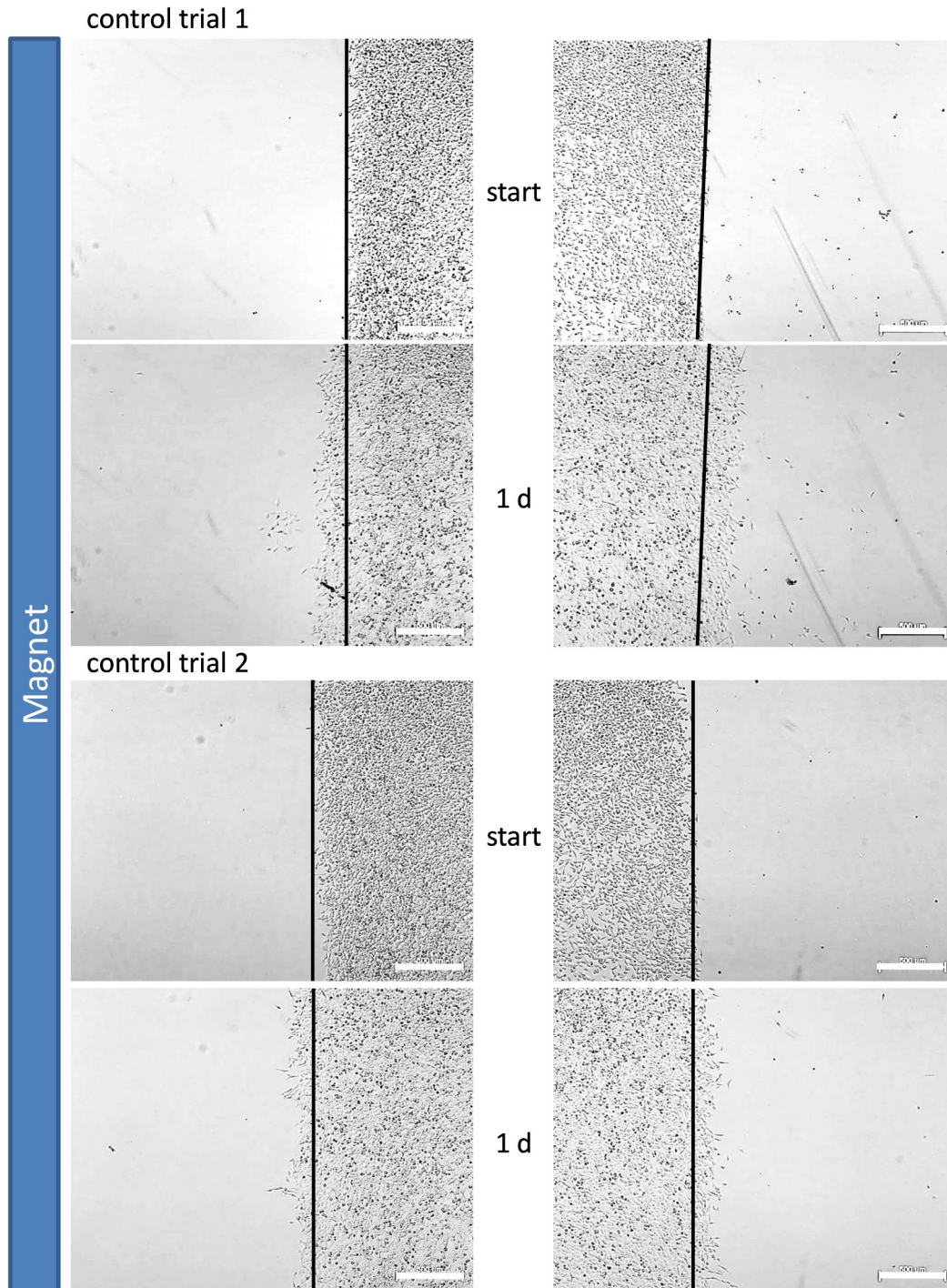
Magnet

Figure 30: Magnetic movement of adherent cells with rhodamine. G62 incubated with 25 µg/mL MA for 1 d were seeded in ibidi inserts without (control) or with 50 µg/mL rhodamine in the medium. A permanent magnet was fixed at the side (marked by the rectangle) and pictures of the edges were taken before (start) and after (1 d) magnetic field incubation. The lines mark the cell fronts. The experiment was repeated, showed in rhodamine 2 and control 2, scale = 500 µm.
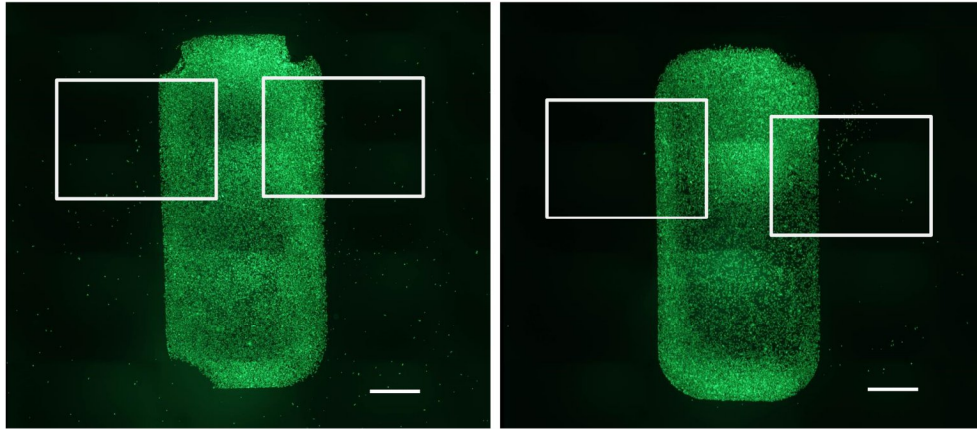
Figure 31: Density check of cells with rhodamine in ibidi insert assay. G62 were incubated with 25 µg/mL MA for 1 d following rhodamine staining (bright). Left 1st trial, right 2nd trial. The magnet was subsequently fixed on the right side of each well, scale=1 mm.
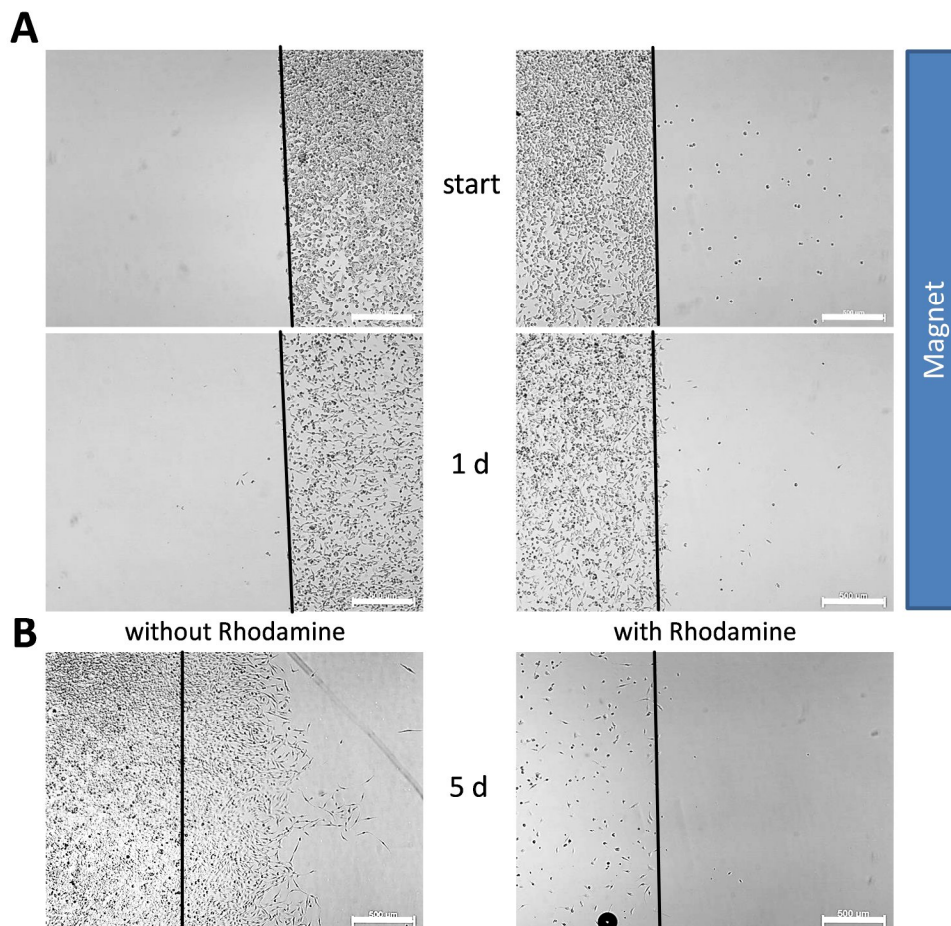
Figure 32: Ibidi insert assay with rhodamine and FS. A: G62 were incubated with 25 µg/mL FS for 1 d and seeded in a spot with ibidi inserts. A magnet was placed at the right side (rectangle) and incubated for 1 d. B: Comparison between FS-loaded G62 with or without rhodamine treatment after 5 d incubation, scale = 500 µm.

Figure 33: Magnetic movement with HGF. G62 cells were incubated with 25 µg/mL MA for 1 d, before HGF was added to the medium and a magnet (marked by the rectangles) was fixed at the side for 1 d. The control shows MA-loaded G62 without HGF, scale = 500 µm.

Transswell assay

In order to quantify the migrating cells, the number of cells that passed a membrane was counted in the transwell assay. The magnet below the plate should increase the movement of the MNP-loaded cells through the pores of the membrane in comparison to control cells without MNPs.

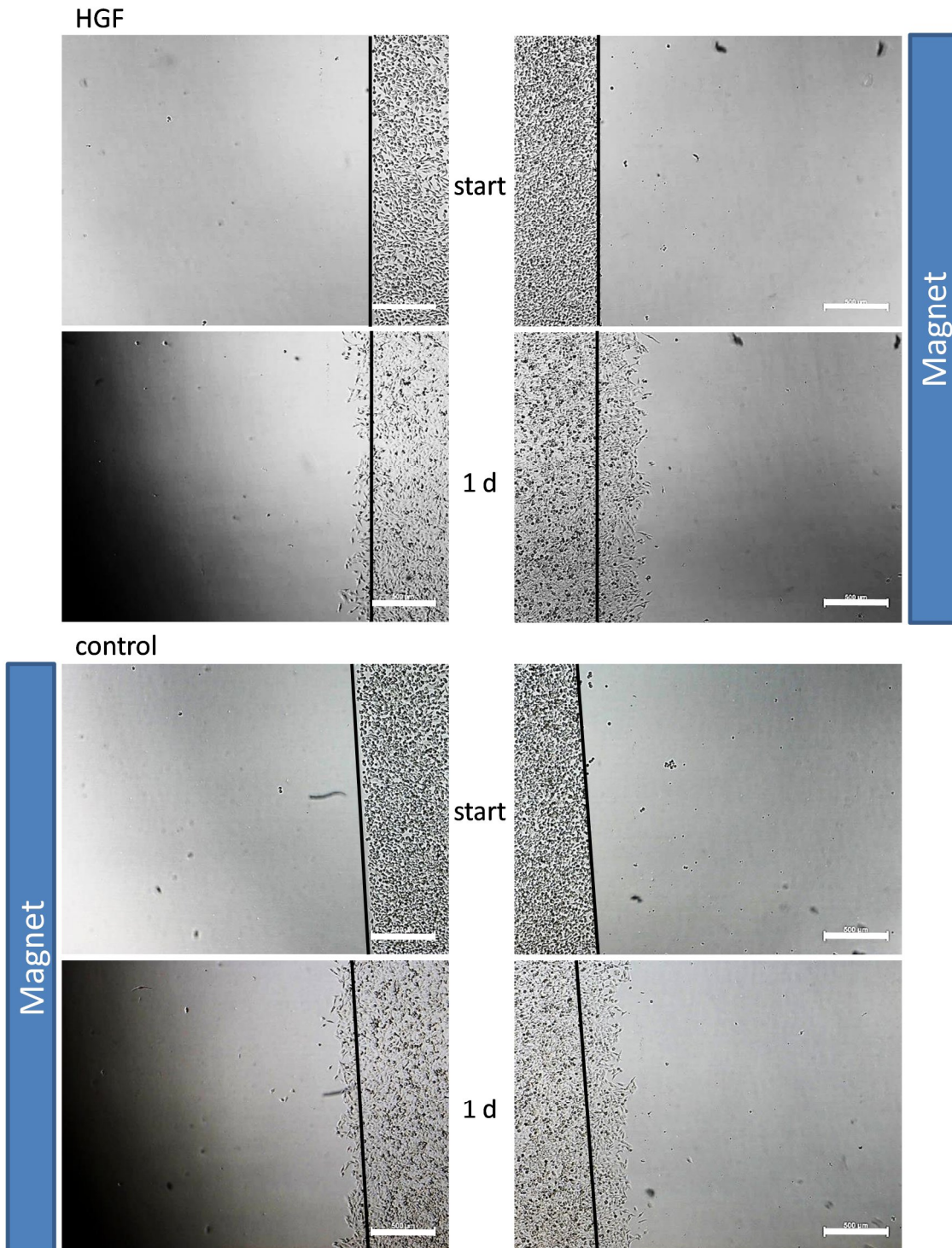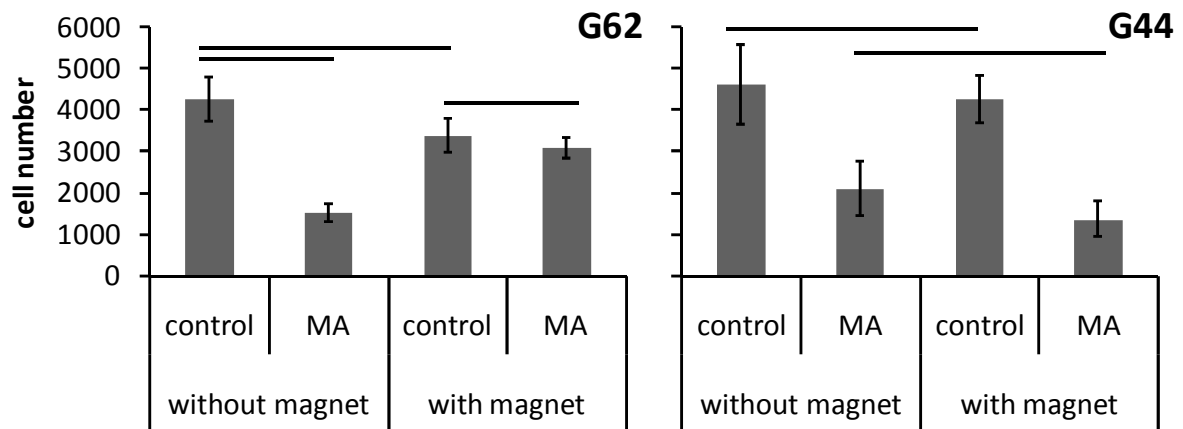**Figure 34: Transwell inserts for magnetic movement.** G62 and G44 were incubated without MNPs (control) or with 25 µg/mL MA for 3 d and transferred to the membrane of the insert. After in the magnetic field, the cells below the membrane were trypsinized and counted by microscopy, lines p≤0.05 (two-way ANOVA), n=6 (duplicates, 3 technical replicates).

In this setup, control G62 cells placed on a magnet showed slightly fewer cells in the compartment (4275 cells) below the membrane, compared to control cells without magnetic field treatment (3385 cells). In contrast, control G44 cells did not show any significant differences between incubation without or with a magnetic field (4640 and 4268 cells). If loaded with MA, both G62 and G44 showed a significantly reduced cell number in the lower compartment compared to control cells (1516 and 2124, respectively). When a magnetic field was applied, G62 cell number significantly increased in the lower compartment to 3084 cells, whereas G44 cell number slightly decreased compared to no magnetic field incubation (1369 cells).

As the MNP-loading decreased the cell number passing the membrane, compared to control cells, the setup was likely not suitable for the magnetic attraction experiment. Additionally, the handling of the assay revealed some drawbacks, as for example the cells could not be observed during migration.

12-well assay

In the 12-well assay, the distribution of cells cultured in 12-well plates was evaluated before and after the magnet incubation, avoiding outgrowth from a spot. As the magnet was

positioned at the outer wall of the well, it did not disturb the visualization of the cells and was still in close vicinity of the cells. The staining of the cells prior to the magnet incubation could influence the results, but was necessary for the cell quantification.
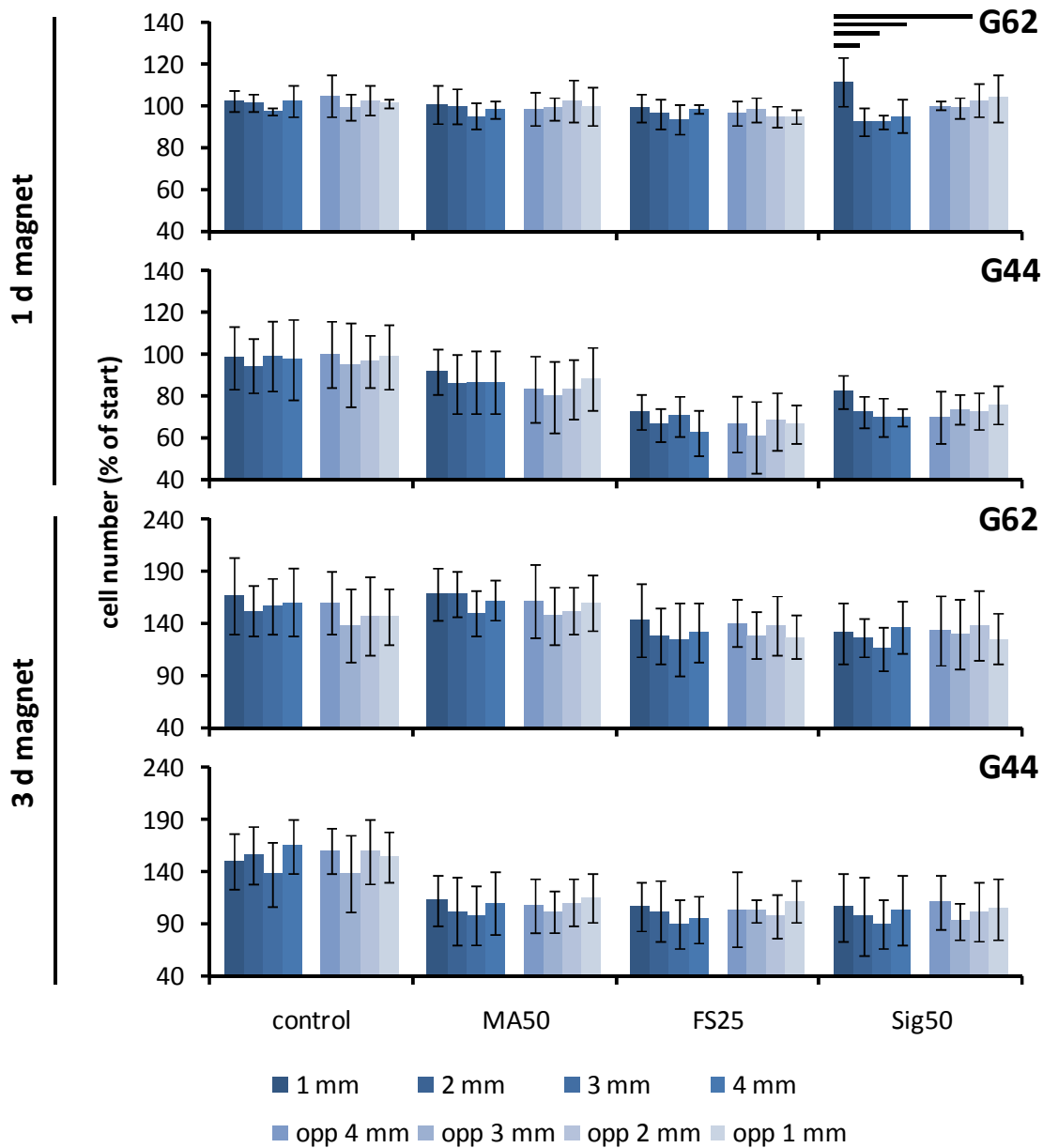
Figure 35: Adherent cell movement in a magnetic field in the 12-well setup. In a 12-well assay, control and MNP-loaded G62 and G44 cells were incubated with a magnet fixed besides the well for 1 or 3 d. Before (start) and after magnet application, pictures were taken and 1 mm areas in increasing distance to the magnet (1-4 mm) and at the other well side (opp 1-4 mm) were counted and related to each other (% of start), lines show p≤0.05, 2-way ANOVA (Holm-Sidak post-hoc analysis), n=6.

After 1 d in the magnetic field, there was no significant difference of remaining cells between all areas near the magnet or on the opposite side of the cell culture well (Figure 35). One exception were G62 cells treated with Sig, where the cell number in the area nearest the magnet increased significantly (112 %) compared to the areas farer away from the magnet (92-96 %). A similar trend was visible in G44 cells loaded with Sig (82 % nearest magnet, 70-72 % farer magnet); however, the differences were not significant. A reduction of the cell number between the samples was detected in G44 cells treated with MA (80 %) and particularly with FS (61 %) and Sig (70 %), compared to control cells (95 %).

After 3 d magnetic field incubation, no significant difference between all areas was detected, even within Sig treated samples. The cell loss in G44 cells was still visible in MNP treated cells compared to control, whereas it was less intense (minimal 90 % with FS).
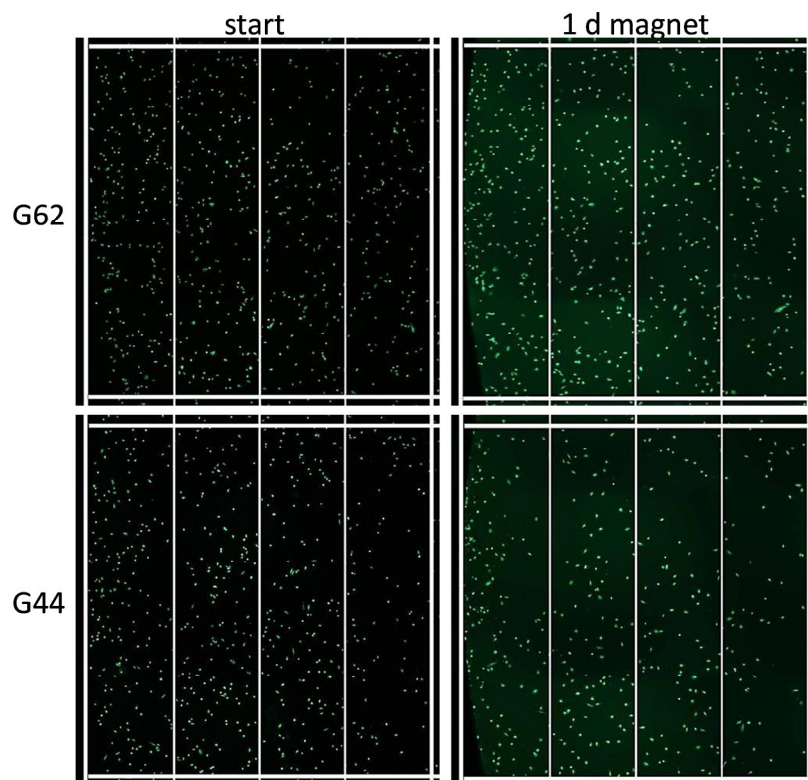
Figure 36: Stained cells of the 12-well assay. For the 12-well assay, G62 and G44 were incubated with Sig for 3 d, followed by Calcein staining and incubation with a magnet fixed on the left side, areas (separated with white lines) are 1 mm broad and 4 mm long.

In Figure 36, examples images of the 12-well assay are presented. In comparison with the amount of cells (green spots) at the beginning of the experiment, G44 showed a loss of cells after 1 d incubation in the magnetic field. The cell number of G62 cells under similar

condition was comparable with the start image. Thus, this loss of cells was not caused by a miscounting and the cells seemed to disappear during the magnet incubation time.

The 12-well assay could not show a directed cell migration towards the magnet of cells loaded with MA or FS, however, a cell displacement was detected with Sig-loaded G62 cells. As a similar, yet not significant trend was observed in G44 cells, an MNP-related effect was assumed. Thus, live-cell imaging was performed with NEDD9-2 cells treated with Sig.

Live-cell imaging

The movement of Sig-loaded cells detected in the 12-well assay was examined by live-cell imaging, where a video was taken to follow the cell movement in the magnetic field.

Figure 37: Pictures of live-cell imaging. NEDD cells were incubated with Sig prior to magnet application (left side) and live microscopy. White circle marks cells detaching during cell division and floating to the magnet, time between pictures = 20 min.

In the live-imaging experiment, NEDD9-2 cells loaded with Sig showed movement to the magnet, attached at the side of the well. However, before the movement to the magnet, the cell rounded up and detached from the surface. Some filaments, that attached the cell on the surface, were stretched and torn as the force from the attracted cell became too strong. Although the NEDD9-2 cells are not glioblastoma cells, their migration principles and the cell culture conditions are similar to most cell types *in vitro*. Thus, the results of the live-cell imaging can be transferred to the Sig-loaded glioblastoma cells in the 12-well assay, illustrating their movement mechanism.

Discussion

The work was divided in several parts:

- characterization of the main actors, thus MNPs, cells and magnetic field

- loading of the cells with MNPs under different conditions

- potential side effects of the MNP loading and the magnetic field

- development of setups for the examinations of cell movements in the magnetic field

- examination of non-adherent and adherent cell movement in a magnetic field.

Characterization of the material influences

MNP reaction to the cell culture medium

One of the main actors of MNP loading is the type of MNPs. The MA and FS were chosen because of their magnetic properties and biocompatibility. Their small size should facilitate the uptake into the cells, leading to higher iron amounts inside the cells and thus to a higher magnetization ability. It is known, that the kind of fluid, in which the MNPs are suspended influences their properties, for example the aggregation of MNPs is affected by several parameters like pH or ionic strength [48]. Particularly the proteins in the serum are known to affect the MNP size by forming a so-called corona [62]. Thus, the MNPs were suspended in normal cell culture medium and a size measurement was performed to evaluate the behavior of the MNPs.

MA and FS showed a different size distribution when diluted with water, as MA particles were bigger with a more dispersed size and FS showed a clear peak. This difference in size appeared likely due to the coating, as the iron oxide core of both MNP types was quite similar with about 6 nm diameter. If diluted with cell culture medium containing FBS, the size of MA increased only slightly, while FS size nearly doubled which can be attributed to an adherence of serum proteins or an agglomeration of the particles. The relatively low protein influence on MA is in accordance with a study by Avdeev et al. [117], where the great stability of MA was demonstrated. The adherence of proteins at the surface of the MNPs is called a corona, which establishes within the first minutes after MNP contact to proteins and changes over time [62]. Bajaj et al. [58] demonstrated that the protein corona reduced the uptake of MNPs. However, the addition of FBS is crucial for the growth of most cell types *in vitro* and proteins are also of importance *in vivo*, e.g. in the blood plasma [140], so that these effects have to be accepted in MNP uptake studies. Interestingly, FS still showed a smaller peak of the original particle size, indicating that not all FS were affected by the medium.

Also in the course of time MA and FS behaved differently in the medium: After 3 d of incubation, more agglomerates appeared in FS samples, while the size distribution of the MA samples did not change remarkably. Even after 3 d incubation, in both MNP types particles in the nano-range were still detectable, so that potentially the loading of cells could continue even after a longer incubation time. That is the reason why the incubation over a longer time was chosen in subsequently loading experiments. The optimal loading size of NPs examined in former studies was between 30 and 50 nm [50], [51], which is also in the size range of the less effective NP transport to the cell surface, as both the diffusion and the sedimentation speed are the lowest [141]. Thus, a longer incubation time could increase the MNP amount at the cell surface and therefore the cellular uptake. A large loading with the MNPs was aimed because of the small iron core of the MNPs, which is however responsible for the magnetic attraction forces.

Cell donor variability

Another main actor of the MNP loading is the cell type. As for all tumors, a high patient variability influences the cell properties, while leading to a similar kind of malignancy. This donor variability can be partially transferred to the *in vitro* setups by cell lines derived from the similar tumor classification but different patients. For example, the glioblastoma cell lines used for this study consist of a different karyotype but were all derived from glioblastoma tumors [124]. Conversely, the cellular behavior *in vitro* could indicate the reaction of the different tumors *in vivo*. Tucker et al. [142] suggested that the general tumor cell characteristics like growth or hypoxia were weak indicators for a clinical outcome; however, the survival tested *in vitro* was well predictive. Indeed, it was shown that even if a target of a chemotherapeutic was expressed in all glioblastoma cell lines in a study, the response of the tumors was highly variable [143]. Taken the donor variability and the weak correlation of general cells properties to a therapy success together, testing a therapeutic substance or treatment requires different cell lines to proof the effectiveness of a potential therapy.

The three glioblastoma cell lines from different human donors were chosen to examine the donor-related differences in cell properties and behavior. It is known that the glioblastoma cells are mostly small and have variable shapes (glioblastoma multiforme) [1], what could be also seen within the glioblastoma populations examined. Nevertheless, the differences in morphology and growth behavior *in vitro* between the glioblastoma cell lines G62, G44 and G112 were more remarkable. Considering the growth rate, G62 and G112 reached similar cell numbers in a comparable time frame, while G44 grew slower. Also, the cell diameter was similar between G62 and G112, while G44 cells were bigger. This may lead to the assumption, that G62 and G112 could show similar behavior. However, considering the cell

membrane integrity, G62 showed a remarkable robustness, while G44 and G112 reacted more sensible to increasing cell numbers.

Also, the differences in morphology pronounce the glioblastoma cell line variations. The cell shape and spreading on the culture well surface differed remarkably from each other and the microscopic pictures showed divers shape conversions in the course of proliferation time. Particularly the G112 islet growth differed from G62 and G44 behavior. This might indicate that G112 cells did not move far after cell division, thus explaining why the cells in the center of the islets were smaller and rounder than at the edges. Additionally, this could explain the decrease in cell viability of G112, as the cells in the islet center die, while the maximal confluence is not yet reached. The pronounced shape conversion of G44 fits to the high viability loss in the proliferation assay, suggesting that these cells react sensible towards higher cell density. In contrast, G62 cells with their stable viability showed only a minor shape change, pronouncing a potential high robustness at least against space limitation. This could indicate, that G62 cells are in general robust against sub-optimal culturing conditions, for example the addition of cell dyes or magnetic fields, and maybe also against possible adverse effects of the MNP loading. Additionally, the even distribution of the cells in culture might suggest a high migration potential. Thus, G62 could be the ideal cell type for the magnetic movement experiments.

Apart from the obvious similarities and differences of the cell lines itself, the cell density as a seeding condition had a strong impact on the cell properties. This was demonstrated in the proliferation assay by using different seeding densities in parallel. The parallel plateau formation of the cell number and the diameter showed a high dependence of cell properties towards each other. However, this plateau was not reached at the same time point using similar cell densities, probably due to different initial cell sizes and growth patterns. The influence of the seeding density on growth was also shown in a study with MSCs, where also the growth pattern of cultures was found to differ because of seeding density [144]. This shows that the original cell donor variations are aggravated by the *in vitro* conditions selected for the experiments. To obtain results that are not too much influenced by the seeding conditions, it is important to focus on the individual cell size and growth rate. Then, the cell seeding density could be adapted in advance of a cell-based study or, if not possible, the seeding conditions should be considered in the experiment evaluations. Thus, for the loading experiments, the seeding density of G44 was reduced compared to G62 and G112, because of the dramatic changes in morphology after a longer cultivation.

The human astrocytes used as control group showed extreme differences compared to the glioblastoma cells. The cells were not much larger in diameter than G44, but much more

spread on the surface of the cell culture well. As usual for most healthy primary cells, they grow much slower than the tumor cells; however, they followed the similar relation of growth and diameter development. Due to the different behavior, large differences to glioblastoma cells in MNP loading were expected, although it was unsure, whether the loading would be more or less effective. The loading of the astrocytes would give an insight into the side effects of the cancer therapy with MNPs, as the affected area of the MNP-based therapy in the brain could be probably not restricted to glioblastoma cells. Because of their high abundance in the brain and their role in the iron metabolism [145], astrocytes were chosen as ideal control cells for the MNP loading and toxicity experiments.

Differential loading within glioblastoma cell lines

The aim of the MNP loading experiments was to investigate,

- which MNP type lead to higher iron loads per cell,

- whether the cell types accumulate MNPs in a similar amount and

- how the incubation conditions (MNP concentration and time) affect the loading.

In order to get information about the cellular MNP amount, the iron level of the cells after the MNP treatment was detected. As the MNP concentration added to the cells was also calculated on the basis of the iron concentration, a direct comparison between the iron in suspension and in the cells could be made. Also, a comparison between the MNP types was possible. Because of the nearly similar iron core diameter of MA and FS and the same core material, it was assumed that the particle concentration was also similar.

The cells incubated with FS had in general a higher level of iron than those with MA. In contrast, in a study by Soenen et al. [146], neuronal progenitor cells were loaded to a higher degree with lipid- compared with dextran-coated MNPs. However, even small changes on the MNP coating were shown to affect the cellular uptake [54], [53], so that loading differences between MNPs with similar coatings can occur. As there are no guidelines about loading conditions like MNP (or iron) concentration or incubation time, a direct comparison of loading results of different studies is nearly impossible. Moreover, transfection agents such as Lipofectamine are often added to facilitate the MNP uptake [147], [146], which in turn increases the complexity of the loading conditions and the cell toxicity. Thus, it is suggested that the loading capacity of MNPs has to be checked for each special MNP type in the individual experimental setup.

The strong concentration-dependent increase of iron load with FS offers the possibility to increase the iron load easily with increasing dose. The comparatively low loading of FS with

5 µg/mL concentration may be explained by the observation, that very small MNPs are only taken up after they assembled into bigger cluster on the membrane [46]. Thus, too few FS could have bind at the cell surface to trigger the uptake, while higher amounts of FS were sufficient for an incorporation. The binding of serum proteins to FS shown in the size measurement could have reduced the cell loading especially with low MNP concentrations. Else, the corona formation did not seem to inhibit the loading, as a linear increase of cellular iron was detected. The dose-increase of MA was far less connected with an increase of iron amount per cell, possibly due to a saturation of loading. The saturation of the MA loading suggests that MA was taken up by an active mechanism because of the restricted workload of transport mechanisms. In contrast, lipid-based MNPs were supposed to fuse directly with the membrane without using energy for active transport and thus are taken up easier by the cells [46]. The lipid coating-based fusion of MA with the cell membrane could be hampered by the adhesion of proteins at the MNP surface. However, the size increase of MA was low in the DLS experiment, indicating only few protein adherence. Prior to the uptake, the adsorption of MNPs on the cell surface is necessary. This adhesion is only possible at special sites of the membrane and thus a saturation may occur, if all sites are already blocked. As the membrane consists of areas of different charges, the saturation of the binding sites is true for both, lipophilic and lipophobic particles [148]. So, the saturation of MA loading is not a proof for an active loading mechanism, but could also demonstrate a saturation of the cell surface binding sites. For FS, this saturation was not observed in the present study. This leads to the assumption, that the cells are using a different cell loading mechanism for MA and FS, especially because the iron amount in the medium was kept similar for both MNPs.

The assumption of a different loading mechanism is supported by the time-dependent loading behavior, where FS showed a nearly linear increase, whereas MA iron loading was less homogenous and even decreased in some cases. An explanation can be the cell growth, which has to be considered in long-term experiments. As the loading with MA was more depending on the growth, the uptake of MA was assumed to be more slowly. This could also explain the decrease in iron detected in G44 between day 1 and 2. If the cells are growing faster than the uptake proceeds, the iron amount per cell is diluted during cell division. Similar observations were published by Kim et al. [61], who found out that the iron load per cell also depends on the cell cycle phase: right after division, the iron load per cell is lower compared to other phases. Thus, in a later culture period, where the cell division was reduced due to space limitation, the iron amount per cell increased largely. In contrast, FS loading was far less affected by the growth of the cells, indicating a faster loading mechanism.

Another effect of the cell growth was shown in the iron visualization in the cells: the iron amount varied greatly within the cell population. One reason could be the different cell cycle phases as described above, another could be the asymmetric cell division. In a study with gold particles [149], the uneven distribution of particle-containing vesicles was demonstrated. The unpredictable loading of the single cells was assumed to be a kind of a risk management of the cells, where potential toxins in endosomes are burden on only one of the daughter cells. However, in another study [66], an equal distribution of MNPs after cell division was observed. For a therapy concept based on MNP incorporation, the uneven MNP distribution has to be considered. That is the reason why in magnetic trials of this study, no pre-selection of MNP-containing cells was performed and a quantification of magnetically moved cells was preferred.

Considering the cells, not only the growth rate played a role in the MNP loading. Although G62 and G112 had similar growth rates, G112 reached far lower iron loads than G62 with both MNP types. This was also shown in the iron staining trial, where small iron signals were detected mostly in the center of the islets. As the islet growth was the biggest difference towards the other glioblastoma cell lines, this special G112 cell property might be the reason for their low iron loads. An explanation could be the small cell body spreading on the surface. It is known, that the cell surface area is important for the uptake of NPs and that smaller cells take up less MNPs than bigger ones [146]. This would also explain that similar or more iron was detected in G62 and G44 cells, as G44 cells were bigger and more spread than G62, offering more surface for the FS loading.

Another reason of the low MNP loading of G112 might rely on the different growth rate of the cells within the colonies. The cells in the center are not dividing due to space limitation and thus can accumulate more iron while the cells at the edge are diluting their MNP load fast. Described in a scenario, the initial uptake of iron into a G112 cell was relatively high and only few diluted during division. The daughter cells were not migrating far from the mother cell which could explain the islet formation. This leads to a proliferation stop of the mother cell, which is keeping its iron. In the mean time, the cells more at the edge of the colony grow faster due to more space availability and thus, the iron was faster diluted. Taken together, this study indicates that not only the speed of growth but also the growth pattern influences the final load of MNPs in a cell population and in a single cell. This is in accordance with Snijder et al. [150], who found that cell population parameter influences the properties of a single cell, as for example the cell size or the endocytosis.

Summers et al. [149] stated that the uptake of nanoparticles in a single cell is unpredictable, due to the cell heterogeneity and random particle dynamics. Furthermore, the uneven

distribution of MNPs after cell division and the differential loading between MNP and cell types [59] impairs the prediction. In the present study, the MNP loading differences were also specified for cell lines of glioblastoma origin and expanded by cell culture conditions. These results implement such a high complexity of the interaction between MNPs and cells that it is nearly impossible to assume the success of a MNP-based therapy without pre-trials *in vitro*. This is maybe also the reason why only few MNP formulations and therapeutic or diagnostic approaches made their way into the clinic so far. The individualized medicine concept describe the development of patient-targeted therapies with the help of individual tests prior to a medication [151]. This concept is time-consuming and expensive, but may be the only way to allow successful application of MNPs in the medical field.

Comparing the cancer cells with the astrocytes, the time- and concentration-related loading behavior was similar. This supports that the influence of general cell properties, like growth, and MNP characteristics are more important for MNP loading than special cell type variations. The loading efficiency was similar or even higher in astrocytes compared to glioblastoma cell lines, although it was shown that healthy cells usually take up less MNPs in comparison with cancer cells. The hypothesis for this relation is the bad nutrition situation in the tumor area that favors the uptake by unspecific endocytosis [59]. Thus, maybe the large spreading of the astrocytes and their slow proliferation in comparison with the glioblastoma cells favors the MNP uptake, in contrast to other healthy cells. According to their natural function, including the feeding of neurons [152], maintaining the ion homeostasis and clearing the synaptic gap from neurotransmitters [153], the uptake of molecules is mandatory for astrocytes. Indeed, Geppert et al. [154] showed, that astrocytes take up MNPs after a relatively short incubation time of 6 h. Thus, the remarkable MNP loading of astrocytes detected is probably due to their special properties in cell culture in combination with their natural function. Considering the planned aim to apply a force at the MNP-loaded cells by a magnetic field, the relatively high MNP loading of astrocytes could lead to pronounced side effects of this therapy approach. As the migration ability of the astrocytes is lower than of glioblastoma cells [155], the effect of the magnetic movement should be far less than for high motile glioblastoma cells. Additionally, the further toxicity evaluation of both the MNPs and the magnetic field is important for the application of MNPs in the brain.

Similar to the quantitative detection of the MNPs, the visualization of the MNPs was achieved by iron detection. The localization of iron signals near the nuclei after MA treatment is typical for MNP uptake in astrocytes [156]. This iron localization is also a hint that the MNPs are really taken up by the cells and not only attached at the cell surface. The difficulties of the staining after MA treatment could be addressed to the detection limit of the

Prussian blue visualization. However, the detection limit of the microscopic evaluation of iron stained by Prussian blue is 0.2 pg/µm² [157], so that the staining would not have been successful at all for the iron amounts/cell detected in this study, even if the cell body area in culture is estimated small with 100 µm². The difficulty to apply the detection limit on cells loaded with MNPs could rely on the very uneven MNP distribution within the cell population, so that in some cells, the iron content is much higher compared to others. Furthermore, the MNPs are likely localized in vesicles, so that in certain areas of the cell, the iron level is potentially much higher. Thus, the detection limit for Prussian blue could not be compared with the MNP loading quantification data. However, a drop below the detection limit would be in accordance with the successful iron staining in MA-treated G62 cultures with a very high cell density and thus a reduced proliferation. Similar to the G112 cell loading scenario, the inhibition of cell growth could enhance the cellular iron level due to the lack of division-derived MNP dilution. Furthermore, a more dense packing of MNPs in vesicles could explain, why the MA detection was successful in astrocytes, although the mean iron load per cell did not differ very much.

Very unusual was the iron distribution in astrocytes treated with FS. The high signal at the edges or possibly outside the cells could indicate an export of the MNPs. However, even with an incubation with a more than four times higher MNP dose (225 µg iron/mL), Geppert et al. [65] detected only a marginal decrease of intracellular iron concentration and a stable amount of MNPs in densely-packed vesicles during the 7 d post-incubation phase. The visualization of MNP-filled vesicles in MA-loaded astrocytes could indicate a MNP type-dependent reaction. Perhaps, the loading with FS is based on a different uptake mechanism than MA, as already suggested in the quantitative loading evaluation. Another explanation could be an unusual fast trafficking of the MNPs to iron, which is then exported. The MNPs or iron near the cell edges could be the reason for the growth in islets that only occurred in FS treated astrocytes (see appendix, Figure 42). Perhaps, the iron "belt" inhibited the expansion and finally the growth of the cells demonstrated by the lower confluence.

Side effects of cell loading with MNPs

Considering the effects of the MNP loading on cells, one have to face the MNPs itself, but also the components of the MNPs (i.e. the iron oxide and the coating material) after their dissolution in the cell lysosomes. As the liberation of iron out of the MNPs likely occur as early as already one day after MNP treatment to sufficient amounts to induce ferritin up-regulation [65], iron has to be included in the evaluation of MNP loading side effects. Negative effects on cells can be explained by the mechanical hindrance of natural cell processes of MNPs as well as chemical reactions of iron or coating molecules. Positive

effects of MNPs are likely supporting the cell metabolism, where the single molecules are more powerful than whole MNPs. There are basically two main aspects about the increased iron level influencing the cell metabolism: the positive effect of iron as co-factor of cellular enzymes [158] and the negative effect because of dangerous oxide radicals production [159].

As a parameter for the MNP reaction inside the cells, the cell number variation after MNP loading was examined. The glioblastoma cell number was affected by the loading with MNPs, however, only to a small extent. In a study by Schäfer et al. [160], no difference in cell number was detected in mesenchymal stem cells, which were transfected with MNPs for 4 h, following re-seeding and cell counting at 90 % confluence. In comparison with the present study, the incubation time was very short and thus, probably the iron amount was too low for any effect on cell growth. Indeed, most reductions of cell number occurred with the highest MNP concentration and a longer incubation time, so that likely the higher MNP load per cell was responsible for this decreases. This is consistent with the toxicity testing of 24 different nanoparticles in various cell lines, which showed a concentration- and time-dependent increase of cytotoxicity in all cell types [135]. A similar reaction was observed by Soenen et al. [161], who incubated neural progenitor cells and endothelial cells with comparatively high MNP doses (500-1000 µg iron/mL) for 24 h, following washing and incubation in normal cell culture medium without MNPs. At high doses, a reduction of proliferation was observed after 3 d, whereas after longer incubation this reduction was recovered. The authors explained this transient effect with a dilution of MNPs because of cell division. A transient effect in the present study was not shown, probably because the cells were challenged with MNPs until the end of the experiment.

The reasons for the cell number reductions were examined in a study by Grudzinski et al. [162], where a cell cycle arrest was detected in glioma cells after MNP treatment, proposing a resting phase of the cells for the DNA repair. It was even suggested that this could indicate a potential therapy; however, the repair of cancerous DNA was not proven in the publication. Else, the reduction of cell number could be also addressed to an increase of cell death. However, the few changes in membrane integrity of glioblastoma cells suggested, that the reductions in cell number were more likely due to an inhibition of cell growth than a toxic effect. This is supported by the cytoskeleton staining results, showing no clear damages of the actin structure in the cells after MNP loading, unlike observed in other MNP studies [163], [161].

The relationship, that samples with a higher iron load per cell included fewer cells compared to control cells, was observed in most cell lines. However, it was only significant in astrocyte samples. This may be because astrocytes gathered more MNPs, so that the relation was

stronger visible, or the healthy cells reacted more sensible to the MNP loading. The high astrocyte cell number reduction after FS treatment indicate that the unusual localization of the MNPs at the cell edges is related with enhanced cell stress. Interestingly, the FS treatment did not lead to reductions of the astrocyte membrane integrity, whereas the MA loading clearly did. This does not only demonstrate the higher sensibility of astrocytes, but indicate the divers handling of the MNP types inside the cells. Thus, side effects could occur, if MNPs are used for a possible therapy concepts in the brain.

Interestingly, very small rises of the glioblastoma and astrocyte cell number were also detected, mostly after short-term incubation and with little MNP concentrations. The small increases of cell numbers may be due to an iron increase after MNP disintegration. Bai and Wu et al. [164] showed that the growth of Chinese hamster ovary cells reduced drastically in a low-iron basal medium, whereas cells grown in the same medium supplemented with iron showed stable proliferation even after 5 passages.

In order to gain more insight in the metabolic status of the cells, a MTT assay was performed. The effects of MNP loading were more visible with metabolic activity detection, compared to the membrane integrity measurement. This is consistent with the observation of Lanone et al. [135]. In their study, a higher impact of the MNP loading was detected using the MTT assay rather than the Neutral red assay, which is based on the cell membrane integrity. Similar results were also shown after MNP loading of astrocytes [165]. Interestingly, the metabolic activity was not only reduced but also increased after the MNP loading, which support the enhanced cell proliferation detected.

The increase of metabolic activity was described in several studies after MNP loading. Some researchers suggest that nanoparticles may interact with biochemical assays. Holder et al. [166] summarized that particles could (I) interact with the light absorption or fluorescence, (II) undergo chemical reactions with the assay substances or (III) adsorb the assay compounds at the surface. Kroll et al. [167] found increases of metabolic activity after incubation with diverse nanoparticles, especially titanium oxide (TiO_2) nanoparticles, after 24 h incubation. They showed that the scattering of light during the detection of the formazan product led to enhanced absorbance values; however, they indicated also that other unknown mechanisms must play a role. A transient increase was also detected in a study by Bahring et al. [168], where the metabolic activity of human brain microvascular endothelial cells was tested with three different assays based on colorimetry (MTS), fluorescence (PrestoBlue) or luminescence (CellTiter-Glo) after 3 h of MNP loading. They found out that luminescence-based assays showed no scattering effects of MNPs, however, still a small increase of activity

was demonstrated. This leads to the assumption, that the increases detected were at least not only due to the detection method but based on cellular reactions.

In a study by Arbab et al. [169], transient increases of metabolic activity in HeLa cells and MSCs after 1-3 d MNP incubation were explained by an enhanced activity due to free iron. However, in another study, the transient increase was also shown with cerium and copper nanoparticles [135]. Au et al. [165] found significant increases of metabolic activity in astrocytes incubated with MNPs for 6 h. They suggest an uncoupling of the mitochondrial membrane as a reason for this phenomenon. Indeed, in a study with dicumarol, which uncouples the mitochondrial NADH-cytochrome, a transient increase of metabolic activity detected by the MTT assay was shown. This was supposed to rely on other oxidative effects than mitochondrial electron-chain associated ones, that are more sensible towards cellular stress. The subsequent decline of activity might be because of a ROS-related cell damage [170]. Possibly, similar processes explain the transient increases of metabolic activity after MNP loading.

A theory might be that the iron is released from the MNPs, leading to positive effects on cell metabolism and in parallel to ROS damage enhancement via the Fenton reaction. So, both, positive and negative effects on metabolic activity could be addressed to the iron release from the MNPs. This is supported by the observation, that MA and FS both lead to similar transient increases of metabolic activity followed by a decrease, despite of a different coating material. As the membrane integrity and the cell number are only slightly affected in glioblastoma cells, the toxicity of the MNPs could be considered as low. Nevertheless, the metabolic activity showed that the cells are reacting towards the MNP burden. Astrocytes reacted more sensible to MNP loading, probably due to their higher iron load and their lack of cancer cell-related robustness. This could indicate that MNP-based therapies in the brain could suffer from high side effects. However, these side effects might be overcome by the proper design of MNPs, as especially the reaction of astrocytes differed between the MA and FS treatment. As the reaction of glioblastoma cells was less variable between the MNP types, the MNP application success should be more evaluated after the healthy cell reaction.

Magnetic field effects

Besides the culture conditions and the MNP loading, the magnetic field could influence the cell health. The toxicity of magnetic fields has been discussed controversial in literature. Particularly static magnetic fields alone were mostly considered as little toxic for cells [93]. However, toxic effects on glioblastoma cells, like morphology changes and apoptosis at 300 mT, were already described [171]. Also, genotoxicity was detected in glioblastoma cells with a magnetic field in combination with X-Ray treatment [172]. In other studies presenting

MNP-loaded cells in a magnetic field, no or only few toxicity was detected, whereas morphological changes were common. For example Smith et al. [173] observed an alignment of the actin fibers with the magnetic field, if a neodymium magnet was placed beneath the cell culture well, creating a 350 mT field. Huang et al. [174] also showed an actin alignment in high static magnetic fields according to the field lines. Schäfer et al. [160] found an alignment of MSCs in a magnetic field only after incubation with MNPs.

As the glioblastoma populations consist of cells with often completely variable morphology, it was difficult to judge any changes of the actin cytoskeleton by the magnetic field. Furthermore, due to the setup, the distance to the magnet was approximately 7 mm and thus the magnetic field of the permanent magnet was only 100 mT. Perhaps higher field strengths would have been necessary to reach drastic morphological changes. However, also in other experiments with 300 mT, no apoptostic cell morphology was observed, as described by Teodori et al. [171]. Also the alignment of the cells in direction of the field lines could not be observed. Astrocytes seemed to be more affected by the MNP loading than by the magnetic field, as especially after FS treatment, more connections between the actin fibers appeared. This is in accordance to the observation of an islet formation after FS incubation. So, morphological changes did not seem to matter for the magnetic direction experiments.

Aberrations of the metabolic activity in a 200 mT magnetic field of a permanent magnet were detected, but were relatively low and barely reproducible. Furthermore, control cells without MNP treatment also showed alterations in their metabolic activity. However, dose-dependent decreases of metabolic activity occurred, indicating that the MNPs were indeed responsible for at least some reactions. Additionally, the decreases significant towards the control were only detected in samples with the highest MNP concentration. In a study with MSCs, neither the cell proliferation nor the viability (membrane integrity) was significantly affected after the treatment with MNPs and subsequent incubation with permanent magnets [160]. In contrast, Bae et al. [99] found decreases of viability (ATP production) with increasing concentration of MNP and intensity of a static magnetic field alone, and with longer incubation time. These contradictions could be explained by the sensitivity of the assays used.

In order to test whether a much stronger magnetic field could cause side effects, FS-loaded cells were incubated in a 7 T MRI device. Although the temperature was carefully controlled, the small differences in metabolic activity between the conditions may be due to temperature variations. Differences between control and MNP-loaded cells were of statistic relevance but nevertheless quite small, what demonstrated that a highly homogenous magnetic field cannot cause remarkable toxic effects in cells loaded with MNPs. Thus, effects seen in trials with

permanent magnets may be due to the field gradients rather than insufficient field strength. Indeed, the kind of magnetic field is known to matter for biological responses [84]. For example, alternating fields were shown to destroy MNP-loaded cells without remarkable temperature increase, as used for hyperthermia [175].

A probable reason for the magnetic field effects was described by Bae et al. [99], who found that MNPs needles formed by the static magnetic field inside the cells or added afterwards lead to similar cell viability reductions. Thus, a mechanical hindrance of cell processes could be possible for MNP-related magnetic field effects. The aggregate formation was a concentration-dependent process, so that a high MNP uptake was regarded more hazardous. Another reason for the increase of cytotoxicity could be the enhanced uptake of the MNPs attached to the cell surface via the magnetic forces, which then enhances the iron load and thus the ROS-related damages. Interestingly, also increases of metabolic activity were measured in glioblastoma cells, especially with short incubation time and lower MNP concentration, what may refer to an aggravation of the already shown MNP loading effects by the magnetic field. Astrocytes showed the clearest dose-dependency, which was enhanced with longer MNP incubation, indicating a higher iron load causing more disturbances of the cell metabolism in the magnetic field. This behavior supports the findings of the MNP toxicity, where astrocytes also reacted more sensible compared with the glioblastoma cells. However, the absolute effects of the field types and strengths tested were low, so that the risk of side effects due to the magnetic field application in further trials was not considered crucial, even for MNP-loaded cells.

MNP-derived magnetic movement

After gaining experience in how much MNPs can be loaded by which cell line and whether there are toxic effects or not, the magnetic attraction of the MNP-loaded cells was studied. For the attraction experiment setups, mostly 10 mm magnets were chosen, due to their high field strength at the surface (360 mT), their sharp gradient and their good field penetration distance. Additionally, because of their size, they were easy to handle and fit besides the well of a multi-well plate. Only for the swimming discs experiment, bigger magnets were preferred, as they covered a broader area of the well and had a deeper penetration, which was necessary to overcome the gap between magnet and disc. By the visualization of the MNP attraction by the magnetic field, MA seemed to be better attracted than FS. As the iron core size is similar, maybe the coating of the MNPs was responsible for the differences. Indeed, Daou et al. [176] showed that the coating play a role in the magnetic properties of MNPs, as carboxylated molecules lowered their magnetization, while phosphonated ones did not. Nevertheless, the treatment with FS lead to higher iron amounts/cell, indicating more

incorporated MNPs, which was found to increase the attraction by a magnetic field [81]. Thus, the MNP type and the amount of iron per cell could apparently both influence the attraction of a MNP-loaded cell by a magnet. Therefore, both MNP types were used for magnetic movement induction experiments.

Non-adherent movement

For a fast and easy examination, non-attached cells were chosen first for "physical" attraction experiments. By comparing the pictures taken after seeding cells above a permanent magnet, the attraction patterns of MA- and FS-loaded cells were similar, although the iron load per cell was higher with FS. This was a hint that indeed the relatively good attraction properties of the MA in combination with their weaker loading led to similar magnetic attraction as the low-attracted FS, which were taken up to a higher amount. It was also shown that not all cells were attracted by the magnet, as some cells remained distributed over the whole surface, like in the control cells without MNP treatment. This could be explained by the unequal MNP loading of the cells, shown by the iron staining. In contrast to MA and FS, Sig-treated cells attached mainly in the middle of the well, so near the magnet, and showed a pattern like the cells were directed by the field lines. This MNP type showed a higher agglomeration than MA or FS [123], a faster and better attraction by a magnet and a massive iron loading of cells in preliminary trials. However, the effects of the Sig loading and the magnetic field on the cells was not determined. The good attraction of Sig-loaded cells supports the importance of choosing MNPs for magnetic attraction after both, physical and biological properties. The setup nevertheless showed some weaknesses: the seeding distribution of cells in the well was not perfectly regular, demonstrated by an accumulation of control cells in the middle. The difference between control and MNP-loaded cells was remarkable but the uneven seeding was supposed to mask smaller differences in magnetic attraction between the MNP types. Furthermore, a quantification of the data was not possible, due to the problem to mark the exact magnet position below the culture well and the accumulation of the cells.

That is the reason why an assay with a swimming disc was developed. The idea of this setup was to move MNP-loaded cells against their sedimentation behavior to the top, where only the attracted cells can be counted on the disc. The results of this assay also suggested that cells without MNPs do not remarkably react to the magnetic field, while the MNP-loaded cells could be attracted by the permanent magnet. G112 showed the fewest attraction, in accordance with the low iron load detected. However, less FS-loaded cells were attracted in the swimming disc trial, although the MNP loading with FS was much higher compared with MA. Also, G62 were better attracted than G44 cells, whereas the MNP loading was at least similar between both kinds of cell. It could be assumed that the bigger size of G44 cells lead

to a faster sedimentation, so that the magnetic attraction was not sufficient to overcome the gravitational forces. Another reason could be a worse adherence of G44 cells on the discs, what was indeed generally observed during G44 cell culture. In some swimming disc trials the standard deviation was quite high, indicating a low reproducibility of the experiments. This may rely on the differences of dropwise seeding and the time until placement of the discs.

To overcome these problems, a horizontal setup was developed, where non-attached cells could roll on a surface. In a study by Kim et al. [80], a microfluidic chip was used to separate labeled circulating tumor cells from blood cells by a magnetic field. In this setup, the blood containing the tumor cells flow through a channel where a magnetic field is applied in a special pattern, so that the tumor cells are pushed to an outlet at one side of the channel. In this channel setup, a quantification of the magnetized cells was possible and thus, in the present study, also a channel with floating cells was used. In a so-called magnetophoresis setup, MNP-loaded cells were moved horizontally towards a magnet, while the velocity of the cells was detected with a camera [177]. As an investigation of the whole cell population was preferred in the present study, the counting of whole areas after fixed time periods was performed.

In the magnet channel assay, the magnetic attraction was also the lowest with G112, like in the swimming discs experiments. Another similarity was the higher attraction of cells with a longer MNP incubation time. Both could be explained by the impact of cellular iron loads. In accordance with the magnetic seeding experiment, there were only few significant differences between MA and FS samples, although the iron loads per cell for FS were more than twice as high as for MA. Only with very high differences of iron load (4.6 times), the magnetic attraction differed remarkably. This supports the assumption that not only the iron content governed the magnetic properties of the cells and is the reason why both MA- and FS-loaded cells were examined further. However, G112 cells were excluded from further trials due to the low loading efficiency and weak attraction by the magnet.

Another issue examined with the magnet channel setup was the distance to the magnet sufficient for the cell movement, as this had to be considered in later adherent cell setups. According to the magnet channel trial, the magnetic field was able to attract MNP-loaded cells only in few millimeters distance to the magnet surface, as nearly all loading conditions lead to no significant difference at latest 5 mm distance. This measurement is in accordance with the results from the flux density measurement, where it was shown that the magnetic field weakened drastically within the first millimeters distance. Thus, 100 mT was regarded

as the minimal field strength to attract the MNP-loaded cells on a surface in a non-attached state.

Adherent migration

After the movement of non-attached MNP-loaded glioblastoma cells towards a magnet was shown, the development of a suitable setup for the examination of attached cells was focused. The method of choice for such complex migration studies would be live-cell imaging, since it enables a time-resolved observation. However these techniques have also drawbacks and were not available in the laboratory. The main disadvantage is the equipment complexity needed and thus the high costs: To create optimal humidity, warmth and gas composition, a large incubator or a small box has to be installed at the microscope [178], to maintain stable conditions to keep the focal plane of the sample [179]. Depending on the experiment, a compromise between high quality and speed has to be chosen [178]. The phototoxicity is another drawback, describing the process of heat generation by light in the cells or even worse the generation of ROS, if fluorescent dyes are applied [178]. One of the biggest problem is the evaluation of the data. The most commonly used technique is the manual tracking, where the centers of the cells are followed in a time sequence by a point-and-click procedure. The variability between the operators in terms of the choice of the observed cells and the cell center was found to be very high [180]. Many software packages are available for cell tracking, each having advantages and disadvantages [181], while the usability is often insufficient for a scientist without informatics knowledge [182]. Additionally, the time needed for an evaluation of migration data is quite high, for example for the evaluation of 10 frames with 156 cells, 5-20 min and in another software even 2 h were required [183].

Therefore, setups with endpoint-detection were chosen, so that it was possible to incubate the cells at optimal conditions during the magnetic field application. Several setups were tested, while it was demonstrated that each of them has its negative and positive aspects (Table 5).

The setups with the best optical control were the cylinders and ibidi® inserts, but this is connected with the worst possibility to quantify the amount of migrating cells. The simpler handling of the ibidi® inserts were due to the silicone material, however, the inserts were also more expensive than the cloning cylinders. It was possible to observe the cells without a staining, which may potentially influence the cell behavior, but a coating of the surface was not applicable without causing detachment of the cylinder or insert. The biggest problems encountered were the influence of the cell seeding density on the results and the relatively far distance to the magnet, that reduced the cells attraction as seen in the magnet channel assay trials.

Table 5: Advantages (+) and disadvantages (-) of the adherent cell migration setups

	cylinder	ibidi	transwell	12-well
quantification	-	-	+	+
optical control	+	+	-	+
coating possible	-	-	+	+
no cell loss	+	+	-	+
fast evaluation	+	+	-	-
no staining	+	+	-	-
costs	+	-	-	+
small magnet distance	-	-	-/+	+
easy handling	-	+	-	+
cell density irrelevant	-	-	+	+

The transwell inserts allowed a quantification of the cell migration, but without any optical control. In a comparison of different migration setups, Hulkower and Herber [184] also criticized the non-physiological membrane that the cells have to pass. The most prominent problem was the trypsinization step between the magnet application and evaluation. This led potentially to cell losses, operator-related differences and inaccuracies of the volume after centrifugation, as not the whole supernatant above the cell pellet could be removed without risking cell aspiration. The seeding density was probably less relevant, as the whole surface of the membrane was used for the migration evaluation. The pore size of the membrane might affect the ability of the cells treated with MNPs to pass the membrane, indicated by the lower number of MNP-treated cells detected below the membrane without the magnetic field. Although the biggest pore size available was chosen (8 µm), it might be possible, that the agglomeration of MNPs inside the cells inhibited the plasticity of the cell body necessary to migrate through the pores. However, in a study by Weis et al. [123], no steric hindrance of the MNP-loaded cells was detected, while the cells migrated through a 3D matrix of connective tissue. Thus, maybe also other effects might have played a role in the lower migration of MNP-loaded cells in comparison with control cells.

The most trustworthy data were achieved from the 12-well assay. As the cells were not seeded in a spot, the assay was probably the closest to reality, as the glioblastoma cells seem

to migrate alone or in small groups and thus are scattered in the brain tissue [108]. Due to the cell observation at the beginning and the end of the magnetic field application without medium exchange or other manipulation in between, a cell loss could be excluded. The magnet was very close to the cells, i.e. only separated by the wall of the cell culture vessel (ca. 1 mm), what was shown optimal in non-adherent magnet channel trials. This setup showed a clear advantage to the quite similar setup of Riggio et al. [113], where the cells were counted by eye in areas quite far from the magnet (5, 10 and 15 mm) only after magnetic field application. So, seeding density variations could not be addressed at all. Furthermore, according to their scheme, the magnets were fixed always at the right side for MNP and on the left side for control cells. In the 12-well assay, for each sample, left and right side magnet position were mixed to avoid cell seeding differences and the cell number after magnet incubation was related with the initial cell number.

The disadvantages lie in the time-consuming image evaluation, offering a quantification of the results though. Another drawback is the necessity of the fluorescence cell staining, suspected to affect the cell behavior. For example, fast blue, a common dye for cell tracking experiments, is supposed to reduce the cell adherence, proliferation and viability [185]. Calcein-AM was regarded as a very good stain in a review [186], comparing several types of fluorescent dyes for migration and proliferation experiments. Calcein-AM has a high intensity, does not bind to cell molecules or membranes and has no effect of cellular functions. Indeed, the cells incubated with MNPs and calcein-AM showed no remarkable influences. However, if the cells were trypsinized after MNP treatment, less metabolic activity was shown, while the effect was worsened by the calcein-AM staining (see appendix, Figure 47). This suggested that the detachment of the cells between MNP-loading and migration was the main reason for the lower activity, and the fluorescent staining interferes in this process.

Nevertheless, the fluorescence staining enabled the evaluation of the cells close to the well edge and thus near the magnet, as the bright field light scattering led to shadows in this area. Another advantage of the fluorescence staining was the ability to quantify the cells more easily in a (semi-) automatic way. In the course of the development and validation of an in-house software, Hand et al. [183] compared different cell tracking softwares. They found that most softwares were designed for fluorescent cell detection, and even the softwares capable of phase-contrast image processing gained higher tracking success, if the cells were stained with a fluorescent dye. The reason for this is the easier segmentation of the cells, i.e. the separation of the cells from the background and other cells.

Rhodamine was selected both because of its fluorescence properties and its suppression of the cell proliferation [187]. The fluorescence is localized in the mitochondria, however, after a longer incubation time, the whole cytosol is stained [188]. This is convenient for a software-based segmentation step for a migration evaluation. The reduction of growth after rhodamine treatment is probably due to the interference of the dye with the mitochondrial energy production [189]. This effect was regarded useful in two ways. Firstly, the outgrowth of the cells out of a spot would be diminished, so that not the growth but more the migration of the cells are demonstrated in the setup. Secondly, it seems that the inhibition of proliferation is directly linked with the enhancement of glioblastoma cell migration. Giese et al. [15] collected information about two distinct glioblastoma subpopulations, one more proliferative and one more invasive type. They suggested that the extracellular matrix and soluble factors could support one cell type or the other. In a model by Hatzikirou et al. [190], it was shown, that this switch from proliferation ("grow") to migration ("go") type was not caused by mutation but by transition of the phenotype in response to the oxygen availability. Thus, the blockage of one transition possibility could move the balance to the other type. To test this, we introduced rhodamine to inhibit the cell proliferation, which was successfully demonstrated in pre-trials (appendix Figure 45), and to provoke a higher cell migration. This artificial enhancement of migration would be helpful to gain faster results in the study of directed migration. In parallel, we checked the suitability of the insert-setup for the migration evaluation.

The growth inhibition due to rhodamine treatment was shown effective in the ibidi® setup, as the outgrowth was reduced. However, the strongly reduced outgrowth was also a hint, that the cell migration was not remarkably enhanced by the proliferation inhibition. Additionally, the interaction of FS-loading and rhodamine staining, which drastically decreased the cell number, indicated a strong impact of rhodamine on the cell function causing cell death. The concentration of rhodamine could not be further decreased, as the proliferation inhibition and the staining might have been too weak for an aimed quantitative evaluation. So, rhodamine was not considered as the best option for further migration testing.

The hepatocyte growth factor (HGF), also called scatter factor, was tested to directly increase the migration of the cells to facilitate the migration evaluation and prevent the setups from artifacts like growth influence. The enhancement of the glioblastoma cell migration was tested with the ibidi® insert setup, which is similar to the fence migration assay published by Lamszus et al. [109]. In this study, HGF increased remarkably the outgrowth of ten glioblastoma cell lines from a spot. However, in the present study, the pronounced difference of adherent movement could not be reproduced with G62. This indicated that HGF was not

able to increase the migration of the cells or to overcome the problems of the setup. Similar results were obtained with a laminin coating (see appendix, Figure 46), showing to improve the motility of glioblastoma cells in other studies [109], [138].

Due to non-reproducible results of the magnetic field-driven migration, the ibidi® insert assay was doubted to be suitable to show the directed cell migration, as probably other parameters have a big influence on the outgrowth. As demonstrated by fluorescence microscopy, the cell density differences between the trials with rhodamine could be such an influence on the setup. The higher initial density, i.e. the higher cell number, could have increased the pressure for the cells to migrate out of the spot. This effect might influence the cell migration more than the magnetic attraction and thus may skew the results. Similar effects were observed in the HGF trials, the cells were moving more to the right side of the spot, regardless the magnet position. For normal migration tests, this uneven seeding density does not hamper the results, as normally a mean diameter of the migrated cells is set. However, for the directed migration, the location of the outgrowth is important. Furthermore, the technique was not suitable for an exact quantification of the migration, so that other methods were introduced further to proof the results of the cylinder and ibidi inserts.

In the transwell setup, G62 cells treated with MA migrated more through the membrane with a magnetic field, whereas MA-loaded G44 did not seem to be influenced by the magnet. In the magnet channel trial, G62 cells were slightly better attracted than G44, thus with G44 the loading might not be high enough to influence the cells. Another reason for the differences could be cell property-related, for example the bigger cell size or a lower plasticity of G44 cells could hinder the cell migration through the pores of the membrane. Relatively low cell numbers were detected in MNP treated samples, both incubated with or without a magnet. As it is difficult to visualize the start point of this assay [191], the initially attached cell number may have been not similar between control and MNP-loaded samples. In studies with astrocytes, the adherence of the cells to the surface was diminished, if MNPs were administered before cell adhesion [102], [165]. Transferred to the transwell experiments, a lower adherence of the MNP-loaded cells could affect the starting cell number and thus also the migrating cell number. So, the results of this trial may be again influenced by other factors making an accurate evaluation difficult.

Due to the results of the 12-well assay, the magnetic field was not able to move MA- or FS-loaded adherent cells. The magnetic field strength was similar to the one in the magnetic channel assay, where the cells could be moved within the first 5 mm distance to the magnet surface. In a study by Pensabene et al. [192], carbon nanotubes-loaded neuroblastoma cells were attracted by a 300 mT magnetic field strength near the magnet, what is similar to the

field strength in the area the closest to the magnet (1 mm) in the present study. The shift of the cell mass in the setup by Pensabene et al. [192] was observed from the area at the other side of the well with 37 mT, what is higher than the 5-13 mT in the opposite area (1-5 mm opp) of the 12-well assay, so that the attraction force could be too low. However, the opposite area of the 12-well assay was actually chosen to serve as control without magnetic cell attraction, so that the lack of cell loss fulfilled the requirements of the negative control. The area size steps of 1 mm could have been too big to detect the cell displacement, whereas neuroblastoma cells managed up to 2 mm distance within 24 h incubation in a magnetic field [114]. Thus, it was assumed, that glioblastoma cells, which are known by their high migration ability, could also overcome distances of 1 mm.

It is possible, that the MNP-loading was not high enough to exert forces on the cells, which could influence the migration direction. As shown in the attraction of non-attached cells, the cellular iron content is not sufficient to guarantee a prediction of the attraction forces. Thus, a comparison with other studies is difficult. Furthermore, it is difficult to predict, which force is optimal to induce a cell displacement by a magnetic field. It was shown that beads binding to integrin receptors at the cell surface provoked a stiffening of the cell cytoskeleton upon force application by a magnetic field [193]. Gardel et al. [103] reviewed, that an increased tension on the cell body was correlated with enhanced adhesion of the cells. Thus, a too high field strength could also hinder the cell migration, due to adverse cell reactions. This is in accordance with a review by Lange and Fabry [194], where the authors remark that even though basic mechanic principles play a role in the cell migration, the biological principles like receptor transduction or gene expression interfere with the physics.

Interestingly, Sig-treated G62 cells showed a significant deviation in the cell distribution pattern in the 12-well assay. This pattern indicates that cells from the more far areas moved to the area the nearest to the magnet. In live-cell imaging videos, performed in a cooperation exchange in the Biophysics laboratory in Erlangen, the detachment of Sig-loaded cells was observed, followed by a non-attached attraction by the magnetic field. A similar phenomenon was also described by Pensabene et al. [192] and shown in the supplemental video of a study by White et al. [112], where the low-adhering microglia cells were pulled to the magnet probably in a non-attached state. Pensabene et al. [192] suggested that the movement of the cells occurred during their cell division and explained the differences of movement efficiency by different cell doubling times. Indeed, in the proliferation study, G62 cells showed a faster proliferation compared with G44, which fits to the higher cell number attracted by the magnet. However, it remains unclear, why MA- and FS- loaded cell did not detach during cell division, as they should be attracted by the magnet in the floating state as well.

Considering the Sig-loaded cells, the unequal cell number distribution among the areas disappeared after a longer incubation in the magnetic field. A lower attraction of MNP-loaded cells after a longer time may occur due to a dilution of the MNP concentration per cell due to cell division, as suggested by Bradshaw et al. [111]. However, in the 12-well assay setup, the accumulated cells near the magnet after 1 d were not removed, leading to even more cells after division. Thus, it seems that the displaced cells did not stay near the magnet. A possible explanation could be that the cells died before moving, so that the detachment was not because of the cell division but the ongoing cell death. Thus, the cells were detected near the magnet and disappeared afterwards due to necrotic or apoptotic processes. Another possibility is the cell death after the movement. If the Sig-loaded cells purely moved in the non-attached state, the MNP-covered cells could have difficulties to attach to the surface again, which is yet necessary for their survival. Indeed, Schaub et al. [102] detected that astrocytes mixed with MNPs before seeding attached to a lower degree. This was explained by the complete cell surface decoration with MNPs after cell detachment, which prevented physically the adherence at the surface. This assumption is supported by the observation of large Sig clusters on the cell surface.

The reduced adherence of the cells after MNP-loading and detachment could also explain why G44 cells treated with MNPs showed generally a decreased cell number after the magnetic field application compared to control cells. The influence of the magnet was regarded as not responsible, as no shift of cell number within the areas was detected. If the cells were attracted or killed by the magnetic field, the effect should have been higher in areas nearer to the magnet. In pictures at the start of the magnetic field incubation, the cells are still round, showing a low adherence to the surface. Although the cells were viable at the beginning (as demonstrated by the positive Calcein staining), they could have died during the following incubation time, leading to a lower cell number in all areas.

Thus, the 12-well assay including its evaluation procedure still demonstrated some weaknesses, which could mask the directed migration of MNP-loaded glioblastoma cells to a magnet. The biggest problem is the need to detach the MNP-loaded cells before seeding in the 12-well plates. This trypsinization probably caused a reduced cell attachment, which interfered with the proper cell migration. A direct seeding of the cells in the 12-well setup would solve this problem, however, the fast cell division of glioblastoma cells in combination with the need of a longer MNP incubation time would lead to a space limitation. A more efficient MNP loading could offer a possibility to overcome this problem. Therefore, a study with a reduced incubation time but a broader range of MNP types could be helpful, as the prediction of the loading success seems to be nearly impossible. It was also found that the

magnet channel assay offered useful information about the MNP-loaded cell attraction, that could help to compare different MNP and cell types for their suitability in magnetic attraction-based studies.

During the present study, drastic artifacts were demonstrated in assays used for cell migration detection, especially in setups based on cell outgrowth from a spot or migration through a membrane. These artifacts might have also played a role in the studies of magnetic field-driven cell migration direction of Riggio et al. [113], Bradshaw et al. [111] and White et al. [112]. Especially the difference between the cell movement adherent at the surface or floating in the medium was difficult to distinguish in most cell culture setups. Developments of live-cell imaging methods could offer a solution for this problem, as well as the production of specialized cell culture chambers by 3D-printing as demonstrated in the study by White et al. [112].

The floating movement mechanism showed by Sig-loaded glioblastoma cells was the only effective way to guide the cells to the magnet. As cancer cells normally divide more often than healthy cells, this mechanism could be used in the cancer treatment for an assembly of MNP-loaded cells with the help of a magnet. However, whether this mechanism also works in the three dimensional matrix of the natural environment, remains unknown. When the cells are embedded in a complex matrix, more attachment points should be available even during cell division. These attachments need to be ripped off and the cells have to be pulled through the matrix by the magnetic force. For this, a very high loading with optimal MNPs and a very strong magnetic field are essential requirements. To test this *in vitro*, a 3D-model with the cells embedded in a matrix could be introduced. This is also of importance, as the cell migration in a 3D construct is guided by different conditions compared to 2D setups [125]. In order to observe the cells in this model, a live cell imaging in all three dimensions would be necessary, which is even further challenging [195].

Conclusion

The manipulation of cells with the magnetic force is a fascinating topic. Already few applications of magnetic fields in a biological context are available, even in the medical field. The magnetic force is known to influence biologic processes and regarded as relatively harmless, especially if static fields are used. In combination with MNPs, the power of this force could be increased, while an enhancement of negative effects has to be carefully investigated. In the present study, an influence of the magnetic field on the cells - with and without MNP treatment - was shown, whereas the effects were small and often not reproducible.

Another problem faced in the present study is the accurate prediction of the MNP loading success, which was not possible. Nevertheless, the loading of the whole cell population (presented as mean iron load per cell) is guided by the incubation time and the concentration of the MNPs, although these parameters are highly affected by the cell growth and the MNP characteristics. The manifold of influences on the MNP loading necessitates a test of different parameters prior to every new MNP application. Similar is true for the toxicity prediction of MNPs, where a test of the metabolic status of the cells seemed to give the best insight, compared to cell growth or membrane integrity.

The main goal of the present study was the directed guidance of MNP-loaded cells' movement by a magnetic field. The movement of non-adherent cells was already demonstrated for different purposes, whereas the publications about adherent movement are sparse. In the present study, the development and evaluation of different setups for the magnetic cell movement research showed various advantages and disadvantages. Especially, the undisturbed observation of the cells, the quantification of the cell movement and the cell adherence led to problems in the proper evaluation of the results. Thus, the counting of stained cells in areas near and more far the magnet before and after the application of the magnetic field, following relation of the values demonstrated the most reliable data.

In the present study, the movement of MNP-loaded cells in a non-adherent state was significantly enhanced by the MNP incorporation. As expected, the distance to the magnet and the iron content of the cells influence the amount of the attraction. However, the MNP properties seemed to affect the success more than the iron content. Thus, MNP loading studies alone are probably not sufficient for a prediction of the cell attraction. An adherent movement of the MNP-loaded cells could not be proven in the present study. The only cell movement in the adherent setup was demonstrated during cell division, where the adherence of the cells is drastically lowered, so that the cells were ripped off and attracted in a non-

adherent state. It needs to be studied, whether this mechanism is still relevant for magnetic cell movement in a 3D construct, where the cell migration is guided by different conditions compared to 2D setups.

References

1. Pschyrembel W (2007) Pschyrembel® Klinisches Wörterbuch. Auflage 261, Verlag W. de Gruyter, Berlin, ISBN 978-3-11-018534-8
2. Louis DN, Ohgaki H, Wiestler OD et al. (2007) The 2007 WHO Classification of Tumours of the Central Nervous System. Acta Neuropathol 114(2): 97–109. doi: 10.1007/s00401-007-0243-4
3. Agnihotri S, Burrell KE, Wolf A et al. (2013) Glioblastoma, a Brief Review of History, Molecular Genetics, Animal Models and Novel Therapeutic Strategies. Arch Immunol Ther Exp 61(1): 25–41. doi: 10.1007/s00005-012-0203-0
4. Ohgaki H, Kleihues P (2005) Epidemiology and etiology of gliomas. Acta Neuropathol 109(1): 93–108. doi: 10.1007/s00401-005-0991-y
5. Stupp R, Mason WP, van den Bent MJ et al. (2005) Radiotherapy plus concomitant and adjuvant temozolomide for glioblastoma. N Engl J Med 352(10): 987–996. doi: 10.1056/NEJMoa043330
6. Stupp R, Brada M, van den Bent MJ et al. (2014) High-grade glioma: ESMO Clinical Practice Guidelines for diagnosis, treatment and follow-up. Ann Oncol 25(suppl 3): iii93. doi: 10.1093/annonc/mdu050
7. Herdegen T, Böhm R (2008) Kurzlehrbuch Pharmakologie und Toxikologie. 328 Tabellen. Thieme, Stuttgart [u.a.], ISBN 978-3-13-142291-0
8. Esteller M, Garcia-Foncillas J, Andion E et al. (2000) Inactivation of the DNA-Repair Gene MGMT and the Clinical Response of Gliomas to Alkylating Agents. N Engl J Med 343(19): 1350–1354. doi: 10.1056/NEJM200011093431901
9. Chinot OL, Wick W, Mason W et al. (2014) Bevacizumab plus Radiotherapy–Temozolomide for Newly Diagnosed Glioblastoma. N Engl J Med 370(8): 709–722. doi: 10.1056/NEJMoa1308345
10. Raizer JJ, Abrey LE, Lassman AB et al. (2010) A phase II trial of erlotinib in patients with recurrent malignant gliomas and nonprogressive glioblastoma multiforme postradiation therapy. Neuro-Oncology 12(1): 95–103. doi: 10.1093/neuonc/nop015
11. Bota DA, Desjardins A, Quinn JA et al. (2007) Interstitial chemotherapy with biodegradable BCNU (Gliadel) wafers in the treatment of malignant gliomas. Ther Clin Risk Manag 3(5): 707–715
12. Bregy A, Shah AH, Diaz MV et al. (2014) The role of Gliadel wafers in the treatment of high-grade gliomas. Expert Rev Anticanc 13(12): 1453–1461. doi: 10.1586/14737140.2013.840090
13. Bergers G, Benjamin LE (2003) Angiogenesis: Tumorigenesis and the angiogenic switch. Nat Rev Cancer 3(6): 401–410. doi: 10.1038/nrc1093
14. Legendre C, Garcion E (2015) Iron metabolism: a double-edged sword in the resistance of glioblastoma to therapies. Trends Endocrin Met 26(6): 322–331. doi: 10.1016/j.tem.2015.03.008
15. Giese A, Bjerkvig R, Berens ME et al. (2003) Cost of Migration: Invasion of Malignant Gliomas and Implications for Treatment. J Clin Oncol 21(8): 1624–1636. doi: 10.1200/JCO.2003.05.063
16. Elong Edimo W, Ghosh S, Derua R et al. (2016) SHIP2 controls plasma membrane PI(4,5)P2 thereby participating in the control of cell migration in 1321 N1 glioblastoma cells. J Cell Sci 129(6): 1101–1114. doi: 10.1242/jcs.179663
17. Mondol AS, Tonks NK, Kamata T (2014) Nox4 redox regulation of PTP1B contributes to the proliferation and migration of glioblastoma cells by modulating tyrosine phosphorylation of coronin-1C. Free Radical Bio Med 67: 285–291. doi: 10.1016/j.freeradbiomed.2013.11.005
18. Joseph JV, Conroy S, Pavlov K et al. (2015) Hypoxia enhances migration and invasion in glioblastoma by promoting a mesenchymal shift mediated by the HIF1α–ZEB1 axis. Cancer Lett 359(1): 107–116. doi: 10.1016/j.canlet.2015.01.010
19. Bernhart E, Damm S, Wintersperger A et al. (2013) Protein kinase D2 regulates migration and invasion of U87MG glioblastoma cells in vitro. Exp Cell Res 319(13): 2037–2048. doi: 10.1016/j.yexcr.2013.03.029
20. Bølge Tysnes B, Mahesparan R (2001) Biological Mechanisms of Glioma Invasion and Potential Therapeutic Targets. J Neuro-Oncol 53(2): 129–147. doi: 10.1023/A:1012249216117

21. Groves MD, Puduvalli VK, Hess KR et al. (2002) Phase II Trial of Temozolomide Plus the Matrix Metalloproteinase Inhibitor, Marimastat, in Recurrent and Progressive Glioblastoma Multiforme. J Clin Oncol 20(5): 1383–1388. doi: 10.1200/JCO.20.5.1383

22. Hu J, Muller KA, Furnari FB et al. (2014) Neutralizing the EGF receptor in glioblastoma cells stimulates cell migration by activating uPAR-initiated cell signaling. Oncogene 34(31): 4078–4088. doi: 10.1038/onc.2014.336

23. Verhaak RG, Hoadley KA, Purdom E et al. (2010) Integrated Genomic Analysis Identifies Clinically Relevant Subtypes of Glioblastoma Characterized by Abnormalities in PDGFRA, IDH1, EGFR, and NF1. Cancer Cell 17(1): 98–110. doi: 10.1016/j.ccr.2009.12.020

24. Stupp R, Wong ET, Kanner AA et al. (2012) NovoTTF-100A versus physician's choice chemotherapy in recurrent glioblastoma: A randomised phase III trial of a novel treatment modality. Eur J Cancer 48(14): 2192–2202. doi: 10.1016/j.ejca.2012.04.011

25. Mrugala MM, Engelhard HH, Dinh Tran D et al. (2014) Clinical Practice Experience With NovoTTF-100A™ System for Glioblastoma: The Patient Registry Dataset (PRiDe). Semin Oncol 41: S4. doi: 10.1053/j.seminoncol.2014.09.010

26. Kirson ED (2004) Disruption of Cancer Cell Replication by Alternating Electric Fields. Cancer Res (Cancer Research) 64(9): 3288–3295. doi: 10.1158/0008-5472.CAN-04-0083

27. Bernstein JJ, Woodard CA Glioblastoma cells do not intravasate into blood vessels. Neurosurgery 1995(36(1)): 124–132

28. Chicheł A, Skowronek J, Kubaszewska M et al. (2007) Hyperthermia – description of a method and a review of clinical applications. Reports of Practical Oncology & Radiotherapy 12(5): 267–275. doi: 10.1016/S1507-1367(10)60065-X

29. Hildebrandt B (2002) The cellular and molecular basis of hyperthermia. Crit Rev Oncol Hemat 43(1): 33–56. doi: 10.1016/S1040-8428(01)00179-2

30. Lal S, Verma J, van Noorden CJ (2014) Nanoparticles for hyperthermic therapy: synthesis strategies and applications in glioblastoma. Int J Nanomed: 2863. doi: 10.2147/IJN.S57501

31. Jordan A, Scholz R, Maier-Hauff K et al. (2006) The effect of thermotherapy using magnetic nanoparticles on rat malignant glioma. J Neurooncol 78(1): 7–14. doi: 10.1007/s11060-005-9059-z

32. Maier-Hauff K, Ulrich F, Nestler D et al. (2011) Efficacy and safety of intratumoral thermotherapy using magnetic iron-oxide nanoparticles combined with external beam radiotherapy on patients with recurrent glioblastoma multiforme. J Neurooncol 103(2): 317–324. doi: 10.1007/s11060-010-0389-0

33. Dürr S, Janko C, Lyer S et al. (2013) Magnetic nanoparticles for cancer therapy. Nanotechnology Reviews 2(4). doi: 10.1515/ntrev-2013-0011

34. Veiseh O, Gunn JW, Zhang M (2010) Design and fabrication of magnetic nanoparticles for targeted drug delivery and imaging. Adv Drug Deliver Rev 62(3): 284–304. doi: 10.1016/j.addr.2009.11.002

35. Gallo J, Long NJ, Aboagye EO (2013) Magnetic nanoparticles as contrast agents in the diagnosis and treatment of cancer. Chem Soc Rev 42(19): 7816. doi: 10.1039/c3cs60149h

36. Wagner B, Drel V, Gorin Y (2016) Pathophysiology of gadolinium-associated systemic fibrosis. Am J Physiol Renal Physiol 311(1): F1. doi: 10.1152/ajprenal.00166.2016

37. Taboada E, Rodríguez E, Roig A et al. (2007) Relaxometric and Magnetic Characterization of Ultrasmall Iron Oxide Nanoparticles with High Magnetization. Evaluation as Potential T1 Magnetic Resonance Imaging Contrast Agents for Molecular Imaging. Langmuir 23(8): 4583–4588. doi: 10.1021/la063415s

38. Halamoda Kenzaoui B, Angeloni S, Overstolz T et al. (2013) Transfer of Ultrasmall Iron Oxide Nanoparticles from Human Brain-Derived Endothelial Cells to Human Glioblastoma Cells. ACS Appl Mater Interfaces 5(9): 3581–3586. doi: 10.1021/am401310s

39. Hadjipanayis CG, Machaidze R, Kaluzova M et al. (2010) EGFRvIII Antibody-Conjugated Iron Oxide Nanoparticles for Magnetic Resonance Imaging-Guided Convection-Enhanced Delivery

and Targeted Therapy of Glioblastoma. Cancer Res 70(15): 6303–6312. doi: 10.1158/0008-5472.CAN-10-1022

40. Fu A, Wilson RJ, Smith BR et al. (2012) Fluorescent Magnetic Nanoparticles for Magnetically Enhanced Cancer Imaging and Targeting in Living Subjects. ACS Nano 6(8): 6862–6869. doi: 10.1021/nn301670a

41. Zhang J, Shin MC, Yang VC (2014) Magnetic Targeting of Novel Heparinized Iron Oxide Nanoparticles Evaluated in a 9L-glioma Mouse Model. Pharm Res 31(3): 579–592. doi: 10.1007/s11095-013-1182-5

42. Kong SD, Lee J, Ramachandran S et al. (2012) Magnetic targeting of nanoparticles across the intact blood–brain barrier. J Control Release 164(1): 49–57. doi: 10.1016/j.jconrel.2012.09.021

43. Stephen ZR, Kievit FM, Veiseh O et al. (2014) Redox-Responsive Magnetic Nanoparticle for Targeted Convection-Enhanced Delivery of O6 -Benzylguanine to Brain Tumors. ACS Nano 8(10): 10383–10395. doi: 10.1021/nn503735w

44. Kaluzova M, Bouras A, Machaidze R et al. (2015) Targeted therapy of glioblastoma stem-like cells and tumor non-stem cells using cetuximab-conjugated iron-oxide nanoparticles. Oncotarget: 1–19

45. Klein S, Sommer A, Distel LVR et al. (2014) Superparamagnetic Iron Oxide Nanoparticles as Novel X-ray Enhancer for Low-Dose Radiation Therapy. J Phys Chem B 118(23): 6159–6166. doi: 10.1021/jp5026224

46. Rivolta I, Panariti, Miserocchi (2012) The effect of nanoparticle uptake on cellular behavior: disrupting or enabling functions? NSA: 87. doi: 10.2147/NSA.S25515

47. Salvati A, Åberg C, dos Santos T et al. (2011) Experimental and theoretical comparison of intracellular import of polymeric nanoparticles and small molecules: toward models of uptake kinetics. Nanomed-Nanotechnol 7(6): 818–826. doi: 10.1016/j.nano.2011.03.005

48. Shang L, Nienhaus K, Nienhaus G (2014) Engineered nanoparticles interacting with cells: size matters. J Nanobiotechnol 12(1): 5. doi: 10.1186/1477-3155-12-5

49. Zhang S, Li J, Lykotrafitis G et al. (2009) Size-Dependent Endocytosis of Nanoparticles. Adv Mater 21(4): 419–424. doi: 10.1002/adma.200801393

50. Lu F, Wu S, Hung Y et al. (2009) Size Effect on Cell Uptake in Well-Suspended, Uniform Mesoporous Silica Nanoparticles. Small 5(12): 1408–1413. doi: 10.1002/smll.200900005

51. Huang J, Bu L, Xie J et al. (2010) Effects of Nanoparticle Size on Cellular Uptake and Liver MRI with Polyvinylpyrrolidone-Coated Iron Oxide Nanoparticles. ACS Nano 4(12): 7151–7160. doi: 10.1021/nn101643u

52. Schlorf T, Meincke M, Kossel E et al. (2011) Biological Properties of Iron Oxide Nanoparticles for Cellular and Molecular Magnetic Resonance Imaging. IJMS 12(1): 12–23. doi: 10.3390/ijms12010012

53. Sun Z, Yathindranath V, Worden M et al. (2013) Characterization of cellular uptake and toxicity of aminosilane-coated iron oxide nanoparticles with different charges in central nervous system-relevant cell culture models. IJN: 961–970. doi: 10.2147/IJN.S39048

54. Murase K, Saito S, Tsugeno M et al. (2012) Impact of surface coating and particle size on the uptake of small and ultrasmall superparamagnetic iron oxide nanoparticles by macrophages. IJN: 5415. doi: 10.2147/IJN.S33709

55. Mahmoudi M, Hofmann H, Rothen-Rutishauser B et al. (2012) Assessing the In Vitro and In Vivo Toxicity of Superparamagnetic Iron Oxide Nanoparticles. Chem Rev 112(4): 2323–2338. doi: 10.1021/cr2002596

56. Safi M, Courtois J, Seigneuret M et al. (2011) The effects of aggregation and protein corona on the cellular internalization of iron oxide nanoparticles. Biomaterials 32(35): 9353–9363. doi: 10.1016/j.biomaterials.2011.08.048

57. Lesniak A, Fenaroli F, Monopoli MP et al. (2012) Effects of the Presence or Absence of a Protein Corona on Silica Nanoparticle Uptake and Impact on Cells. ACS Nano 6(7): 5845–5857. doi: 10.1021/nn300223w

58. Bajaj A, Samanta B, Yan H et al. (2009) Stability, toxicity and differential cellular uptake of protein passivated-Fe3O4 nanoparticles. J Mater Chem 19(35): 6328. doi: 10.1039/b901616c

59. Jordan A, Scholz R, Wust P et al. (1999) Endocytosis of dextran and silan-coated magnetite nanoparticles and the effect of intracellular hyperthermia on human mammary carcinoma cells in vitro. J Magn Magn Mater 194(1-3): 185–196. doi: 10.1016/S0304-8853(98)00558-7

60. Albanese A, Tang PS, Chan WC (2012) The Effect of Nanoparticle Size, Shape, and Surface Chemistry on Biological Systems. Annu Rev Biomed Eng 14(1): 1–16. doi: 10.1146/annurev-bioeng-071811-150124

61. Kim JA, Åberg C, Salvati A et al. (2011) Role of cell cycle on the cellular uptake and dilution of nanoparticles in a cell population. Nature Nanotech 7(1): 62–68. doi: 10.1038/nnano.2011.191

62. Tenzer S, Docter D, Kuharev J et al. (2013) Rapid formation of plasma protein corona critically affects nanoparticle pathophysiology. Nature Nanotech 8(10): 772–781. doi: 10.1038/nnano.2013.181

63. Mahmoudi M, Laurent S, Shokrgozar MA et al. (2011) Toxicity Evaluations of Superparamagnetic Iron Oxide Nanoparticles: Cell "Vision" versus Physicochemical Properties of Nanoparticles. ACS Nano 5(9): 7263–7276. doi: 10.1021/nn2021088

64. Arbab AS, Wilson LB, Ashari P et al. (2005) A model of lysosomal metabolism of dextran coated superparamagnetic iron oxide (SPIO) nanoparticles: implications for cellular magnetic resonance imaging. NMR Biomed. 18(6): 383–389. doi: 10.1002/nbm.970

65. Geppert M, Hohnholt MC, Nürnberger S et al. (2012) Ferritin up-regulation and transient ROS production in cultured brain astrocytes after loading with iron oxide nanoparticles. Acta Biomater 8(10): 3832–3839. doi: 10.1016/j.actbio.2012.06.029

66. Wilhelm C, Gazeau F (2008) Universal cell labelling with anionic magnetic nanoparticles. Biomaterials 29(22): 3161–3174. doi: 10.1016/j.biomaterials.2008.04.016

67. Ray PD, Huang B, Tsuji Y (2012) Reactive oxygen species (ROS) homeostasis and redox regulation in cellular signaling. Cell Signal 24(5): 981–990. doi: 10.1016/j.cellsig.2012.01.008

68. Kowaltowski AJ, Souza-Pinto NC de, Castilho RF et al. (2009) Mitochondria and reactive oxygen species. Free Radical Bio Med 47(4): 333–343. doi: 10.1016/j.freeradbiomed.2009.05.004

69. Prohaska R, Sibon OC, Rudnicki DD et al. (2012) Brain, blood, and iron: Perspectives on the roles of erythrocytes and iron in neurodegeneration. Neurobiol Dis 46(3): 607–624. doi: 10.1016/j.nbd.2012.03.006

70. Toyokuni S (2009) Role of iron in carcinogenesis: Cancer as a ferrotoxic disease. Cancer Science 100(1): 9–16. doi: 10.1111/j.1349-7006.2008.01001.x

71. Jiao Y, Wilkinson J, Di X et al. (2008) Curcumin, a cancer chemopreventive and chemotherapeutic agent, is a biologically active iron chelator. Blood 113(2): 462–469. doi: 10.1182/blood-2008-05-155952

72. Zanotto-Filho A, Braganhol E, Edelweiss MI et al. (2012) The curry spice curcumin selectively inhibits cancer cells growth in vitro and in preclinical model of glioblastoma. J Nutr Biochem 23(6): 591–601. doi: 10.1016/j.jnutbio.2011.02.015

73. Elstner A, Holtkamp N, Deimling A von (2007) Involvement of Hif-1 in desferrioxamine-induced invasion of glioblastoma cells. Clin Exp Metastasis 24(1): 57–66. doi: 10.1007/s10585-007-9057-y

74. Kiessling MK, Klemke CD, Kaminski MM et al. (2009) Inhibition of Constitutively Activated Nuclear Factor- B Induces Reactive Oxygen Species- and Iron-Dependent Cell Death in Cutaneous T-Cell Lymphoma. Cancer Res 69(6): 2365–2374. doi: 10.1158/0008-5472.CAN-08-3221

75. Hartwig V, Giovannetti G, Vanello N et al. (2009) Biological Effects and Safety in Magnetic Resonance Imaging: A Review. IJERPH 6(6): 1778–1798. doi: 10.3390/ijerph6061778

76. Rikken RSM, Nolte RJM, Maan JC et al. (2014) Manipulation of micro- and nanostructure motion with magnetic fields. Soft Matter 10(9): 1295–1308. doi: 10.1039/C3SM52294F

77. Wautelet M, Hoppe B (2008) Nanotechnologie. Oldenbourg, München, ISBN: 978-3-486-57960-4

78. Lohmann KJ (2010) Q&A: Animal behaviour: Magnetic-field perception. Nature 464(7292): 1140–1142. doi: 10.1038/4641140a

79. Inglis DW, Riehn R, Sturm JC et al. (2006) Microfluidic high gradient magnetic cell separation. J Appl Phys 99(8): 08K101. doi: 10.1063/1.2165782

80. Kim S, Han S, Park M et al. (2013) Circulating Tumor Cell Microseparator Based on Lateral Magnetophoresis and Immunomagnetic Nanobeads. Anal Chem 85(5): 2779–2786. doi: 10.1021/ac303284u

81. Moysidis SN, Alvarez-Delfin K, Peschansky VJ et al. (2015) Magnetic field-guided cell delivery with nanoparticle-loaded human corneal endothelial cells. Nanomed-Nanotechnol 11(3): 499–509. doi: 10.1016/j.nano.2014.12.002

82. Souza GR, Molina JR, Raphael RM et al. (2010) Three-dimensional tissue culture based on magnetic cell levitation. Nature Nanotech 5(4): 291–296. doi: 10.1038/nnano.2010.23

83. Laurent S, Dutz S, Häfeli UO et al. (2011) Magnetic fluid hyperthermia: Focus on superparamagnetic iron oxide nanoparticles. Adv Colloid Interfac. doi: 10.1016/j.cis.2011.04.003

84. Markov MS (2007) Magnetic Field Therapy: A Review. Electromagn Biol Med 26(1): 1–23. doi: 10.1080/15368370600925342

85. Brown CS, Ling FW, Wan JY et al. (2002) Efficacy of static magnetic field therapy in chronic pelvic pain: A double-blind pilot study. Am J Obstet Gynecol 187(6): 1581–1587. doi: 10.1067/mob.2002.128026

86. Morris C, Skalak T (2005) Static magnetic fields alter arteriolar tone in vivo. Bioelectromagnetics 26(1): 1–9. doi: 10.1002/bem.20047

87. Detlavs I, Dombrovska L, Klavinsh I et al. (1994) Experimental study of the effect of electromagnetic fields' in the early stage of wound healing. Bioelectroch Bioener 35(1-2): 13–17. doi: 10.1016/0302-4598(94)87004-7

88. Pilla A, Muehsam D, Markov M (1997) A dynamical systems/Larmor precession model for weak magnetic field bioeffects: Ion binding and orientation of bound water molecules. Bioelectroch Bioener 43(2): 239–249. doi: 10.1016/S0302-4598(96)05161-6

89. Buchachenko A (2016) Why magnetic and electromagnetic effects in biology are irreproducible and contradictory? Bioelectromagnetics 37(1): 1–13. doi: 10.1002/bem.21947

90. Lin H, Blank M, Rossol-Haseroth K et al. (2001) Regulating genes with electromagnetic response elements. J Cell Biochem 81(1): 143–148. doi: 10.1002/1097-4644(20010401)81:1<143:AID-JCB1030>3.0.CO;2-4

91. Goodman R, Blank M (1998) Magnetic field stress induces expression of hsp70. Cell Stress Chaperon 3(2): 79–88

92. Glover P, Cavin I, Qian W et al. (2007) Magnetic-field-induced vertigo: A theoretical and experimental investigation. Bioelectromagnetics 28(5): 349–361. doi: 10.1002/bem.20316

93. International Commission on Non-Ionizing Radiation Protection (2009) Guidelines on limits of exposure to static magnetic fields. Health Physics 96(4): 504–514. doi: 10.1097/01.HP.0000343164.27920.4a

94. Rosen AD (2003) Mechanism of Action of Moderate-Intensity Static Magnetic Fields on Biological Systems. CBB 39(2): 163–174. doi: 10.1385/CBB:39:2:163

95. Schenck JF (2000) Safety of Strong, Static Magnetic Fields. J Magn Reson Imaging 12(1): 2–19. doi: 10.1002/1522-2586(200007)12:1<2:AID-JMRI2>3.0.CO;2-V

96. Tenuzzo B, Chionna A, Panzarini E et al. (2006) Biological effects of 6 mT static magnetic fields: A comparative study in different cell types. Bioelectromagnetics 27(7): 560–577. doi: 10.1002/bem.20252

97. Hashish AH, El-Missiry MA, Abdelkader HI et al. (2008) Assessment of biological changes of continuous whole body exposure to static magnetic field and extremely low frequency

electromagnetic fields in mice. Ecotoxicol Environ Saf 71(3): 895–902. doi: 10.1016/j.ecoenv.2007.10.002

98. Ghodbane S, Lahbib A, Sakly M et al. (2013) Bioeffects of Static Magnetic Fields: Oxidative Stress, Genotoxic Effects, and Cancer Studies. BioMed Research International 2013(4): 1–12. doi: 10.1155/2013/602987

99. Bae J, Huh M, Ryu B et al. (2011) The effect of static magnetic fields on the aggregation and cytotoxicity of magnetic nanoparticles. Biomaterials 32(35): 9401–9414. doi: 10.1016/j.biomaterials.2011.08.075

100. Comfort KK, Maurer EI, Hussain SM (2013) The Biological Impact of Concurrent Exposure to Metallic Nanoparticles and a Static Magnetic Field. Bioelectromagnetics: n/a. doi: 10.1002/bem.21790

101. Shaw J, Raja SO, Dasgupta AK (2014) Modulation of cytotoxic and genotoxic effects of nanoparticles in cancer cells by external magnetic field. Cancer Nano 5(1): 14. doi: 10.1186/s12645-014-0002-x

102. Schaub NJ, Rende D, Yuan Y et al. (2014) Reduced Astrocyte Viability at Physiological Temperatures from Magnetically Activated Iron Oxide Nanoparticles. Chem Res Toxicol 27(12): 2023–2035. doi: 10.1021/tx500231f

103. Gardel ML, Schneider IC, Aratyn-Schaus Y et al. (2010) Mechanical Integration of Actin and Adhesion Dynamics in Cell Migration. Annu Rev Cell Dev Biol 26(1): 315–333. doi: 10.1146/annurev.cellbio.011209.122036

104. Fletcher DA, Mullins RD (2010) Cell mechanics and the cytoskeleton. Nature 463(7280): 485–492. doi: 10.1038/nature08908

105. Goldbrunner RH, Bernstein JJ, Tonn JC (1999) Cell-extracellular matrix interaction in glioma invasion. Acta Neurochir (Wien) 141(3): 295-305; discussion 304-5

106. Sharma P, Sheets K, Elankumaran S et al. (2013) The mechanistic influence of aligned nanofibers on cell shape, migration and blebbing dynamics of glioma cells. Integr Biol 5(8): 1036–1044. doi: 10.1039/C3IB40073E

107. Giese A, Rief MD, Loo MA et al. (1994) Determinants of human astrocytoma migration. Cancer Res 54(14): 3897–3904

108. Han J, Daniel JC, Pappas GD (1995) Expression of type VI collagen during glioblastoma cell invasion in brain tissue cultures. Cancer Lett 88(2): 127–132

109. Lamszus K, Schmidt NO, Jin L et al. (1998) Scatter factor promotes motility of human glioma and neuromicrovascular endothelial cells. Int J Cancer 75(1): 19–28

110. Verkhovsky AB, Svitkina TM, Borisy GG (1999) Self-polarization and directional motility of cytoplasm. Curr Biol 9(1): 11–S1. doi: 10.1016/S0960-9822(99)80042-6

111. Bradshaw M, Clemons TD, Ho D et al. (2015) Manipulating directional cell motility using intracellular superparamagnetic nanoparticles. Nanoscale 7(11): 4884–4889. doi: 10.1039/c4nr06594h

112. White EE, Pai A, Weng Y et al. (2015) Functionalized iron oxide nanoparticles for controlling the movement of immune cells. Nanoscale 7(17): 7780–7789. doi: 10.1039/c3nr04421a

113. Riggio C, Calatayud MP, Hoskins et al. (2012) Poly-l-lysine-coated magnetic nanoparticles as intracellular actuators for neural guidance. IJN: 3155. doi: 10.2147/IJN.S28460

114. Raffa V, Vittorio O, Ciofani G et al. (2009) Cell creeping and controlled migration by magnetic carbon nanotubes. Nanoscale Res Lett 5(1): 257–262. doi: 10.1007/s11671-009-9463-y

115. Lauffenburger DA, Horwitz AF (1996) Cell Migration: A Physically Integrated Molecular Process. Cell 84(3): 359–369. doi: 10.1016/S0092-8674(00)81280-5

116. Bica D, Vékás L, Avdeev MV et al. (2007) Sterically stabilized water based magnetic fluids: Synthesis, structure and properties. J Magn Magn Mater 311(1): 17–21. doi: 10.1016/j.jmmm.2006.11.158

117. Avdeev MV, Mucha B, Lamszus K et al. (2010) Structure and in Vitro Biological Testing of Water-Based Ferrofluids Stabilized by Monocarboxylic Acids. Langmuir 26(11): 8503–8509. doi: 10.1021/la904471f

118. Farazi TA, Waksman G, Gordon JI (2001) The Biology and Enzymology of ProteinN-Myristoylation. J Biol Chem 276(43): 39501–39504. doi: 10.1074/jbc.R100042200

119. Pham W, Kircher MF, Weissleder R et al. (2004) Enhancing Membrane Permeability by Fatty Acylation of Oligoarginine Peptides. ChemBioChem 5(8): 1148–1151. doi: 10.1002/cbic.200400063

120. Pham W, Zhao B, Lo EH et al. (2005) Crossing the blood–brain barrier: A potential application of myristoylated polyarginine for in vivo neuroimaging. NeuroImage 28(1): 287–292. doi: 10.1016/j.neuroimage.2005.06.007

121. Li J, Gu B, Meng Q et al. (2011) The use of myristic acid as a ligand of polyethylenimine/DNA nanoparticles for targeted gene therapy of glioblastoma. Nanotechnology 22(43): 435101. doi: 10.1088/0957-4484/22/43/435101

122. Sadhukha T, Wiedmann TS, Panyam J (2013) Inhalable magnetic nanoparticles for targeted hyperthermia in lung cancer therapy. Biomaterials 34(21): 5163–5171. doi: 10.1016/j.biomaterials.2013.03.061

123. Weis C, Blank F, West A et al. (2014) Labeling of cancer cells with magnetic nanoparticles for magnetic resonance imaging. Magn Reson Med 71(5): 1896–1905. doi: 10.1002/mrm.24832

124. Westphal M, Hänsel M, Hamel W et al. (1994) Karyotype analyses of 20 human glioma cell lines. Acta Neurochir (Wien) 126(1): 17–26

125. Zhong J, Baquiran JB, Bonakdar N et al. (2012) NEDD9 Stabilizes Focal Adhesions, Increases Binding to the Extra-Cellular Matrix and Differentially Effects 2D versus 3D Cell Migration. PLoS ONE 7(4): e35058. doi: 10.1371/journal.pone.0035058

126. Xtal Concepts Spectroscatter User Manual

127. Hinderliter PM, Minard KR, Orr G et al. (2010) ISDD: A computational model of particle sedimentation, diffusion and target cell dosimetry for in vitro toxicity studies. Part Fibre Toxicol 7(1): 36. doi: 10.1186/1743-8977-7-36

128. fish WW (1988) [27] Rapid colorimetric micromethod for the quantitation of complexed iron in biological samples. In: Metallobiochemistry Part A, vol 158. Elsevier, pp 357–364

129. Riemer J, Hoepken HH, Czerwinska H et al. (2004) Colorimetric ferrozine-based assay for the quantitation of iron in cultured cells. Anal Biochem 331(2): 370–375. doi: 10.1016/j.ab.2004.03.049

130. Jance JA (2012) Theory and strategy in histochemistry. A guide to the selection and understanding of techniques. Springer, [Place of publication not identified]

131. Riss TL MRNAea (2013) Assay Guidance Manual [Internet]. Cell Viability Assays. http://www.ncbi.nlm.nih.gov/books/NBK144065/

132. Berridge M, Tan A (1993) Characterization of the Cellular Reduction of 3-(4,5-dimethylthiazol-2-yl)-2,5-diphenyltetrazolium bromide (MTT): Subcellular Localization, Substrate Dependence, and Involvement of Mitochondrial Electron Transport in MTT Reduction. Arch Biochem Biophys 303(2): 474–482. doi: 10.1006/abbi.1993.1311

133. Bernas T, Dobrucki J (2002) Mitochondrial and nonmitochondrial reduction of MTT: Interaction of MTT with TMRE, JC-1, and NAO mitochondrial fluorescent probes. Cytometry 47(4): 236–242. doi: 10.1002/cyto.10080

134. Berridge M, Tan A, McCoy K et al. (1996) The Biochemical and Cellular Basis of Cell Proliferation Assays That Use Tetrazolium Salts. Biochem Biophys Res Co(4): 14–19

135. Lanone S, Rogerieux F, Geys J et al. (2009) Comparative toxicity of 24 manufactured nanoparticles in human alveolar epithelial and macrophage cell lines. Part Fibre Toxicol 6(1): 14. doi: 10.1186/1743-8977-6-14

136. Bradley Armen G (2007) Hall Effect Experiment. http://www.phys.utk.edu/labs/modphys/

137. Schmitz S (2007) Der Experimentator: Zellkultur. Elsevier, München, ISBN: 3827415640

138. Joy AM (2003) Migrating glioma cells activate the PI3-K pathway and display decreased susceptibility to apoptosis. J Cell Sci 116(21): 4409–4417. doi: 10.1242/jcs.00712

139. McDonald J (2014) Handbook of Biological Statistics, 3rd edn. Sparky House Publishing, Baltimore, Maryland

140. Jedlovszky-Hajdú A, Bombelli FB, Monopoli MP et al. (2012) Surface Coatings Shape the Protein Corona of SPIONs with Relevance to Their Application in Vivo. Langmuir 28(42): 14983–14991. doi: 10.1021/la302446h

141. Teeguarden JG, Hinderliter PM, Orr G et al. (2006) Particokinetics In Vitro: Dosimetry Considerations for In Vitro Nanoparticle Toxicity Assessments. Toxicological Sciences 95(2): 300–312. doi: 10.1093/toxsci/kfl165

142. Tucker SL, Thames HD (1989) The effect, of patient-to-patient variability on the accuracy of predictive assays of tumor response to radiotherapy: A theoretical evaluation. Int J Radiat Oncol 17(1): 145–157. doi: 10.1016/0360-3016(89)90382-9

143. Batchelor TT, Sorensen AG, Di Tomaso E et al. (2007) AZD2171, a Pan-VEGF Receptor Tyrosine Kinase Inhibitor, Normalizes Tumor Vasculature and Alleviates Edema in Glioblastoma Patients. Cancer Cell 11(1): 83–95. doi: 10.1016/j.ccr.2006.11.021

144. Neuhuber B, Swanger SA, Howard L et al. (2008) Effects of plating density and culture time on bone marrow stromal cell characteristics. Exp Hematol 36(9): 1176–1185. doi: 10.1016/j.exphem.2008.03.019

145. Hohnholt MC, Dringen R (2013) Uptake and metabolism of iron and iron oxide nanoparticles in brain astrocytes. Biochm Soc Trans 41(6): 1588–1592. doi: 10.1042/BST20130114

146. Soenen SJ, Himmelreich U, Nuytten N et al. (2011) Cytotoxic effects of iron oxide nanoparticles and implications for safety in cell labelling. Biomaterials 32(1): 195–205. doi: 10.1016/j.biomaterials.2010.08.075

147. Mailänder V, Landfester K (2009) Interaction of Nanoparticles with Cells. Biomacromolecules 10(9): 2379–2400. doi: 10.1021/bm900266r

148. Wilhelm C, Gazeau F, Roger J et al. (2002) Interaction of Anionic Superparamagnetic Nanoparticles with Cells: Kinetic Analyses of Membrane Adsorption and Subsequent Internalization. Langmuir 18(21): 8148–8155. doi: 10.1021/la0257337

149. Summers HD, Rees P, Holton MD et al. (2011) Statistical analysis of nanoparticle dosing in a dynamic cellular system. Nature Nanotech 6(3): 170–174. doi: 10.1038/nnano.2010.277

150. Snijder B, Sacher R, Rämö P et al. (2009) Population context determines cell-to-cell variability in endocytosis and virus infection. Nature 461(7263): 520–523. doi: 10.1038/nature08282

151. Topol EJ (2014) Individualized Medicine from Prewomb to Tomb. Cell 157(1): 241–253. doi: 10.1016/j.cell.2014.02.012

152. Pellerin L (2005) How Astrocytes Feed Hungry Neurons. MN 32(1): 59–72. doi: 10.1385/MN:32:1:059

153. Khakh BS, Sofroniew MV (2015) Diversity of astrocyte functions and phenotypes in neural circuits. Nat Neurosci 18(7): 942–952. doi: 10.1038/nn.4043

154. Geppert M, Hohnholt MC, Thiel K et al. (2011) Uptake of dimercaptosuccinate-coated magnetic iron oxide nanoparticles by cultured brain astrocytes. Nanotechnology 22(14): 145101. doi: 10.1088/0957-4484/22/14/145101

155. Singh SK, Bhardwaj R, Wilczynska KM et al. (2011) A Complex of Nuclear Factor I-X3 and STAT3 Regulates Astrocyte and Glioma Migration through the Secreted Glycoprotein YKL-40. Journal of Biological Chemistry 286(46): 39893–39903. doi: 10.1074/jbc.M111.257451

156. Pickard MR, Jenkins SI, Koller CJ et al. (2011) Magnetic Nanoparticle Labeling of Astrocytes Derived for Neural Transplantation. Tissue Eng Pt C-Meth 17(1): 89–99. doi: 10.1089/ten.tec.2010.0170

157. Lyon H (1991) Theory and Strategy in Histochemistry. A Guide to the Selection and Understanding of Techniques. Springer Berlin Heidelberg, Berlin, Heidelberg, ISBN: 3642737420

158. Le N, Richardson DR (2002) The role of iron in cell cycle progression and the proliferation of neoplastic cells. BBA-Rev Cancer 1603(1): 31–46. doi: 10.1016/S0304-419X(02)00068-9

159. Crichton RR, Wilmet S, Legssyer R et al. (2002) Molecular and cellular mechanisms of iron homeostasis and toxicity in mammalian cells. J Inorg Biochem 91(1): 9–18. doi: 10.1016/S0162-0134(02)00461-0

160. Schäfer R, Bantleon R, Kehlbach R et al. (2010) Functional investigations on human mesenchymal stem cells exposed to magnetic fields and labeled with clinically approved iron nanoparticles. BMC Cell Biol 11(1): 22. doi: 10.1186/1471-2121-11-22

161. Soenen SJH, Nuytten N, Meyer SF de et al. (2010) High Intracellular Iron Oxide Nanoparticle Concentrations Affect Cellular Cytoskeleton and Focal Adhesion Kinase-Mediated Signaling. Small 6(7): 832–842. doi: 10.1002/smll.200902084

162. Grudzinski IP, Bystrzejewski M, Cywinska MA et al. (2014) Comparative cytotoxicity studies of carbon-encapsulated iron nanoparticles in murine glioma cells. Colloid Surface B 117: 135–143

163. Berry CC, Wells S, Charles S et al. (2003) Dextran and albumin derivatised iron oxide nanoparticles: influence on fibroblasts in vitro. Biomaterials 24(25): 4551–4557. doi: 10.1016/S0142-9612(03)00237-0

164. Bai Y, Wu C, Zhao J et al. (2011) Role of iron and sodium citrate in animal protein-free CHO cell culture medium on cell growth and monoclonal antibody production. Biotechnol Progress 27(1): 209–219. doi: 10.1002/btpr.513

165. Au C, Mutkus L, Dobson A et al. (2007) Effects of Nanoparticles on the Adhesion and Cell Viability on Astrocytes. Biol Trace Elem Res 120(1-3): 248–256. doi: 10.1007/s12011-007-0067-z

166. Holder AL, Goth-Goldstein R, Lucas D et al. (2012) Particle-Induced Artifacts in the MTT and LDH Viability Assays. Chem Res Toxicol 25(9): 1885–1892. doi: 10.1021/tx3001708

167. Kroll A, Pillukat MH, Hahn D et al. (2012) Interference of engineered nanoparticles with in vitro toxicity assays. Arch Toxicol 86(7): 1123–1136. doi: 10.1007/s00204-012-0837-z

168. Bahring F, Schlenk F, Wotschadlo J et al. (2013) Suitability of Viability Assays for Testing Biological Effects of Coated Superparamagnetic Nanoparticles. IEEE Trans Magn 49(1): 383–388. doi: 10.1109/TMAG.2012.2222635

169. Arbab AS, Bashaw LA, Miller BR et al. (2003) Characterization of Biophysical and Metabolic Properties of Cells Labeled with Superparamagnetic Iron Oxide Nanoparticles and Transfection Agent for Cellular MR Imaging1. Radiology 229(3): 838–846. doi: 10.1148/radiol.2293021215

170. Collier AC, Pritsos CA (2003) The mitochondrial uncoupler dicumarol disrupts the MTT assay. Biochem Pharmacol 66(2): 281–287. doi: 10.1016/S0006-2952(03)00240-5

171. Teodori L, Albertini MC, Uguccioni F et al. (2006) Static magnetic fields affect cell size, shape, orientation, and membrane surface of human glioblastoma cells, as demonstrated by electron, optic, and atomic force microscopy. Cytometry 69(2): 75–85. doi: 10.1002/cyto.a.20208

172. Teodori L, Giovanetti A, Albertini MC et al. (2014) Static magnetic fields modulate X-ray-induced DNA damage in human glioblastoma primary cells. J Radiat Res 55(2): 218–227. doi: 10.1093/jrr/rrt107

173. Smith CM, La Fuente Jd, Pelaz B et al. (2010) The effect of static magnetic fields and tat peptides on cellular and nuclear uptake of magnetic nanoparticles. Biomaterials 31(15): 4392–4400. doi: 10.1016/j.biomaterials.2010.01.096

174. Huang C, Wei Z, Bansal V (2015) Concentric Magnetic Structures for Magnetophoretic Bead Collection, Cell Trapping and Analysis of Cell Morphological Changes Caused by Local Magnetic Forces. PLoS ONE 10(8): e0135299. doi: 10.1371/journal.pone.0135299

175. Creixell M, Bohórquez AC, Torres-Lugo M et al. (2011) EGFR-Targeted Magnetic Nanoparticle Heaters Kill Cancer Cells without a Perceptible Temperature Rise. ACS Nano 5(9): 7124–7129. doi: 10.1021/nn201822b

176. Daou TJ, Grenèche JM, Pourroy G et al. (2008) Coupling Agent Effect on Magnetic Properties of Functionalized Magnetite-Based Nanoparticles. Chem Mater 20(18): 5869–5875. doi: 10.1021/cm801405n

177. Fayol D, Luciani N, Lartigue L et al. (2013) Managing Magnetic Nanoparticle Aggregation and Cellular Uptake: a Precondition for Efficient Stem-Cell Differentiation and MRI Tracking. Advanced Healthcare Materials 2(2): 313–325. doi: 10.1002/adhm.201200294

178. Watkins SC, St. Croix CM (2001) Building a Live Cell Microscope: What You Need and How to Do It. In: Robinson JP, Darzynkiewicz Z, Dobrucki J et al. (eds) Current Protocols in Cytometry. John Wiley & Sons, Inc, Hoboken, NJ, USA

179. Stephens DJ (2003) Light Microscopy Techniques for Live Cell Imaging. Science 300(5616): 82–86. doi: 10.1126/science.1082160

180. Huth J, Buchholz M, Kraus JM et al. (2010) Significantly improved precision of cell migration analysis in time-lapse video microscopy through use of a fully automated tracking system. BMC Cell Biol 11(1): 24. doi: 10.1186/1471-2121-11-24

181. Meijering E, Dzyubachyk O, Smal I (2012) Methods for Cell and Particle Tracking. In: Imaging and Spectroscopic Analysis of Living Cells - Optical and Spectroscopic Techniques, vol 504. Elsevier, pp 183–200

182. Carpenter AE, Kamentsky L, Eliceiri KW (2012) A call for bioimaging software usability. Nat Meth 9(7): 666–670. doi: 10.1038/nmeth.2073

183. Hand A, Sun T, BARBER D et al. (2009) Automated tracking of migrating cells in phase-contrast video microscopy sequences using image registration. Journal of Microscopy 234(1): 62–79. doi: 10.1111/j.1365-2818.2009.03144.x

184. Hulkower KI, Herber RL (2011) Cell Migration and Invasion Assays as Tools for Drug Discovery. Pharmaceutics 3(4): 107–124. doi: 10.3390/pharmaceutics3010107

185. Vince GH, Bouterfa H, Goldbrunner R et al. (1997) Fast blue, a fluorescent tracer in glioma cell culture, affects cell proliferation and motility. Neurosci Lett 233(2-3): 148–150. doi: 10.1016/S0304-3940(97)00637-X

186. Parish CR (1999) Fluorescent dyes for lymphocyte migration and proliferation studies. Immunol Cell Biol 77(6): 499–508. doi: 10.1046/j.1440-1711.1999.00877.x

187. Mechem C, Jarrell BE, Koolpe E et al. (1989) Intravital fluorescence microscopy of endothelial cells on vascular grafts. J Surg Res 47(1): 1–7

188. Lampidis TJ, Bernal SD, Summerhayes IC et al. (1983) Selective toxicity of rhodamine 123 in carcinoma cells in vitro. Cancer Res. 43(2): 716–720

189. Modica-Napolitano JS, Aprille JR (1987) Basis for the selective cytotoxicity of rhodamine 123. Cancer Res. 47(16): 4361–4365

190. Hatzikirou H, Basanta D, Simon M et al. (2012) 'Go or Grow': the key to the emergence of invasion in tumour progression? Math Med Biol 29(1): 49–65. doi: 10.1093/imammb/dqq011

191. Staton CA, Reed MWR, Brown NJ (2009) A critical analysis of current in vitro and in vivo angiogenesis assays. Int J Exp Pathol 90(3): 195–221. doi: 10.1111/j.1365-2613.2008.00633.x

192. Pensabene V, Vittorio O, Raffa V et al. (2008) Neuroblastoma cells displacement by magnetic carbon nanotubes. IEEE Trans Nanobioscience 7(2): 105–110. doi: 10.1109/TNB.2008.2000749

193. Matthews BD (2006) Cellular adaptation to mechanical stress: role of integrins, Rho, cytoskeletal tension and mechanosensitive ion channels. J Cell Sci 119(3): 508–518. doi: 10.1242/jcs.02760

194. Lange JR, Fabry B (2013) Cell and tissue mechanics in cell migration. Exp Cell Res 319(16): 2418–2423. doi: 10.1016/j.yexcr.2013.04.023

195. Pampaloni F, Reynaud EG, Stelzer EHK (2007) The third dimension bridges the gap between cell culture and live tissue. Nat Rev Mol Cell Biol 8(10): 839–845. doi: 10.1038/nrm2236

Acknowledgements

Appendix

Astrocytes FBS proliferation

Principle

As the proteins in the FBS of the culture medium is known to influence the aggregation of MNPs and thus the loading of the cells, a similar FBS amount of glioblastoma and astrocyte medium was preferred. In order to check the growth behavior of astrocytes after FBS reduction, astrocytes were cultured with 10 % FBS, and the growth and membrane integrity was measured.

Procedure

Astrocytes were seeded at 2.5×10^4 cells/cm² in 12-well plates in triplicates and adhered for 1 d, before medium exchange to 10 % FBS in half of the samples. At day 1-4, cells were trypsinized and counted by CASY.

Results and discussion

The cell number was reduced at day 3 and more remarkably at day 4 in samples treated with the lower FBS content (Figure 38). However, the membrane integrity was not altered by the lower FBS amount. This indicated that the proliferation was decreased, while the cells stayed healthy. Thus, 10 % FBS was used for MNP loading experiments.
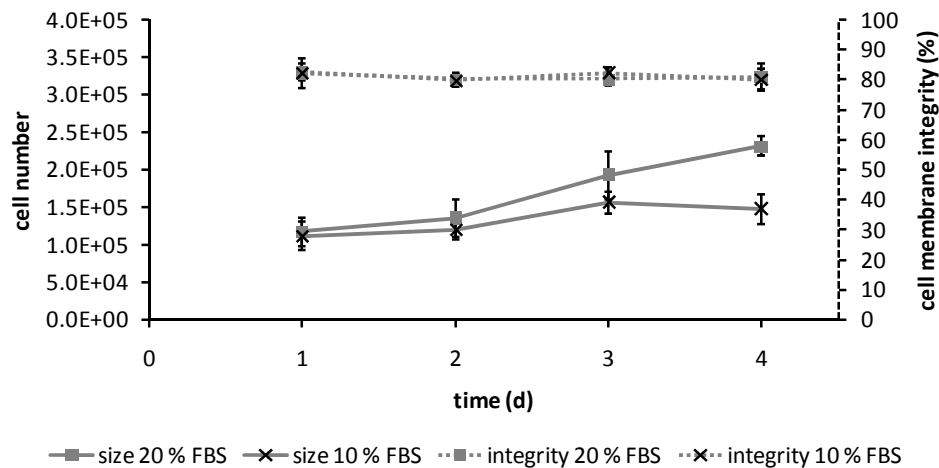
Figure 38: Astrocytes growth without MNP exposure with different FBS concentrations. Means ± standard deviations of cell counts (solid lines) and cell membrane integrity (dotted lines) for 2.5×10^4 cell density after 1-4 d growth. Cross symbol shows cells cultured with 10 % FBS.

Magnetic MNP movement

Principle

Similar to the strength, also the form of the magnetic field could affect the cells. Thus, the magnetic field lines and the attraction of magnetic fluids were visualized with iron oxide nanopowder in air and water.

Procedure

To visualize the magnetic field lines of the magnetic setups used in this study, a sealed petri dish filled with dry iron oxide nanopowder was used. For investigation of the adherent movement setup, the dish was put on top of a 10 mm permanent magnet fixed at the side of a well from a 12-well plate. For the metabolic activity experiment setup, the petri dish was placed on top of a 20 mm permanent magnet fixed on a metal plate. Afterwards, pictures were taken with a Nikon camera.

To get insight in the magnetic attraction pattern of magnetic fluids, the iron oxide nanopowder was resuspended in water and the sealed petri dish was placed on the two magnetic setups for 3 d, followed by picture acquisition.

Results and discussion

The dry iron nanopowder showed the typical magnetic field lines of this type of permanent magnets (Figure 39A), which are also in accordance with the field lines simulated by the femm software.
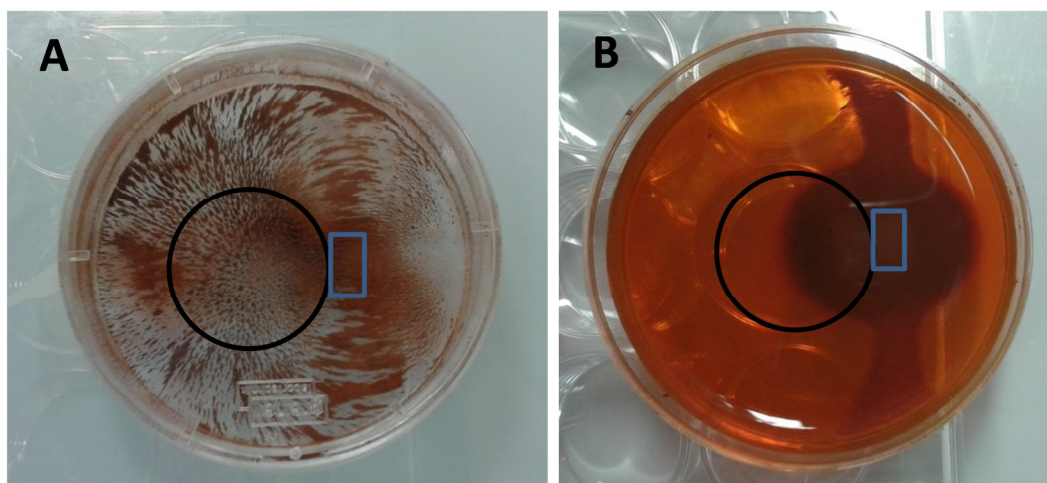
Figure 39: Iron nanopowder attraction by magnets. Dry nanopowder (A) or nanopowder in suspension (B) was put in petri dishes on top of 12-well plates with a magnet fixed at the side, like for the 12-well migration assay setup and pictures were acquired. The blue rectangles show the localization of the 10 mm magnet and the black circles outline the well edges.

It was observed that the MNP reaction to the magnetic field is also detectable at the opposite wall of the well from a 12-well plate, although the field strength was only about 5 mT. The images of the nanopowder suspension in water after a long-term incubation in the magnetic field (Figure 39B) showed that the iron particles from the whole well were attracted to the magnet. This indicates that the MNPs incorporated in cells may also be influenced by the magnetic forces, if they are subjected to a relatively weak magnetic field.

Leibovitz medium test

Principle

During the MRI experiments, the cells had to survive in normal atmosphere. To check the ability of cell seeding in normal atmosphere (without additional gas supply), G62 and G44 cells were seeded with Leibovitz medium, which can buffer the pH via a special composition of phosphates, salts, galactose and amino acids [26]. Additionally, the effect of a heating was tested.

Procedure

For the Leibovitz medium test, G62 and G44 cells were seeded with normal cell culture medium in 12-well plates in triplicates at 2.5×10^4 cells/cm². After 1 d, microscopic pictures were taken and the medium was exchanged to normal cell culture medium (medium control) or Leibovitz medium supplemented with 10 % FBS. The cells were incubated overnight either on a clean table outside the incubator at room temperature (cold) or on a heating block set to 37 °C (warm). In parallel, normal cell culture and Leibovitz medium treated cells were also incubated in a normal cell culture incubator (condition control). The next day, microscopy was repeated and the cells were trypsinized and counted by CASY® twice each.

Results and discussion

As shown in Figure 40, the G62 cell number was reduced largely, if DMEM was used in normal atmosphere incubation, while the decrease was more pronounced in samples incubated on a heating block (warm), compared to room temperature (cold). The cell numbers of G62 cultures incubated with Leibovitz medium were similar in normal atmosphere, if incubated with warmth. The membrane integrity of G62 was less affected than the cell number, however, a slightly higher integrity was detected with Leibovitz medium in the warm setup.
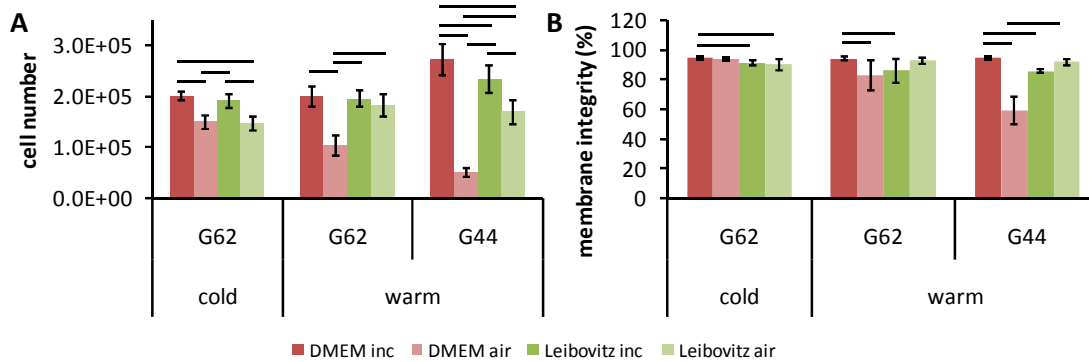
Figure 40: Glioblastoma cell growth and viability in Leibovitz medium. Means ± standard deviations of cell number and membrane integrity of glioblastoma cells incubated in incubator (dark colors "inc") or in normal air (bright colors) in DMEM (red) or Leibovitz (green) medium overnight. "Cold" indicates cells incubated at room temperature, "warm" on a heating plate, lines indicate $p \leq 0.05$, 1-way ANOVA.

This indicated that the Leibovitz medium help the G62 to survive the normal atmosphere conditions, and that a heating would be necessary for MRI experiments to optimize the conditions. G44, incubated with DMEM showed a drop of cell number and also a remarkable decrease in membrane integrity in normal atmosphere (warm). When G44 were incubated with Leibovitz medium, the cell number also decreased, if heat was applied. This suggested that G44 cells are more sensible to culture condition defects, compared to G62 cells. Thus, G62 were chosen for MRI experiments.

MNP loading dataset
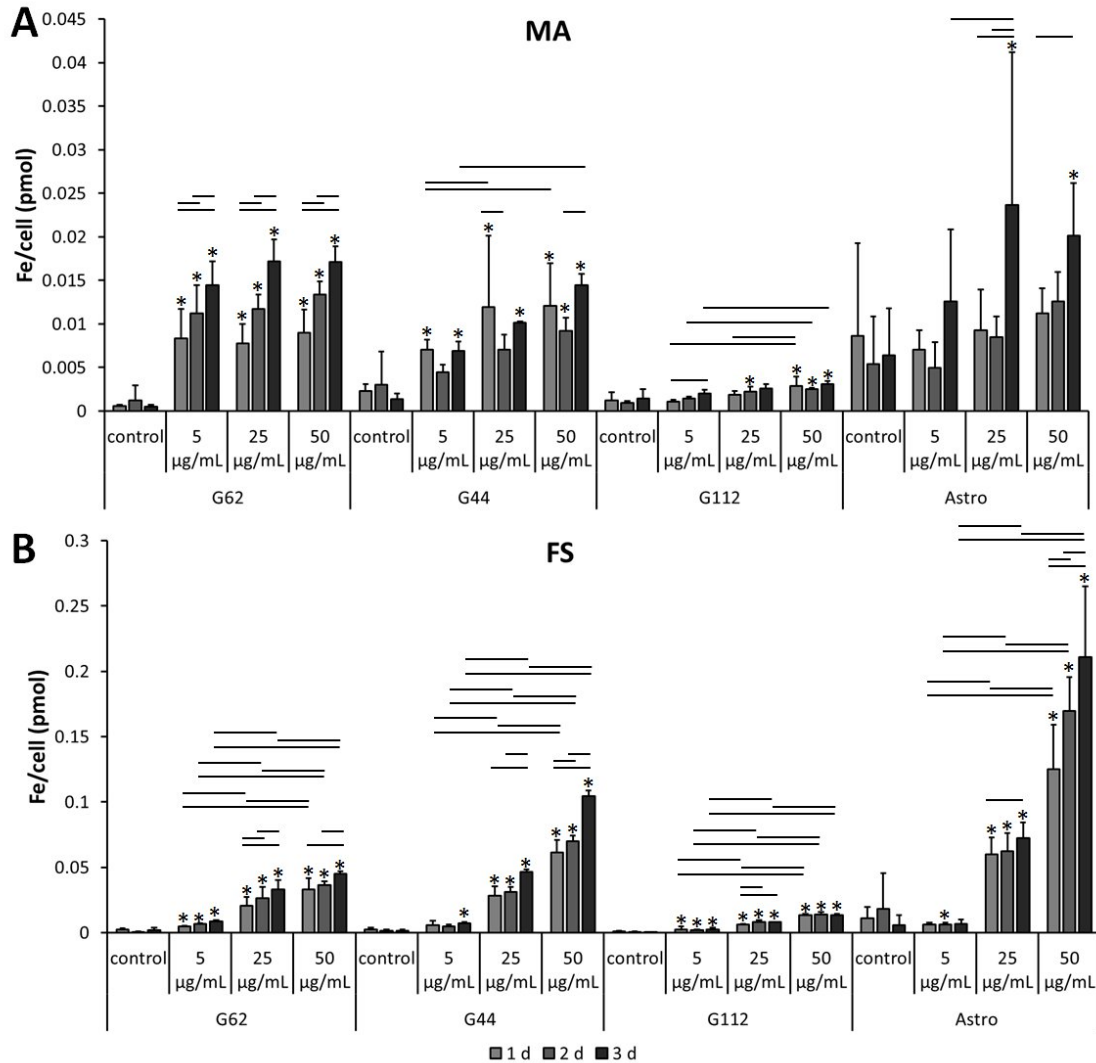
Figure 41: Dataset MNP loading. Means and standard deviation of glioblastoma cells (G62, G44, G112) and astrocytes (Astro) treated without (control) or with MNPs at 5, 25 or 50 µg/mL iron concentration, for 1-3 d. * p≤0.05 towards control, lines between the samples (2-way ANOVA, Holm-Sidak post-hoc test). Methods and discussion as described in the thesis.

Astrocyte - FS islet growth

Principle

Morphological changes are relatively easy to detect and point to adaptations of the cell to inner or outer influences.

Procedure

Astrocytes were grown without MNPs (control) or with 50 µg/mL FS for 1- 3 d and microscopic images were taken.

Results and discussion

Without MNPs, astrocytes grew relatively spread over the whole surface until confluency (Figure 42). If treated with 50 µg/mL FS, the cell spreading was more uneven after 1 d and the cell distribution was less confluent after 3 d. In a higher magnification, an islet-like growth of the cells was shown, if the cells were loaded with FS.

In a publication by Giese et al., less space to adjacent cells was observed, if the cells were not migrating [107], so that the islet growth could indicate in impaired migration behavior, caused by FS treatment.
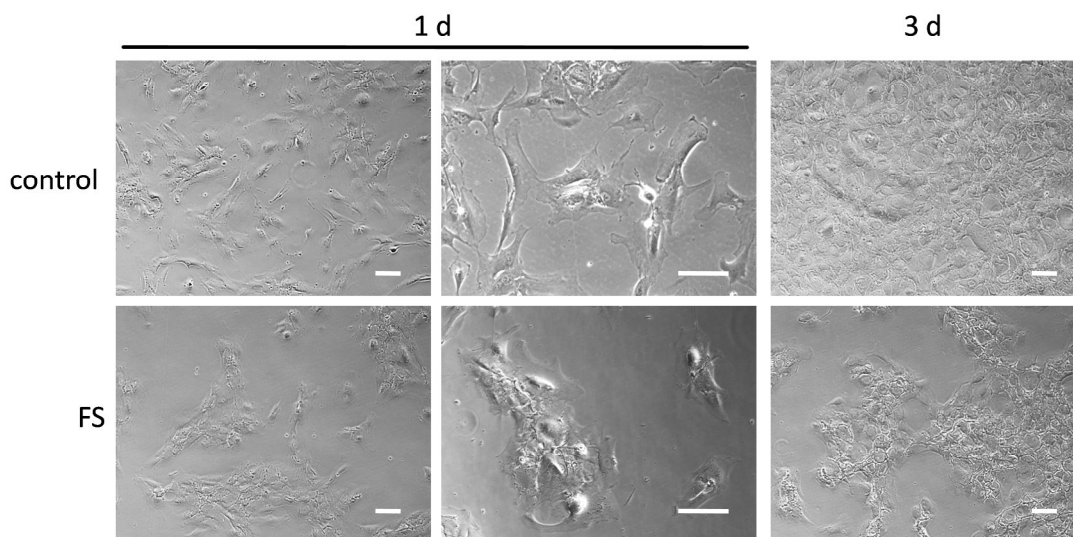
Figure 42: Astrocytes shape conversion with FS 50 µg/mL. Astrocytes without MNPs (control) or treated with 50 µg/mL FS (FS) were grown for 1 - 3 d. The scales show 100 µm.

Cell diameter MNP influence

Principle
The cell size can be affected by the MNP loading.

Procedure
The cells were loaded with MNPs and trypsinized, following CASY examination (see methods part).

Results and discussion
As shown in Figure 43, the cell size was not remarkably affected by any MNP loading condition. However, there are small tendencies, that the cell size is increased with higher MNP loading. This could also indicate, that the cell number was reduced and thus, more space was available for the remaining cells to grow bigger.
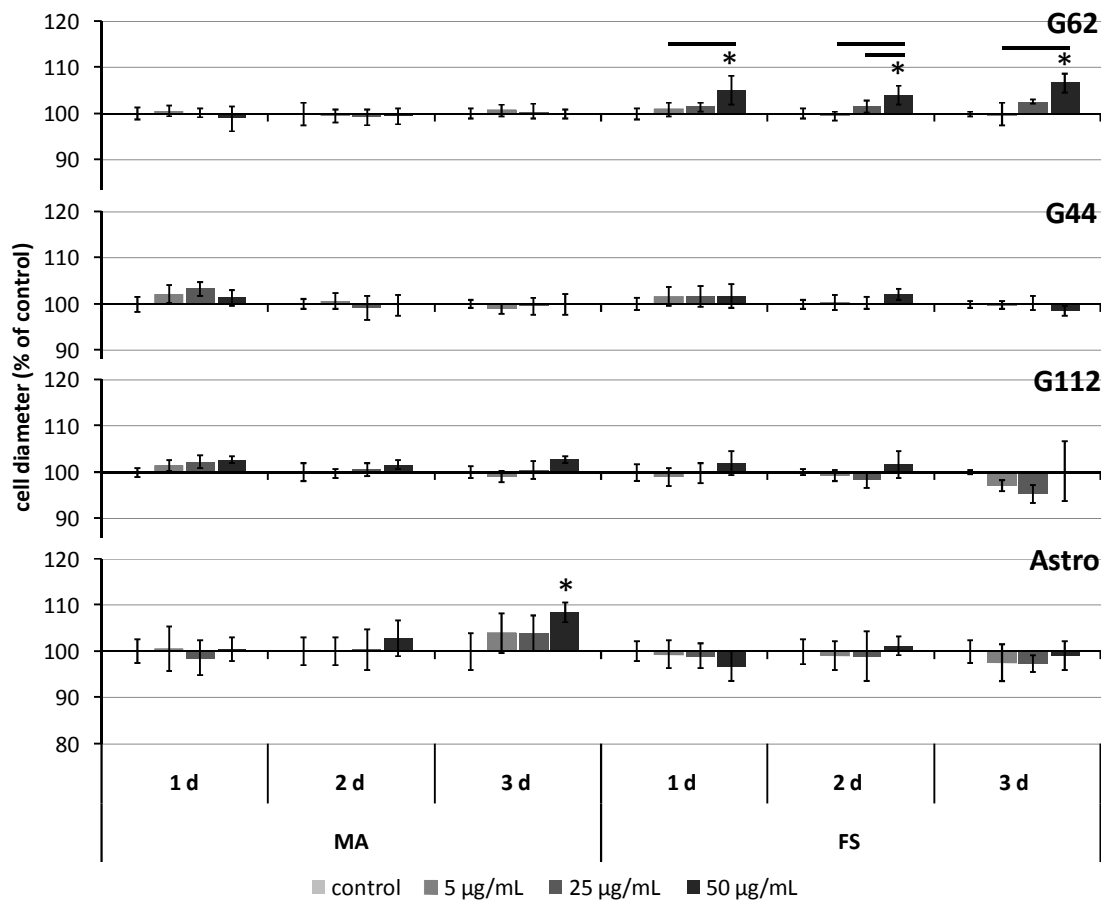
Figure 43: Cell diameter after MNP exposure. Cells were treated with MNPs and the cell diameter was examined by CASY, *p≤0.05, 2-way ANOVA, n=6.

MTT MNP influence

Principle

The influence of the MNPs on the MTT assay procedure was tested. For this aim, MA was mixed with medium and the supernatant of cells treated with MNPs were checked for causing artifacts.

Procedure

In a first trial, MA diluted with medium was incubated with MTT for 4 h, collected in a tube and aliquoted in a 96-well plate. In a second trial, the supernatants from the cells incubated with MA and MTT were collected, centrifuged for 5 min at 13 000 rpm (microcentrifuge) and aliquoted in a 96-well plate. SDS solubilizing solution was added and the mixture was incubated overnight in the incubator. Afterwards, the absorbance was detected and calculated towards control medium (details see methods part).
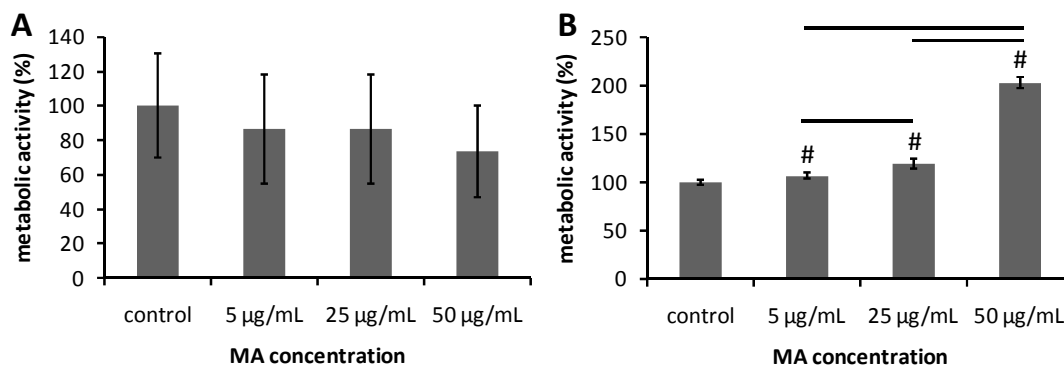
Figure 44: MTT artifacts tests. MA was diluted in medium (A) and cells treated with MA (B) were incubated with MTT for 4 h. The metabolic activity was calculated towards the control without MA, # p≤0.05 to control, line between the samples, 1-way ANOVA, n=9.

Results and discussion

If MA were diluted with medium, a reduction of virtual metabolic activity with the highest MA concentration was detected by MTT assay, compared to control, while the standard deviation was high. Compared with the absolute values gained in experiments with cells, this influence of the MNPs is not affecting the results. This indicated that the MNPs are not inferring with the MTT assay, either by direct reaction with the substances or by scattering.

If the supernatant from the cells treated without (control) or with MA was examined, an increase of absorbance with higher MA concentration was detected, especially with the highest MA concentration (50 µg/mL). As the MNPs itself are not causing high artifacts, a cell component should be responsible for this observation. Possibly, with higher MA concentration, more cells detached and reached the supernatant fraction, where they were dissolved. Thus, the absorbance and the virtual activity increased.

Indeed, this supports the observation, that a higher MNP concentration is leading to a lower adherence of cells.

Rhodamine123 staining proliferation reduction

Principle

The Bromodeoxyuridine (BrdU) assay measures the proliferation of a cell population according to the incorporation of an artificial nucleotide in the DNA during double strand synthesis after cell division.

Procedure

G62 were seeded in 96-well plates and treated with different concentrations of rhodamine123. After 6 h, the cells were washed with medium and pure medium was added.

After overnight incubation, a BrdU assay based on luminescence detection was performed. Controls were cells without any treatment (pure cells), cells treated with the highest DMSO amount used ("DMSO 50") and cells without BrdU (background). According to the manufacturers protocol (Roche), 10 µL BrdU solution (1:10 dilution from stock) was pipetted per well and incubated for 4 h. After medium removal, 200 µL fixation/denaturation solution per well was added for fixation and denaturation of the cells and the cells were incubated for 30 min at room temperature. After removal of the FixDenat solution, 100 µL Anti-BrdU-peroxidase working solution (1:100 dilution) per well was added and incubated for 90 min at room temperature. Then, the antibody solution was washed away 3 times with the washing solution (1:10 dilution) and the bottom was sealed with non-transparent tape. The substrate solution was prepared by mixing component B 1:100 with component A. Afterwards, 100 µL substrate solution per well was added, the plate was incubated 3 min on a shaking platform and the luminescence was measured with the Vicor³V plate reader.

Results and discussion

Even with low rhodamine concentrations in the medium, the proliferation of the cells was significantly decreased (Figure 45). The higher the concentration was, the more growth was inhibited. DMSO alone did not show any effect on cell proliferation.
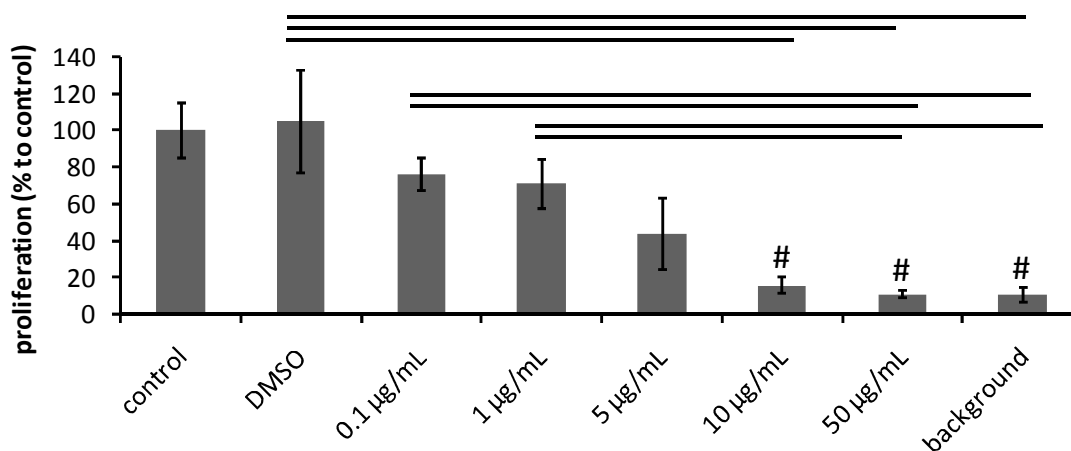

Figure 45: BrdU assay with rhodamine123 treatment. G62 cells were treated with different concentrations of rhodamine (0.1 - 50 µg/mL), or with the highest concentration DMSO used for dissolution of 50 µg/mL rhodamine (DMSO 50). Cells without rhodamine (pure cells) were used as control. Background indicates cells treated without rhodamine and BrdU, # $p \leq 0.05$, line between the samples, 1-way ANOVA, n=8.

Migration with Laminin

Principle

The coating influences the migration capability of cells *in vitro*. Laminin was found to increase the motility of glioblastoma cells, thus the influence of the coating in the magnetic guidance of the cell migration was tested in an ibidi insert setup.

Procedure

The surface of the cell culture wells was coated with 10 µg/mL laminin solution for 1 h at 37 °C and washed with PBS. G62 cells were treated with 25 µg/mL MA for 1 d and seeded in ibidi 4-well inserts, while cells without MNP treatment were set as control, because the lack of magnetic attraction was shown in the non-adherent assays. Then, the migration assay was performed as described in the methods part.

Results and discussion

The outgrowth of the seeding spot was not remarkably increased on the side pointed to the magnet in comparison with the opposite side and with control cells. This indicated that laminin could not support the movement of adherent cells in direction of the magnet.
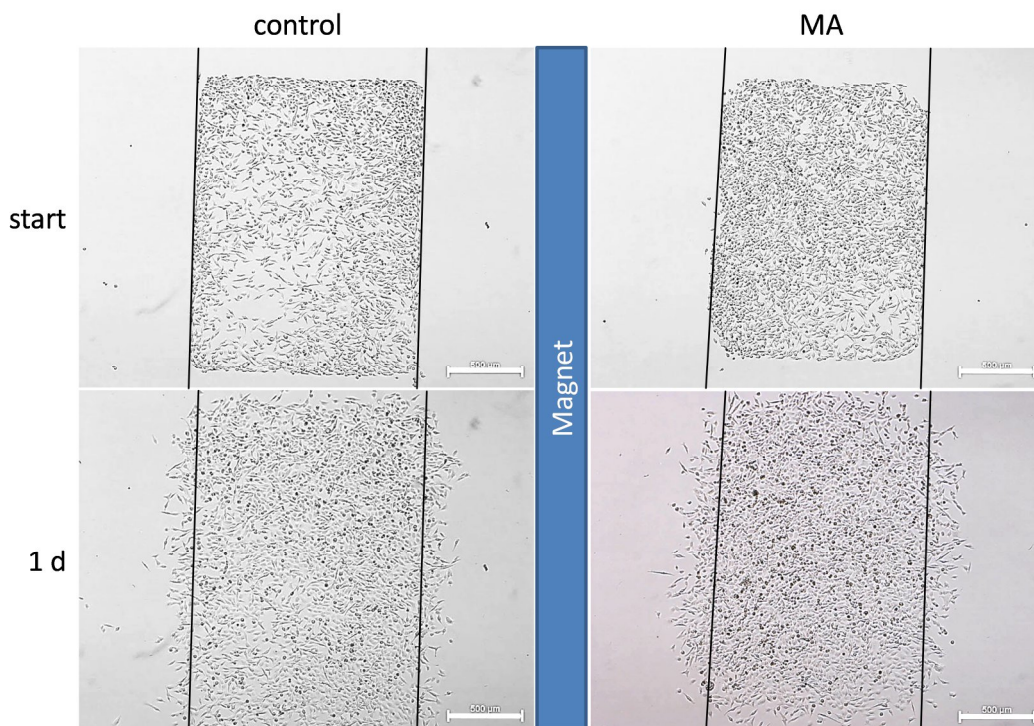

Figure 46: Laminin motility support test. G62 were incubated with 25 µg/mL MA for 1 d or without MNPs (control) and seeded in ibidi 4-well inserts on Laminin-coated surface (10 µg/mL 1 h 37 °C), scale = 500 µm.

Calcein staining effects on cell adherence

Principle

The loss of cells in the 12-well migration assay led to the assumption that the cells died. In order to check the reaction of cells to the double-load with MNPs and Calcein, an MTT assay was performed, that simulated the conditions of the migration assay, including reseeding, magnet incubation and double-staining. In parallel, cells were treated similar, except of the reseeding step, in order to evaluate the trypsinization influence on the cell health.

Procedure

G44 cells were incubated with 25 µg/mL FS for 3 d in either a 96-well plate (72 h adherence) or a 12-well plate (6 h adherence). Cells from the 12-well plate were reseeded in a 96-well plate and let adhere for 6 h. Cells from both 96-well plates were stained with Calcein for 30 min following 24 h incubation with a 20 mm permanent magnet fixed below the plates. Afterwards, the Calcein staining was repeated and MTT assay was performed, as described in the methods part.
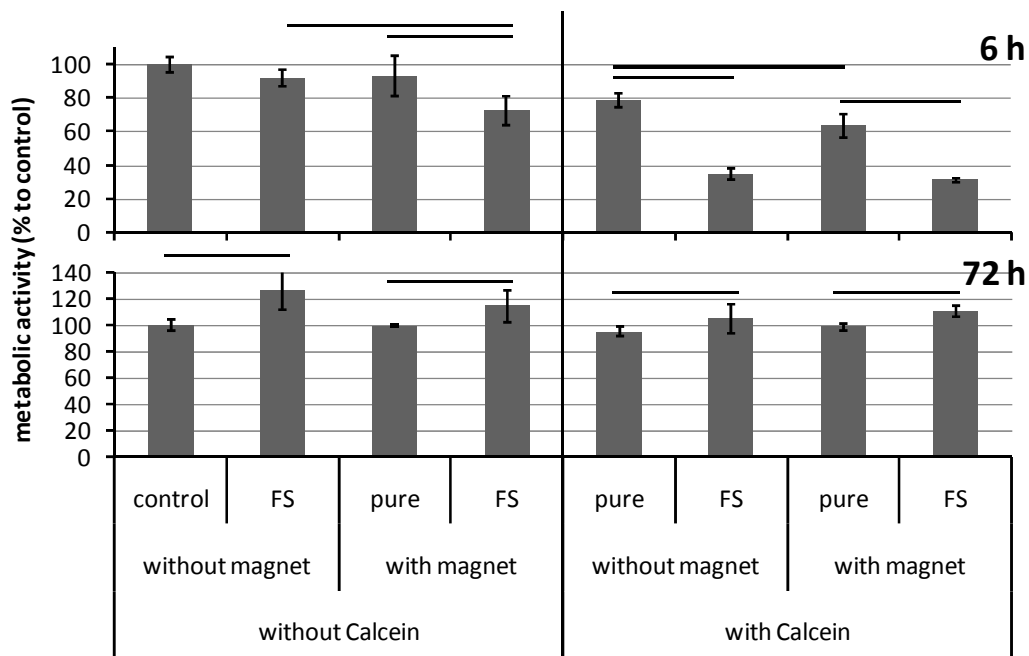
Results and discussion

Figure 47: Calcein influence on G44 cell adhesion. G44 cells were loaded with 25 µg/mL FS (FS) or not (control) for 3 d, following reseeding (6 h adherence) or not (72 h adherence). Then, part of the cells were stained with Calcein and a magnetic field was applied over night. After staining with Calcein, an MTT assay was performed, $p \leq 0.05$, 2-way ANOVA, n=4.

Without trypsinization step (72 h adherence), Calcein did not show large effects on metabolic activity of G44 cells, either without or with magnetic field application. However, with the seeding/staining protocol for the migration assay (6 h adherence), there were pronounced declines in metabolic activity (Figure 47). These were even enhanced by the magnetic field.

A possible reason could be that the cells could not fully adhere if treated with Calcein before. Thus, the Calcein staining might be responsible for the lower G44 cell numbers counted in the migration assay. Cells might not adhere after the first staining (start) but still be counted. During the magnetic field application phase, the cells might die and could not be detected afterwards. G62 cells showed faster adherence and higher robustness in cell characterization studies and thus might not underlie this phenomenon.

List of hazardous chemicals

Table 6: Hazardous chemicals used in this study

Chemical name	CAS-number	GHS category	Hazard statement	Precautionary statement
formaldehyde solution	50-00-0	GHS05, GHS06, GHS08	H301 + H311 + H331-H314-H317-H335-H341-H350-H370	P201-P260-P280-P301 + P310 + P330-P303 + P361 + P353-P304 + P340 + P310-P305 + P351 + P338-P308 + P311-P403 + P233
hydrochloric acid fuming	7647-01-0	GHS05, GHS07	H290-H314-H335	P260-P280-P303 + P361 + P353-P304 + P340 + P310-P305 + P351 + P338 + P310
iron(III)chloride, reagent grade	7705-08-0	GHS05, GHS07	H290-H302-H315-H318	P280-P301 + P312 + P330-P305 + P351 + P338 + P310
laminin from human placenta, liquid	114956-81-9	GHS07	H315-H319-H335	P261-P305 + P351 + P338
potassium hexacyanoferrate (II) trihydrate, ACS reagent	14459-95-1		H412	
potassium permanganate ACS reagent	7722-64-7	GHS03, GHS05, GHS07, GHS09	H272-H302-H314-H410	P210-P220-P260-P280-P305 + P351 + P338-P370 + P378
sodium hydroxide solution,	1310-73-2	GHS05	H290-H314	P280-P303 + P361 + P353-P304 + P340 + P310-P305 + P351 + P338
thiazolyl blue tetrazolium bromide	298-93-1	GHS07, GHS08	H315-H319-H335-H341	P261-P281-P305 + P351 + P338
Triton™ X-100 for molecular biology	9002-93-1	GHS07, GHS09	H302-H319-H411	P301 + P312 + P330-P305 + P351 + P338

Table 7: Explanation of GHS categories

GHS	pictogram	explanation
GHS03		Oxidizing gases, category 1 Oxidizing liquids, categories 1,2,3
GHS05		Corrosive to metals, category 1 Skin corrosion, categories 1A,1B,1C Serious eye damage, category 1

GHS06		Acute toxicity (oral, dermal, inhalation), categories 1,2,3
GHS07		Acute toxicity (oral, dermal, inhalation), category 4 Skin irritation, category 2 Eye irritation, category 2 Skin sensitisation, category 1 Specific Target Organ Toxicity – Single exposure, category 3
GHS08		Respiratory sensitization, category 1 Germ cell mutagenicity, categories 1A,1B,2 Carcinogenicity, categories 1A,1B,2 Reproductive toxicity, categories 1A,1B,2 Specific Target Organ Toxicity – Single exposure, categories 1,2 Specific Target Organ Toxicity – Repeated exposure, categories 1,2 Aspiration Hazard, category 1
GHS09		Hazardous to the aquatic environment - Acute hazard, category1 - Chronic hazard, categories 1,2

Eidesstattliche Versicherung

Hiermit versichere ich an Eides statt, die vorliegende Dissertation selbst verfasst und keine anderen als die angegebenen Hilfsmittel benutzt zu haben.

Ich versichere, dass diese Dissertation nicht in einem früheren Promotionsverfahren eingereicht wurde.

Datum, Unterschrift